Oxidation State Roulette:

Synthesis and Reactivity of Cobalt Complexes Containing SNS Ligands

By

Brandon Fitchett

Thesis submitted to the University of Ottawa in partial fulfillment of the requirements for the degree of Masters of Science in Chemistry

Department of Chemistry and Biomolecular Sciences
Faculty of Science
University of Ottawa

Abstract

The use of rare and expensive noble metals in the chemical industry as organometallic catalysts has grown exponentially in the past few decades due to their high activity, selectivity and their ability to catalyze a wide range of reactions. With this growth in use has also come a proportional growth in concern as these toxic metals inevitably leach into the environment and their negative effects on public health and our ecosystems are becoming better understood. First-row transition metal catalysts provide both environmental and economic benefits as alternatives to these noble metals due to their lower toxicity and cheaper costs. The two-electron chemistry that makes the noble metals so attractive however, is more challenging to accomplish with first-row transition metals.

Intelligently designing the ligand scaffold which surrounds the metal can mitigate or even eliminate some of the shortfalls of these first-row metals. Some key features that should be considered when designing a ligand are: 1) a strong chelating ability so the ligand can stay attached to the metal, 2) incorporation of strong donors to favour low-spin complexes, 3) inclusion of hemilabile groups to allow for substrate activation and metal stabilization throughout various oxidation states, 4) redox activity to be able to donate or accept electrons, and 5) inclusion of Lewis base functionalities which are able to assist the substrate activation. Ligands which incorporate these features are known as bifunctional ligands as they can accomplish more than one function in the catalytic cycle. Developing first-row transition metal complexes containing these ligands may enable these species to replicate the reactivity and selectivity generally associated

with the precious metals. Being able to replace the noble metals used in industry with these catalysts would have tremendous environmental and economic benefits.

The objective of this thesis is to advance the field of bifunctional catalysis by examining the behaviour of two sterically svelte, tridentate SNS ligands containing hard nitrogen and soft sulphur donors when bonded to cobalt. Previous work with iron provides a template of the ligand behaviour to which cobalt can be compared, allowing us to contrast the effects exerted by the different metals. After an introduction to bifunctional catalysis in **Chapter 1**, **Chapter 2** describes the reactivity of the amido ligand, $S^{Me}N^{H}S^{Me}$, with precursors ranging from Co(I) to Co(III), all of which yielded the $19e^-$ pseudooctahedral cobalt(II) bis-amido complex, $Co(S^{Me}N^{-}S^{Me})_2$ characterized by ^1H NMR spectroscopy, single-crystal X-ray crystallography and cyclic voltammetry. Although this complex has a similar structure as the Fe analogue, the cobalt bis-amido complex did not exhibit the same hemilabile behaviour that allowed for simple ligand substitution of one of the thioether groups. Instead it reacted reversibly with 2,2'-bipyridine while 1,2-bis(dimethylphosphino)ethane (DMPE) and 2,6-dimethylphenyl isocyanide both triggered additional redox chemistry accompanied by the loss of protonated $S^{Me}N^{H}S^{Me}$. In contrast, protonation gave the cobalt(II) amido-amine cation, $[Co(S^{Me}NS^{Me})(S^{Me}N^{H}S^{Me})](NTf_2)$, which allowed for substitution of the protonated ligand by acetonitrile, triphenylphosphine and 2,2'-bipyridine based on ^1H NMR evidence. The ability of $Co(S^{Me}NS^{Me})_2$ to act as a precatalyst for ammonia-borane dehydrogenation was also probed, revealing that it was unstable under these conditions. Addition of one equivalent of DMPE per cobalt, however, resulted in better activity with a preference for

linear aminoborane oligomers using ammonia-borane and, surprisingly, to a change in selectivity to prefer cyclic products when moving to methylamine-borane.

Chapter 3 delves into the chemistry of the thiolate ligand, $S^{Me}N^{H}S$, which formed a new 18e$^-$ cobalt(III) pseudooctahedral complex, Co(S^-NC^-)(SMe)(DEPE), from oxidative addition of the C_{aryl}-S^{Me} bond. Scaling up this reaction resulted instead in formation of an imine-coupled $[Co(N_2S_2)]^-$ anion which was characterized by ^{1}H NMR/EPR spectroscopy, single-crystal X-ray diffraction, cyclic voltammetry and DFT studies. The latter revealed an interesting electronic structure with two electrons delocalized in the ligand, demonstrating the non-innocent nature of the N_2S_2 ligand. While the analogous iron complex proved to be an effective pre-catalyst for the hydroboration of aldehydes with selectivity against ketones, this behaviour was not observed with $[Co(N_2S_2)]^-$ which gave a slower rate and less selectivity.

The knowledge acquired from this thesis work has advanced the field of bifunctional catalysis by extending the application of these two SNS ligands from iron to cobalt, revealing unpredictable differences in reactivity between the metals. By comparing the behaviour of these ligands with iron and cobalt, we gain a better understanding of the chemistry that is accessible by these ligands and the applications for which they may be used. This increased knowledge contributes to our long-term goal of replacing expensive and toxic noble metals with more benign first-row transition metals, improving the sustainability of the chemical industry.

Acknowledgements

The first and most significant thanks I must give for helping me finish this thesis is to my supervisor, Professor R. Tom Baker, whose guidance and experience were essential in steering this thesis to completion. Thank you, Baker, for being such a welcoming and approachable mentor over the past two and a half years, always willing to put down what you were doing to answer my questions. Your constant excitement and passion for chemistry is inspiring and has taught me that there is just as much value in understanding the process as there is in the final result. I would not have been able to come this far without your constant injections of positivity and optimism into my project when I was growing frustrated. You are an exemplary scientist and it has been a privilege to learn from you as your student. Thanks for everything.

I must also take this opportunity to thank my other mentors in the Baker group who have taught me over the years. Cassandra, Uttam and Mehdi, thank you for teaching me everything I know about working in a lab and always answering my questions, regardless of how obvious the answer may have seemed. I wouldn't be where I am today without your guidance and will carry your lessons with me throughout my career. To the other members of the Baker group, past and present, thank you for your constant suggestions and assistance. I was very fortunate to be able to be a part of such a friendly group of co-workers. Specifically, I also need to thank Karine for growing into such an amazing friend over the last few years, I'm going to miss not working in the same building as you anymore. Your friendship and sense of humor has made the frustrations of grad school much more bearable, thanks for helping me through it.

I would also be doing an injustice to the rest of my friends that I have made over the past seven years at the University of Ottawa by not mentioning how they have changed my life for the better. Thank you for showing me that university isn't defined by the little piece of paper that you get at the end, but instead by the bonds that you form along the way. You have helped shape me into the person that I am today and hope you know that our friendships mean the world to me. So here's to you guys: Duncan, Brendan, Ethan, Mitch, Jack, Steven, Katie, Kendra, Winston, Charly, Brian, Miguel,

Kate, Robin, Evan, Amber, Fraser and Meaghan, thanks for everything. I'll meet you at Maison.

And finally, I need to thank my family without whom I would have never made it this far. Mom and Dad, I cannot thank you enough for being such supportive parents. Thank you for believing in me and convincing me that I can accomplish whatever I set my mind to. Thank you for your endless emotional support and bringing my mind to ease when I was stressed out about an exam or a project. Thank you for every sacrifice and gesture that you have made to raise me into who I am today. I hope I have made you proud. To my little brother Chris, thanks for always being able to cheer me up. It's good to know I can count on you to make me smile whenever I need it most. To Nanna and Poppa, I couldn't ask for more amazing grandparents. I cherished the time that we had together and will always miss you. I don't know where you are now, but I hope that you are together.

Thanks again to you all,

Brandon

Table of Contents

List of Schemes

List of Tables

List of Figures

Abbreviations

AB	Ammonia-borane
Bipy	2,2'-Bipyridine
CD_3CN	Deuterated acetonitrile
CNAr	2,6-Dimethylphenyl isocyanide
DCM/CH_2Cl_2	Dichloromethane
DEE	Diethyl ether
DEPE	1,2-Bis(diethylphosphino)ethane
DFT	Density functional theory
DMPE	1,2-Bis(dimethylphosphino)ethane
EPR	Electron Paramagnetic Resonance
Equiv.	Equivalent
h	Hour
FTIR	Fourier Transform Infrared
MeAB	Methylamine borane
Me/CH_3	Methyl group
MHz	Megahertz
NMR	Nuclear magnetic resonance
NTf_2	N-(trifluoromethyl sulfonyl)
^oC	Degrees Celsius
ORTEP	Oak Ridge thermal-ellipsoid plot
OTf	Trifluoromethanesulfonate
PMe_3	Trimethylphosphine
PPh_3	Triphenylphosphine
ppm	Parts per million
RT	Room Temperature
$S^{Me}N^HS^{Me}$	Amido ligand before deprotonation
$S^{Me}N^HS$	Thiolate ligand before deprotonation
THF	Tetrahydrofuran
TMS	Trimethylsilyl
Triphos	Bis(2-diphenylphosphinoethyl)phenylphosphine)

List of Contributions

Publications:

1. **Fitchett, B.W**.; Hayes, C.E.; Koob, J.; Brennessel, W.W.; Gabidullin B.M.; Baker R.T. *"Cobalt SNS, SNC, and N_2S_2 thiolate complexes"* manuscript in preparation.

2. **Fitchett, B.W**.; Gabidullin, B.M.; Baker, R.T. *"Cobalt SNS amido complexes"* manuscript in preparation.

Presentations:

1. **Brandon W. Fitchett**, B. Gabidullin, R. T. Baker, *"Oxidation State Roulette: Synthesis of Novel Cobalt SNS Complexes"*, Canadian Society for Chemistry Conference, Edmonton, AB, May 2018 (Poster Presentation)

2. **Fitchett**, **B.W.**; Hayes, C.E.; Gabidullin, B.M.; Baker, R.T. *"Oxidation State Roulette: Synthesis of Novel Cobalt SNS Complexes"*, Canadian Society for Chemistry Conference, Toronto, ON, May 2017 (Poster Presentation)

Work contributing to the knowledge of science but not in this thesis, performed in year one in the Natural Resources Canada labs in collaboration with Dr. R. W. Hughes:

1. Tan, Y.T.; **Fitchett, B.W.**; Hughes, R.W. *"Investigation into layered double hydroxides for thermochemical energy storage."* manuscript in preparation.

Chapter 1: Introduction

1.1. Introduction to Bifunctional Catalysis

Since the initial discovery and presentation of Zeise's salt ($K[PtCl_3(C_2H_4)]\bullet H_2O$) as the first documented organometallic compound by William Christopher Zeise in 1830,[1] the fascination with this class of compounds in the scientific community has grown rapidly due to their incredible applications as stoichiometric reagents and more importantly, homogeneous catalysts. Research focusing in this area has exploded over the last hundred or so years and with it has come a more fundamental understanding of the cooperative roles that ligands play in these organometallic systems. Bifunctional ligands are ligands that cooperate with the metal to assist in the activation of the substrate, either through redox activity or through Lewis acid/base behaviour. Catalysts that incorporate such ligands are known as bifunctional catalysts, as the ligand accomplishes more than one function in the catalytic cycle. In these catalysts, the metal-bound ligand is not simply a bystander but can play an essential function influencing the outcome of catalytic reactions such as small molecule activation, functionalization or the selective conversion of certain substrates. This has led to the design and implementation of new ligand systems when attempting to develop more efficient and sustainable metal catalysts in chemical research.

For a ligand to be effective in modern transition metal catalysis, it should possess the following properties: 1) strong chelating ability to ensure it remains bound to the metal, 2) multiple donor groups that are compatible with different metal atoms, 3) inclusion of multiple strong donor atoms such as P,C or S to favour low-spin, diamagnetic metal complexes, 4) some level of hemilability to allow for the substrate to

associate to the metal centre and 5) redox activity to enable the acceptance or donation of electrons.[2] In addition to these attributes, the ligand should ideally be easy to synthesize from affordable materials and have a low level of toxicity if possible. Ligands which incorporate these properties are known in this context as bifunctional ligands as they allow the metal centre to accomplish more than one function in the catalytic system. As such, bifunctional ligands have emerged as an important class of ligands in catalysis and chemical research in general. Their inclusion in first row transition metal systems has enabled the activation of small molecules and catalysis for chemical transformations with activity and selectivity more generally observed with the precious metals.[2–7]

1.1.1. Catalysis in Nature: Active Sites in Reductive Enzymes

Nature has long acted as a source of inspiration for chemists while designing new catalysts. Natural selection has had an almost unimaginable length of time to optimise its catalytic systems in the form of enzymes, perfecting them over many, many centuries of trial and error. Enzymes, as will be shown below, provide perfect examples of the types of systems that can be developed with bifunctional catalysis and the potential that these systems hold. In enzymatic systems, the mode of activation is often based on cooperative effects that are initiated by the ligand scaffold surrounding the enzyme active site. Such examples are common in biology and play essential roles in the catalytic transformations that make up an organism's metabolism.

The enzyme [FeFe]-hydrogenase is found in a massive number of microorganisms and is thought to be billions of years old, dating back to when the earth had a hydrogen-rich atmosphere.[8,9] This family of enzymes catalyzes the reversible

splitting of dihydrogen into electrons and protons ($H_2 \rightleftharpoons 2H^+ + 2e^-$) in order to provide the organism with energy as well as to balance the redox potential of the cell.[9] The active site of these enzymes houses a thiolate-bridged dinuclear iron unit with a nearby amine pendant motif on the bridging thiolate ligand.[8–11] This amine pendant has been demonstrated both experimentally and theoretically to play an essential role in the activation of the dihydrogen bond (**Scheme 1.1**).[9,12–15]

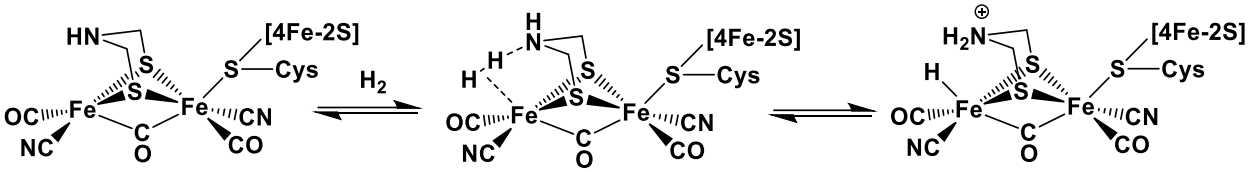

Scheme 1.1: Dihydrogen activation at [FeFe]-hydrogenase.

Similar bifunctional activity has been observed in a family of enzymes that serve a very similar role to the [FeFe]-hydrogenases. The heterobimetallic [NiFe]-hydrogenase family of enzymes is also capable of reversibly splitting the dihydrogen bond. This family of enzymes contains both iron and nickel in the active site which are bridged with two thiolate ligands.[16] Both metal centres are suspected to be essential to the activation of dihydrogen as well as much supporting evidence that the nearby cysteine thiolate is protonated during the process.(**Scheme 1.2**)[16–19]

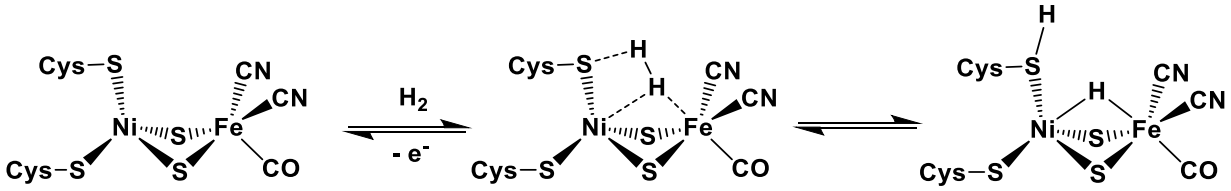

Scheme 1.2: Dihydrogen activation at [NiFe]-hydrogenase.

Many other metalloenzymes make use of these multi-metallic cooperative effects for selective, catalytic transformations such as non-heme iron enzymes including nitrile

hydratases[20,21], superoxide reductases[20,22], copper oxygenases[23] and nickel ureases[24] among others.

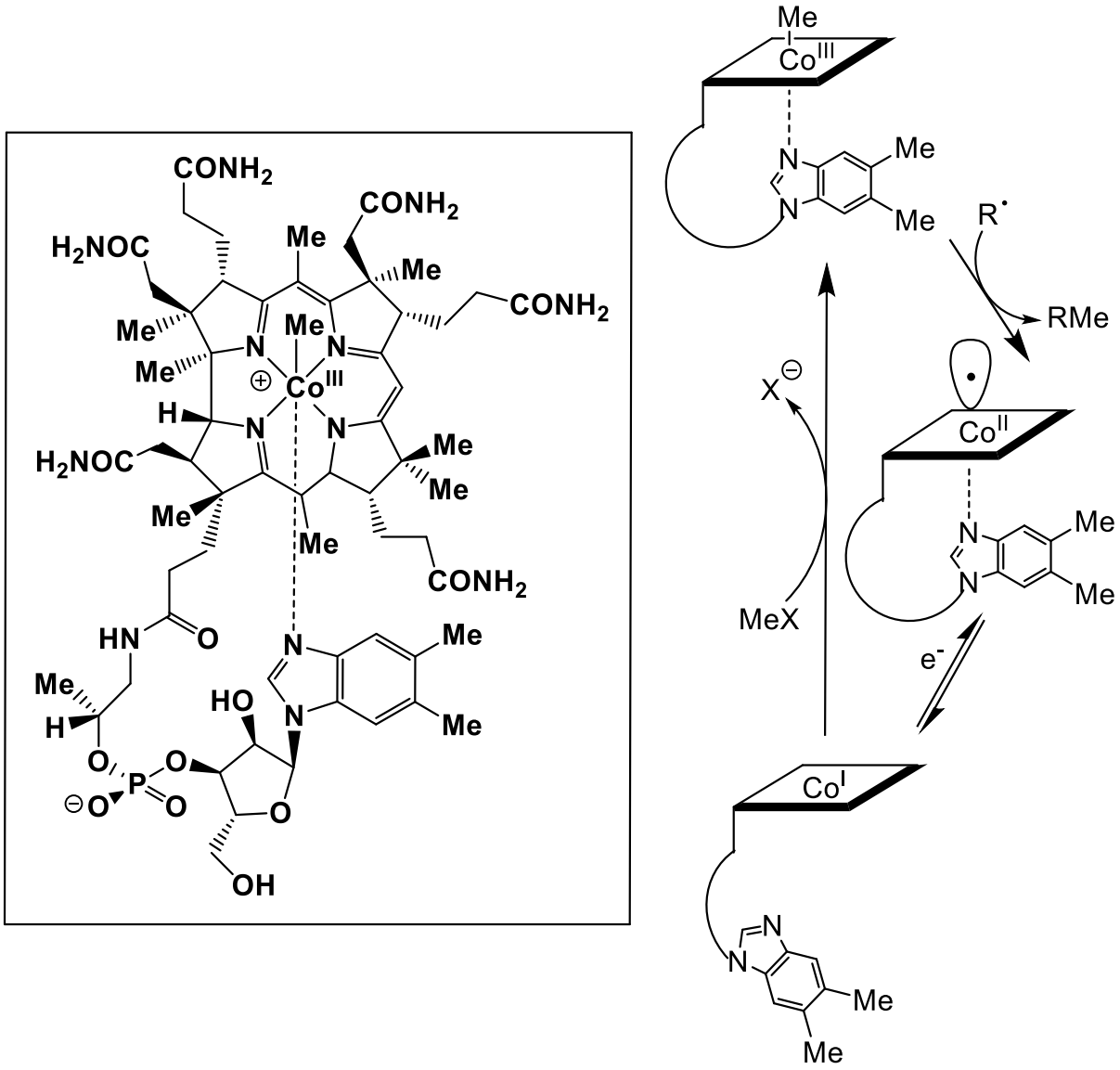

Scheme 1.3: Methylcobalamin (left) and a symbolic illustration depicting the major structural changes occurring during its catalytic cycle.

In addition to designing its ligand systems to assist in the activation of the substrate, biological ligands have also evolved to stabilize the electronic requirements of their metals throughout their catalytic cycles. The vitamin B_{12} derivative methylcobalamin acts as a co-factor in methylation reactions and is hypothesized to act

as a methyl radical donor.[25,26] Methylcobalamin initially exists in a pseudooctahedral 18e$^-$ complex stabilized by the tethered nucleotide base functionality below the plane of the corrin ring (**Scheme 1.3,** top of cycle). Following the abstraction of the methyl radical and reduction to Co(I), the tethered base is able to dissociate from the metal forming the more electronically stable square-planar 16e$^-$ Co(I) structure. Subsequent abstraction of another methyl group from a thiolate nucleophile regenerates Co(III). Now less electronically stable as a square-pyramidal structure, the tethered base is able to again coordinate, reforming the closed-shell Co(III) species.[25,26]

By taking inspiration from the properties that have been distilled from enzymatic systems, chemists can design new ligands which incorporate some of these properties such as redox activity and hemilability to synthesize new catalysts that are able to mimic the chemistry that is observed in nature.

1.1.2. Early Bifunctional Catalysis

Multidentate nitrogen and phosphorus donor ligands are among the most thoroughly studied ligand systems in homogeneous catalysis with applications in bifunctional catalysis being explored as far back as the mid-1980s.[27,28] This area of research was pioneered by the work of Fryzuk *et al.* with the first example of heterolytic splitting of the dihydrogen molecule by Rh and Ir amido-phosphine complexes.(**Scheme 1.4**)[27,28]

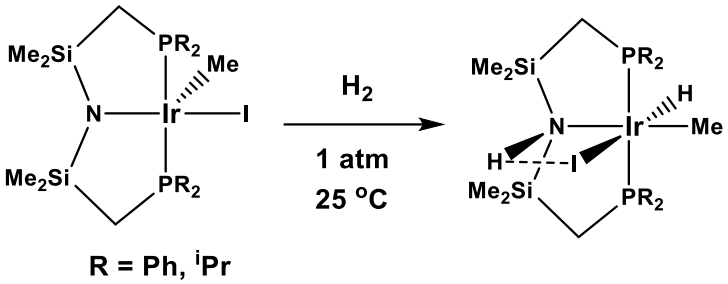

Scheme 1.4: Dihydrogen cleavage by Fryzuk's iridium PNP complex.

This transformation proceeds with bifunctional participation from the amido base accepting a proton from the dihydrogen substrate while the metal centre accepts the hydride, yielding the six-coordinate pseudooctahedral iridium complex. Strangely though, the hydride and proton are not found *cis* to each other across the amido-iridium bond but *trans*. This is rationalized by hydrogen bonding between the proton and the iodo group creating a stabilizing force that highly favours this isomer. [28] The discovery of this reaction created the foundation for later work that would come in developing nitrogen and phosphorus containing ligands for the purposes of bifunctional catalysis.

During a similar time, Shvo *et al.* discovered a bifunctional Ru catalyst which was supported with a tetraphenyl-substituted hydroxycyclopentadienyl ligand system. This complex was also shown to cleave the H-H bond and serve as a stable precatalyst for both hydrogenation and dehydrogenation reactions. Isolated as a dinuclear precatalyst, the complex undergoes dissociation in solution with both parts working in tandem to hydrogenate carbonyls to alcohols or *vice versa*. [29,30] In this dissociation, one ruthenium complex would bring with it both the metallic hydride and alcohol proton while the other is left with an empty coordination site (**Scheme 1.5**).

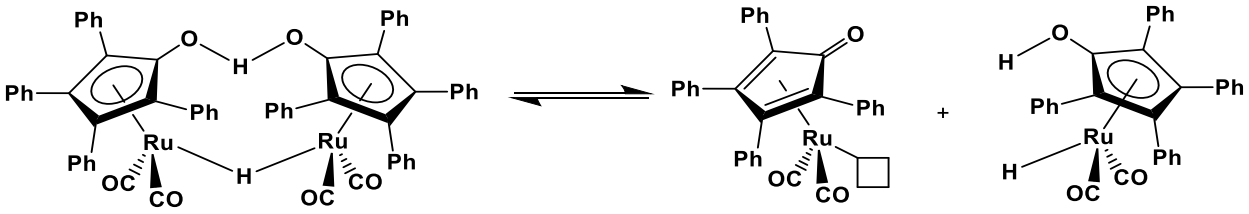

Scheme 1.5: Activation of Shvo's catalyst.

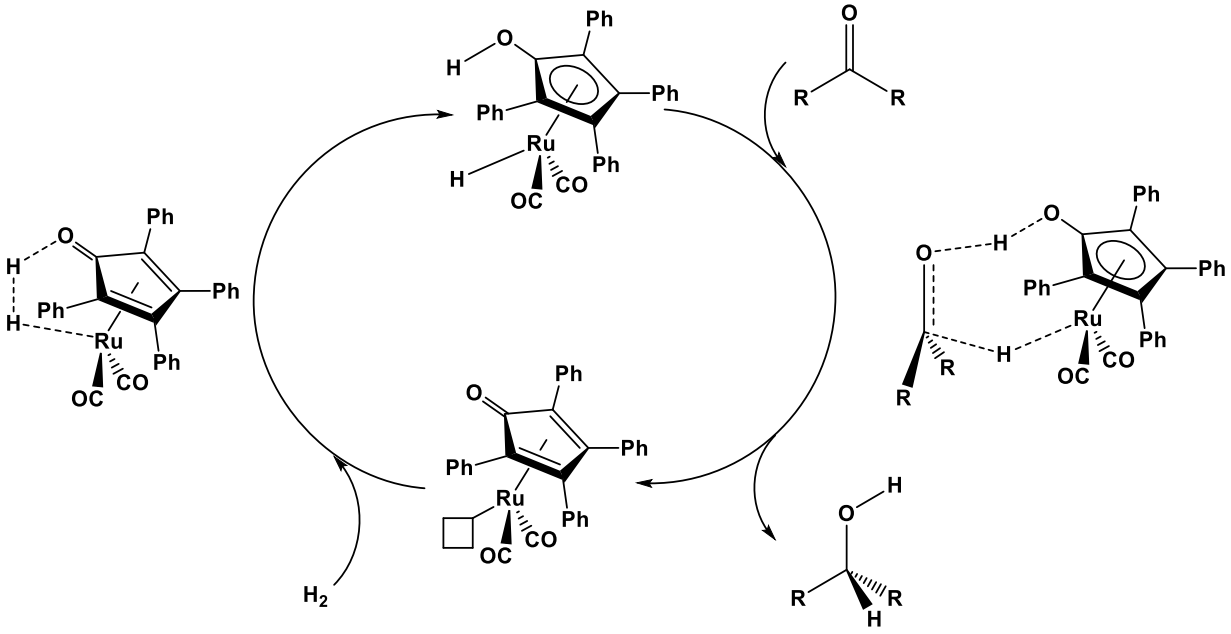

Scheme 1.6: Hydrogenation of a ketone with Shvo's catalyst.

Ruthenium is then able to accept dihydrogen into the open coordination site and, through cooperation with the ligand system, is able to separate it into a hydride and proton. The ketone is then hydrogenated in a concerted mechanism again with participation from the cyclopentadienyl ligand (**Scheme 1.6**).[30] These two discoveries laid the foundation for future exploration in the world of metal-ligand bifunctional activity and the development of ever more complex metal-ligand bifunctional systems.

1.1.3. Bidentate Bifunctional Ligands

Another benchmark discovery in the field of bifunctional catalysis was accomplished by Noyori *et al.* with a Ru catalyst which enabled a conceptually new

hydrogenation process with unprecedented activity and enantioselectivity for the reduction of ketones and imines.[31–33] This family of ruthenium complexes composed of ruthenium(II) ligated with chiral bidentate phosphorus and nitrogen containing ligands was found to be highly effective for the enantioselective hydrogenation of a variety of substrates in the presence of KOH. [31–33] Several of these Noyori-type Ru bifunctional catalysts are depicted below (**Figure 1.1**).

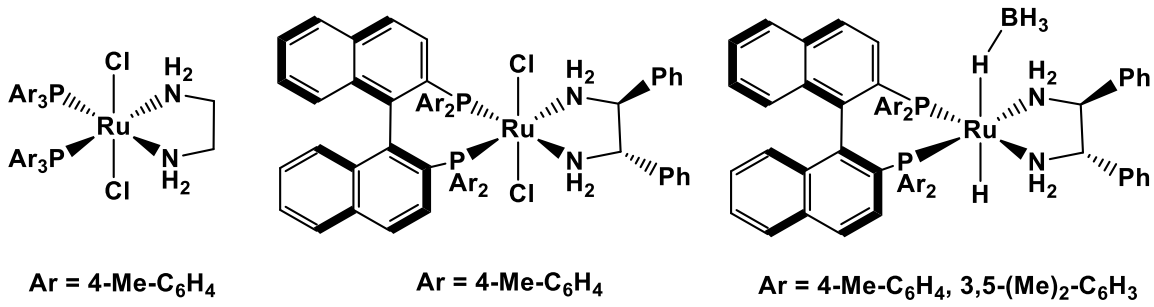

Figure 1.1: Bisphosphine diamine bifunctional ruthenium catalysts for ketone hydrogenation.[5]

These Noyori-type catalysts proceed through a similar mechanism as previous examples where the amine functionality plays an essential role in the hydrogenation of the substrate. This “NH effect” has been reinforced through studies with N-Me analogues such as TMEDA with which the activity significantly drops comparatively under identical conditions.[5] The classical Noyori mechanism of ketone hydrogenation was originally hypothesized to occur *via* an outer-sphere mechanism. In this mechanism, the proton from the nitrogen-hydrogen bond transfers to the oxygen atom while the hydride from the ruthenium metal centre attacks the carbon atom of the carbonyl. Hydrogen gas then associates to the ruthenium regenerating the active species. This mechanism has the advantage of orienting the substrate into a position which explains the observed enantioselectivity. However, recent mechanistic studies by

Dub, Gordon and co-workers have provided evidence that the hydrogenation occurs in a two-step process with the catalyst regeneration being mediated by alcohols present in solution (**Scheme 1.7**).[34–37]

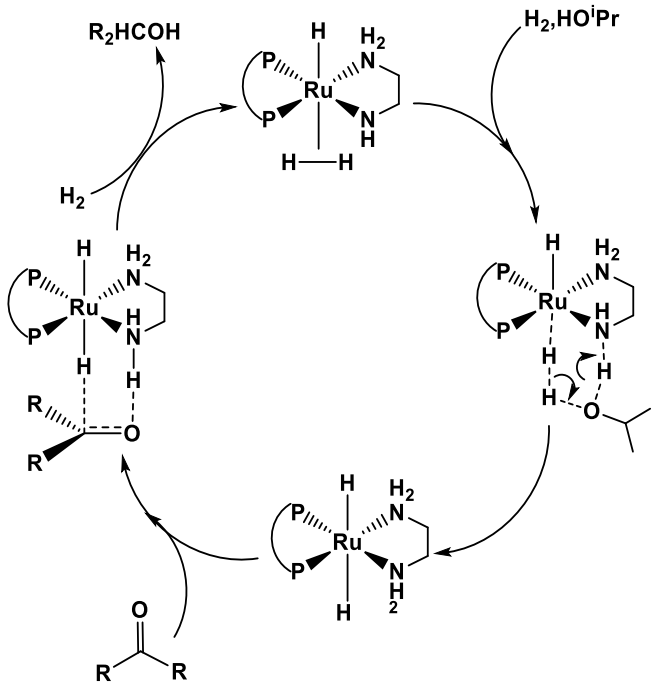

Scheme 1.7: Proposed catalytic cycle for the hydrogenation of ketones under basic conditions.

Following the discovery of this “NH effect” in ruthenium catalysis, this strategy was expanded to a number of other catalytic systems by incorporating amine functionalities into new ligand designs for hydrogenation/dehydrogenation catalysis. Application of this strategy entered new fields of catalysis such as the dehydrogenation of ammonia-borane for dihydrogen release. Examples of such new systems include the P- and N-donor bifunctional ligands which have been reported by Fagnou[38], Schneider[39] and Baker[40,41] (**Figure 1.2**).

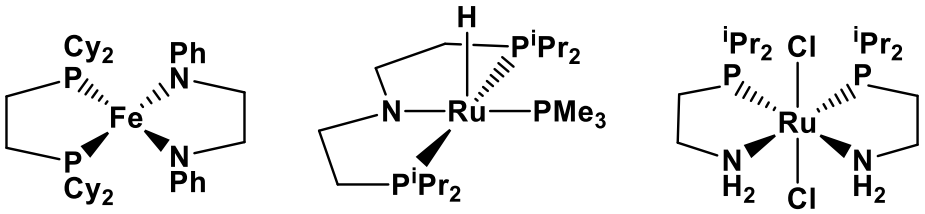

Baker 2012 Schnieder 2010 Fagnou 2008

Figure 1.2: P- and N-donor bifunctional ligand catalysts for ammonia borane dehydrogenation.

Another area of catalysis in which this bifunctional effect has been utilised is in the hydrosilylation of aldehydes, ketones and esters to alcohols using an Fe(II) N-phosphinoamidine system from Ruddy *et al.*[42] These transformations were accomplished with noticeably low catalyst loading, mild reaction conditions and with a very high conversion to the corresponding alcohol. Later work from the same group demonstrated that the cobalt(II) analogue was also able to accomplish selective hydroboration of alkenes.[43]

1.1.4. Tridentate Bifunctional Ligands

Tridentate systems have also been thoroughly studied in the context of bifunctional catalysis. Tridentate ligand systems have the advantage of an additional donor group to further improve the chelating ability of the ligand allowing it to more strongly bind to the metal atom at the cost of one less coordination site in the coordination sphere. One of the first classes of bifunctional tridentate ligands was the family of aliphatic phosphorus and nitrogen containing structures generally referred to as PNP ligands. The common layout of this family is a central amide/amine/imine N-donor group with terminal P-donors which coordinate to the metal in a meridional

configuration. The terminal arms bond strongly to the metal from opposite ends which has earned these ligands the title of ‘pincer’ ligands.

This ‘pincer’ ligand layout was originally envisioned by Shaw in 1975 when he developed his 2,6-bis[(di-t-butylphosphino)methyl]phenyl iridium complex in which an aryl donor resulting from carbon-hydrogen bond activation served a similar role as N-donors in later ligand designs.[44] From this initial pincer ligand design, new ligands which incorporated both phosphorus and nitrogen donor groups in the same layout rapidly gained popularity and have become some of the most extensively studied bifunctional ligand systems in homogeneous catalysis to date. Many different aliphatic PNP ligands have been designed since then and have been paired with many transition metals to yield a wide range of catalyst systems. Some examples are shown below (**Figure 1.3**).

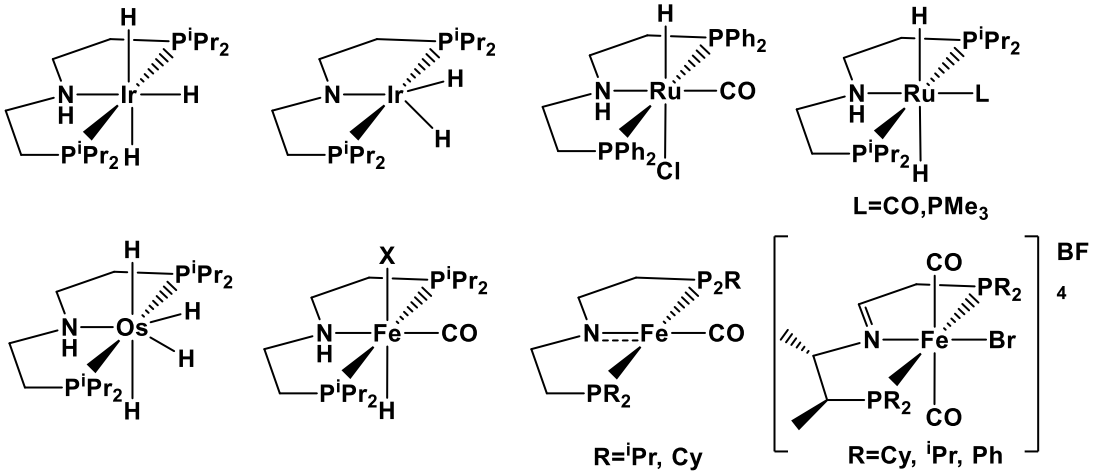

Figure 1.3: Examples of bifunctional complexes with aliphatic PNP pincer ligands.[5,45]

These PNP pincer systems have been successfully utilized in both direct and transfer hydrogenation of ketones, imines, esters, amides as well as the dehydrogenation of alcohols and amine-boranes.[5] Even the conversion of carbon

dioxide to formate was accomplished with a water-soluble iridium PNP catalyst from the Hazari lab which demonstrated turnover numbers as high as 348,000 and yields of up to 70%[46] (**Scheme 1.8**).

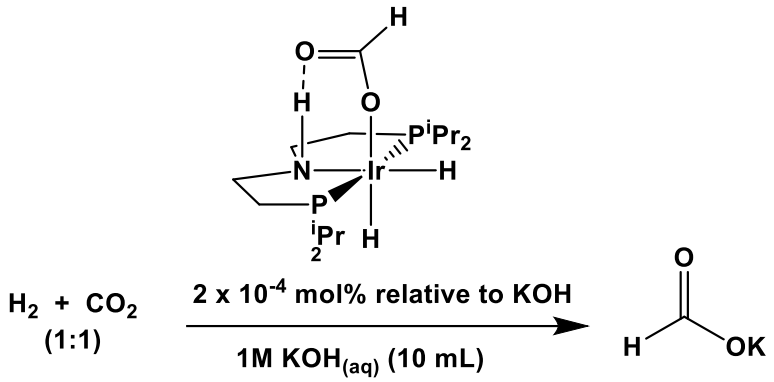

Scheme 1.8: Formation of formate from CO_2 and H_2.[46]

As observed previously with bidentate examples, the metal-amide/amine interaction is believed to be essential within these catalyst systems. This is strongly supported by mechanistic studies using the ligand analogues where the nitrogen-hydrogen bond is replaced with a nitrogen-methyl bond thereby removing the 'NH interaction'. The results are a dramatic decrease in the catalytic activity, reinforcing the importance of the NH bond in these bifunctional systems.[47]

In addition to the aliphatic PNP ligands, phosphorus and nitrogen containing ligands which also contain aryl groups have become common in bifunctional catalysis. The addition of aromatized carbon in the ligand backbone increases the rigidity of the system and forces a more planar conformation upon the ligand, improving its ability to 'pinch' onto the metal. These ligands frequently utilize a pyridine sub-unit as the central nitrogen donor group with a wide variety of terminal functional groups that can be

attached to the main ring.[5] Some examples of these types of neutral pincer ligands are illustrated below (**Figure 1.4**).

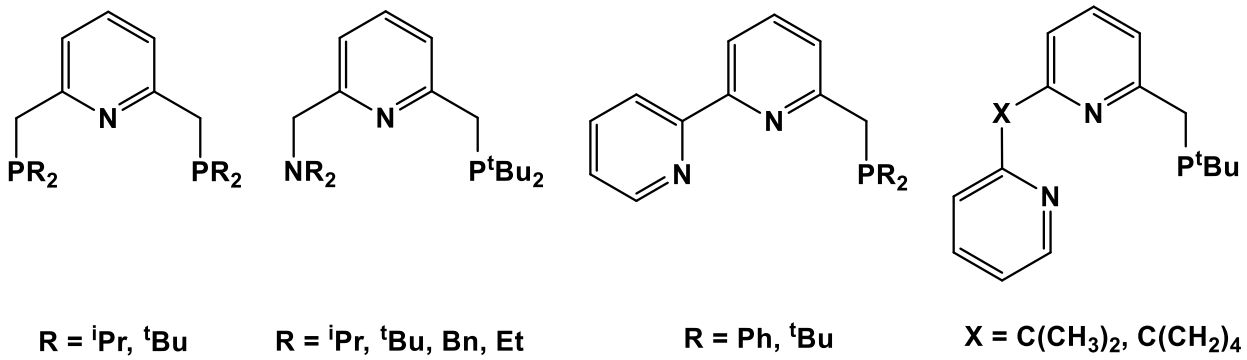

Figure 1.4: Examples of phosphorus and nitrogen pincer ligands containing aryl groups.[5]

An interesting consequence of introducing an aromatic group so close to the metal is that in the presence of a strong base it is possible to deprotonate the methylene group adjacent to the ring forming an exocyclic double bond and breaking the aromatization.[5,48,49] This subsequent double bond then acts as a new reactive centre for metal-ligand cooperation and the nitrogen atom can now be considered as an amide donor to the metal. In such a situation there are now two platforms for metal ligand cooperation, the nitrogen metal bond and the exocyclic double bond with the regeneration of aromatization acting as the driving force for these transformations.[48,49]

Milstein *et al.* in 2006 developed a ruthenium NNP system that provides a perfect example of the chemistry that these pyridine-based ligands can achieve. As shown in **Scheme 1.9**, deprotonation of the ruthenium chloride pre-catalyst results in the formation of the exocyclic double bond which then in unison with the ruthenium atom is able to split hydrogen, forming the active di-hydride species.[5,50] This di-hydride species is then able to go on and efficiently hydrogenate esters into their corresponding

alcohols, achieving selective conversions in excess of 80%.[50] The hydrogenation is proposed to occur *via* the bifunctional mechanism below.

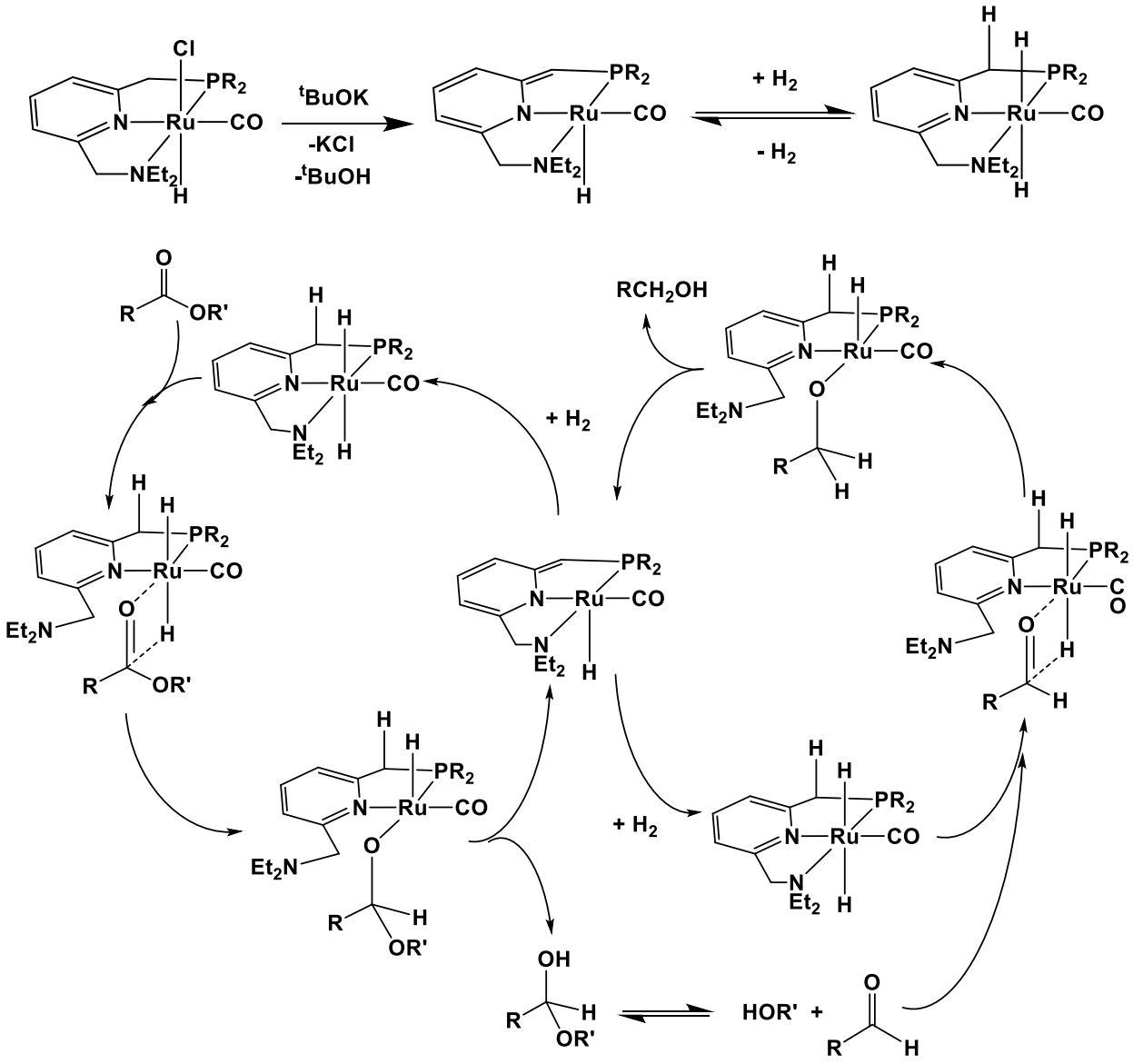

Scheme 1.9: Activation and corresponding mechanism of ester hydrogenation using Milstein's NNP ruthenium catalyst.[5,50]

In addition to the pyridine-based ligands, bifunctional ligands that incorporate more than one aryl group have also been developed. The Ozerov group has reported a palladium complex bearing a diarylamide PNP ligand system which activates

dihydrogen, terminal alkynes and thiols using a bifunctional mechanism. The activation occurs through initial coordination of HX to the palladium centre, followed by intermolecular proton transfer from the HX group to the amide nitrogen facilitated by an external Brønsted base (the triflate counter-ion or solvent).[51]

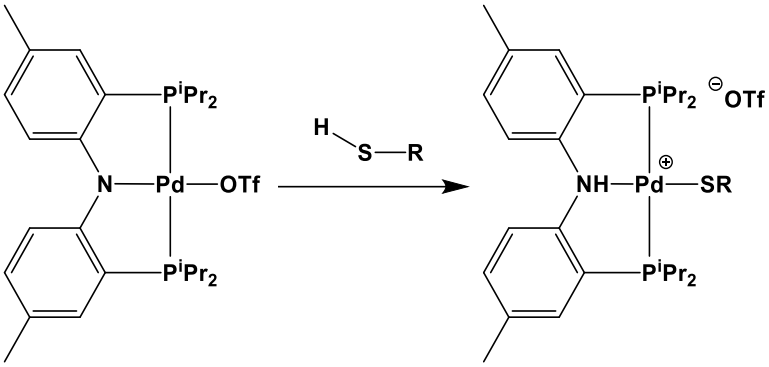

Scheme 1.10: Activation of thiol H-S bond using Pd diarylamide complex.

1.1.5. Sulphur and Nitrogen-Based Bifunctional Systems

Thus far, discussion of bifunctional ligand design has centred on the many examples of phosphorus and nitrogen containing systems that have been successful in this field. Phosphorus, however, is not a common donor in metalloenzyme chemistry and thus not a good model for biomimetic studies. Sulphur however is well known to participate in the bifunctional catalysis observed in nature.[16–19] As such, incorporating sulphur donor groups into bifunctional ligand systems is of great interest to better mimic biological systems as well as to gain a more fundamental understanding of metal-ligand cooperative catalysis. Sulphur containing ligands usually contain either a thiolate or thioether functional group and can be coupled with amine, imine or amide nitrogen donors. In the case of the thiolate features, the sulphur is able to behave as both a sigma and pi donor and also act as a Brønsted base to assist in bifunctional substrate activation making it a complementary group to the previously discussed nitrogen

donors. Some examples of sulphur and nitrogen containing ligands are shown below in **Figure 1.5**.

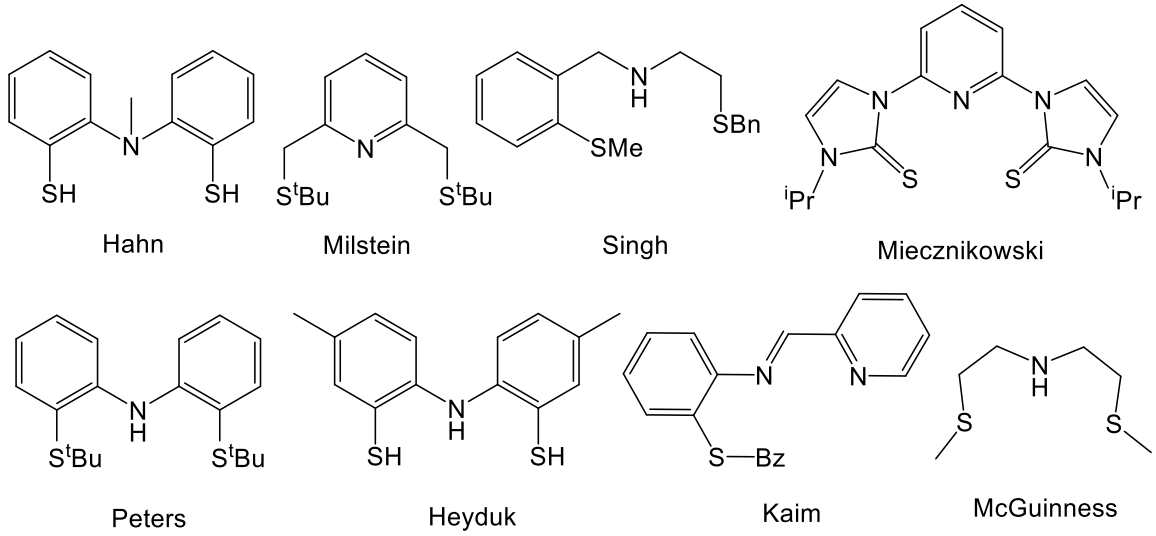

Figure 1.5: Examples of sulphur and nitrogen containing ligands.[52–59]

One example of catalytic activity that can be accomplished with sulphur-containing bifunctional systems is the rhodium(II) system developed by Seino and Mizobe. This complex contains both a tridentate nitrogen donor ligand coupled with a bidentate dithiolate ligand arranged in a pseudooctahedral geometry. This complex has been demonstrated to split dihydrogen in a bifunctional mechanism in the presence of triethylamine followed by hydrogenation of a wide scope of imines. The reaction is catalyzed under ambient conditions and with a catalyst loading of 1 mol%. Furthermore,

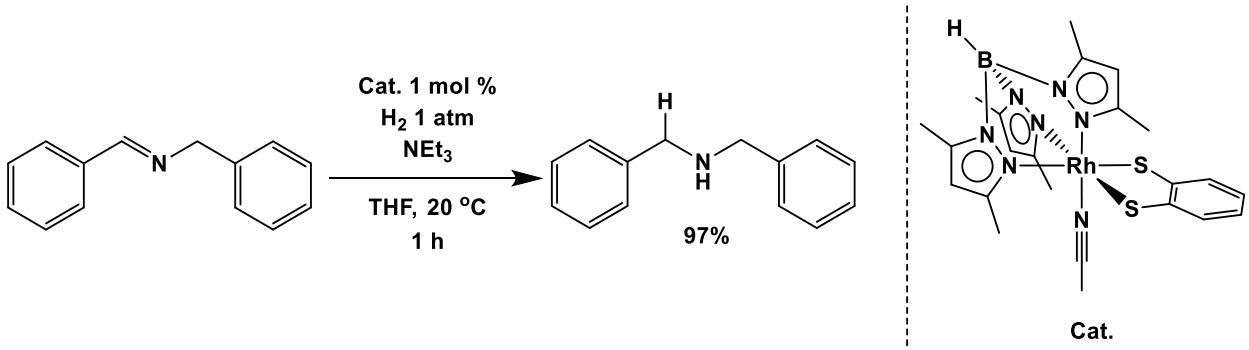

Scheme 1.11: Hydrogenation of imines under ambient conditions by Seino and Mizobe's rhodium dithiolate catalyst.[60]

the system has been shown to be chemoselective, selectively hydrogenating imine functionalities over various aldehyde or ketone groups in the substrate scope.[60]

Another example of bifunctional catalysis with nitrogen- and sulphur-containing ligands is from the work of Sellmann *et al.* with their ruthenium complex containing a pentadentate mixed nitrogen and sulphur donor ligand. Coordination of the pentadentate ligand to the ruthenium atom yields a thiolate-bridged dinuclear species that has been shown to activate the H-H bond through a bifunctional mechanism. The metal and sulphur atom work in unison to cleave the dihydrogen bond, accepting a hydride and proton respectively.[6,61]

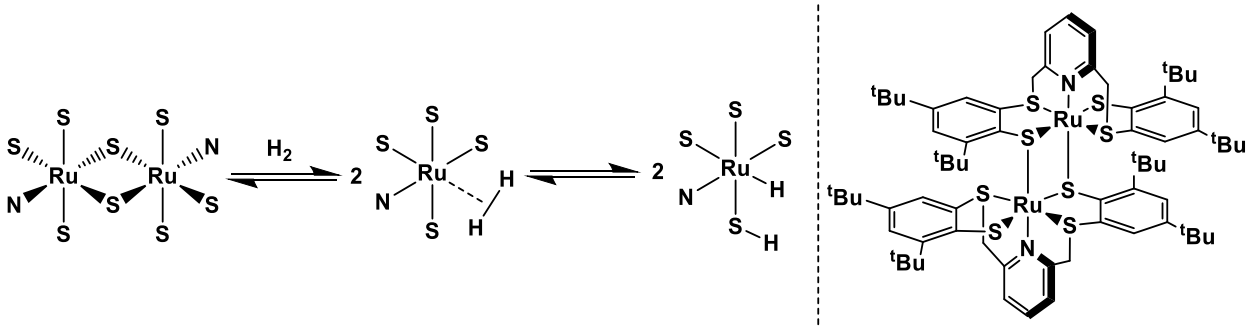

Scheme 1.12: Activation of dihydrogen by Sellmann's ruthenium catalyst *via* a bifunctional mechanism.

The inclusion of sulphur into bifunctional ligand design preserves the presence of a strong donor group in the ligand to favour low-spin metal complexes, a role that was previously accomplished by phosphorus in the PNP ligands. Low-spin electron configurations disfavour radical formation (a key goal in bifunctional catalysis) as electrons are already paired on the metal. Unlike phosphorus however, sulphur donors, specifically thiolate moieties, have the added benefit of being able to act as more

effective Brønsted bases, allowing them to facilitate bifunctional substrate activation in a similar manner to nitrogen donor groups as seen with the examples shown above. This dual functionality of sulphur donors is a potentially beneficial addition to bifunctional ligand design, providing a strong soft-soft interaction with the metal as well as providing an additional platform for bifunctional activity. Inclusion of sulphur into ligand design also more accurately replicates the activity observed in metalloenzymes such as [NiFe]-hydrogenases, allowing for more precise mimicking of the activity of these enzymes which may be of interest for research towards a more fundamental understanding of bifunctional catalysis.

1.2. Hemilabile Ligands

In coordination chemistry, hemilability is a common strategy that is frequently utilized in the design of ligands for new catalytic systems. The ability of one donor of a multi-dentate ligand to reversibly bind and release from the metal to accommodate any electronic changes or to accept a potential substrate is extremely advantageous. In the absence of substrate, the labile component is able to fill a vacant coordination site, preventing any unwanted reactions that could lead to decomposition of the catalyst, potentially extending the catalyst lifetime. This strategy has been successfully employed in a variety of applications such as hydrogenation, carbonylation, hydroformylation, epoxidation, olefin metathesis and ring-opening metathesis polymerization.[62,63] The importance of hemilability is also reflected in many biological systems and is present in many metalloenzymes.[64]

Incorporating hemilability into multidentate ligands can be accomplished in a number of different ways. Typically, the labile donor group is attached to a pendant arm

which tethers the labile group to the rest of the ligand that is bound to the metal by a strongly coordinating donor. Steric interactions, ring strain and weaker metal-heteroatom bonding can all lead to weaker coordination which encourages that bond to be broken. However, since the donor group is tethered to the rest of the ligand scaffold, it is relatively easy for the group to coordinate once again, making the overall process reversible.[62,63] Since this type of reversible dissociation is only observed for the weakly binding moiety while the stronger binding donor is firmly attached, the ligand can be said to be hemilabile as only one group demonstrates the labile behaviour.[62,65] The temporarily vacated coordination site is then free to accept a small molecule or organic substrate which can then lead to further activation by the metal centre.

The thioether represents a promising functional group for the implementation of hemilabile behaviour due to its general low affinity for transition metal coordination but also its ability to act as a pi acceptor under suitable conditions. This behaviour has been previously demonstrated in conjunction with functionalized phosphines,[66,67] mixed donor chelating ligands [68,69] and more uniquely with N-heterocyclic carbenes.[70]

One example of the hemilability of the thioether group is from the work of Bassetti *et al.* who reported the hemilability of a thiobenzyl pendant on their SNS lutidine based ligand. When coordinated to rhodium this complex undergoes oxidative addition of MeI accommodated by the labile pendant thioether arm.[71] This transformation is initiated by the dissociation of one of the thioether arms from the rhodium(I) centre forming the transient three coordinate species. The open coordination site then allows for the metal centre to get close enough to the methyl iodide substrate for it to undergo oxidative addition, forming the 18-electron Rh(III) octahedral complex.

The methyl group then performs a migratory insertion generating the five-coordinate 16 electron acetyl species.[71]

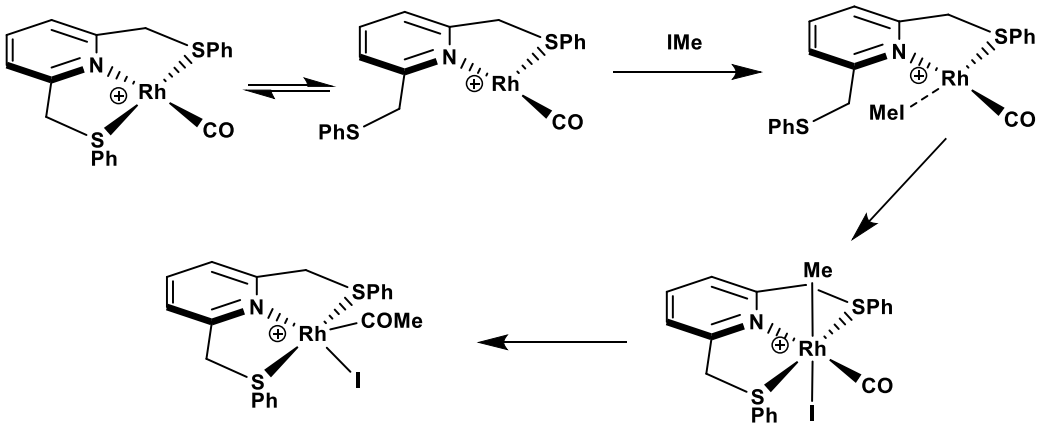

Scheme 1.13: Oxidative addition of methyl iodide to a rhodium(I) SNS complex facilitated by the hemilabile activity of the thioether pendant arm.

Kinoshita *et al.* in 2017 also observed the hemilabile activity of the thiomethyl functionality in their dinuclear iron(II) SCN carbonyl complex. Pending dissociation of one of the carbonyl groups, the thiomethyl arm is able to occupy the empty coordination site of the iron. This iron-sulphur interaction remains stable upon the addition of Lewis bases such as dimethylphenylphosphine and 4-(dimethylamino)-pyridine (DMAP) which break up the dinuclear complex. The products of this reaction are the mononuclear and thiolate-bridged species respectively.[72]

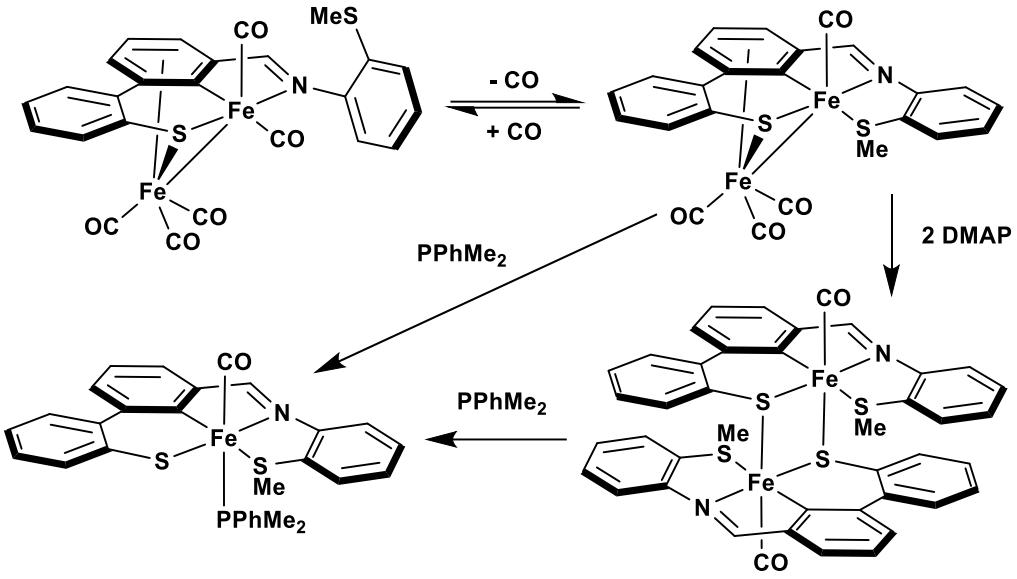

Scheme 1.14: Hemilabile behaviour of a thioether arm in a diiron carbonyl complex.

Kaim and co-workers reported an iridium(III) 4,6-di-*tert*-butyl-2-(2-methylthio) amidophenolate complex that demonstrates the lability of the thioether arm when it undergoes a reversible single electron oxidation. Following oxidation of the ligand to a radical species, the thioether arm is able to coordinate to the iridium(III) centre to account for some of the lost electron density, stabilizing the species as a pseudo four-coordinate complex. Following the subsequent reduction, the thioether is able to dissociate, restoring the original species.[73]

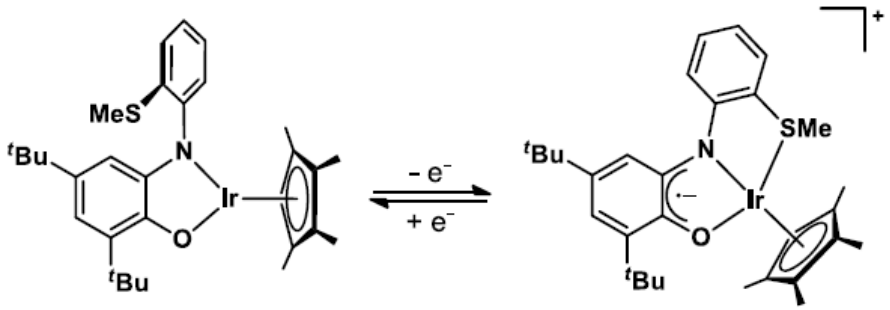

Scheme 1.15: Hemilabile activity during the redox cycle of Kaim's iridium complex.

The introduction of hemilability into ligand design can be incredibly useful as the previous examples have demonstrated. Weakly coordinating labile groups are able to stabilize the catalyst while in the absence of substrate but also able to dissociate to provide a free coordination site for those substrates to approach the metal when present ensuring substrate activation is still possible. The presence of a moiety that is able to associate and disassociate to stabilize the metal while passing through multiple oxidation states is also highly advantageous for catalytic systems as a change in oxidation state is frequently an essential component of catalytic reactions. As has been shown, the thioether functionality excels at this application due to its general weak metal-sulphur interaction. But as was the case in the final example from Kaim *et al.* redox activity must also be considered in bifunctional ligand design.

1.3. Redox-Active Ligands

As can be seen from the previous example, some classes of ligands are able to participate in electron transfer reactions in which they can be oxidized or reduced. These redox active or 'non-innocent' ligands as they are commonly known, represent a distinct class of ligands in organometallic chemistry that provide numerous advantages in the field of homogeneous catalysis. Due to their more accessible energy levels they can be oxidized or reduced at energies comparable to that of the metal which enables them to act as electron reservoirs or sinks. That means that they can potentially assist in the facilitation of multi-electron processes that are otherwise difficult to achieve for base metals.[74,75] This is in distinct contrast to more common ligands in organometallic chemistry such as triphenylphosphine or ammonia which require a far greater energy to oxidize or reduce than the energy needed to change the oxidation state of the metal.[76]

The presence of accessible ligand oxidation states is particularly advantageous in the context of base metal catalysis since base metals more generally prefer one-electron redox processes unlike the two-electron transformations more commonly associated with the precious metals. With the addition of these redox active ligands there is sufficient electron density in the base metal catalyst to potentially enable two subsequent, single electron transfer processes, mimicking the two-electron chemistry observed with the noble metals.[74] The obvious economic and environmental benefits of using base metals for traditional noble metal transformation has driven the recent growth of research into redox-active ligand systems.[74–78]

As is the case with many areas of chemical research, chemists in this field have drawn inspiration by the redox cooperation between metal and ligand that has been observed in nature. Multi-electron reactions are occur frequently in redox metalloenzyme chemistry in which the ligand scaffold surrounding the active site plays a crucial role. This strategy avoids the formation of free radical species that can have damaging effects within an organism while still achieving an effective two electron transfer reaction.[75,76]

One of the most well studied examples of ligand non-innocence in nature comes from the metalloenzyme galactose oxidase which is utilised in some fungal species to produce hydrogen peroxide for lignin degradation by oxidation of the sugar galactose. This metalloenzyme contains a copper(II) metal centre in a square pyramidal geometry that is responsible for accepting the electrons from the oxidized sugar.[79,80] The two-electron chemistry seems at first impossible for a single copper ion going between Cu(I) and Cu(II) but is possible due to the involvement of a redox cofactor in the form of the

tyrosinate functionality that can be oxidized to a tyrosyl radical during the catalytic cycle (**Scheme 1.16 a**).[79,80] Delocalization of the radical throughout the phenoxyl ring significantly stabilizes the radical species, preventing any unwanted radical chemistry from taking place (**Scheme 1.16 b**). When the substrate galactose enters the active site, it is oxidized in two subsequent electron transfers to the copper, the first of which immediately reduces the ligand back to its paired electron state while the second reduces the Cu(II) to Cu(I) (**Scheme 1.16 c**).[79,80] This copper-mediated two electron oxidation is only possible with the assistance of the ligand scaffold acting as an electron sink for one of the two electrons from galactose, demonstrating the importance of ligand redox ability in biological systems. Ligand redox activity is believed to be prevalent in metal-containing redox proteins, however, it is difficult to detect when two radicals are present due to the strong coupling through the central metal atom which is likely to be present.[81]

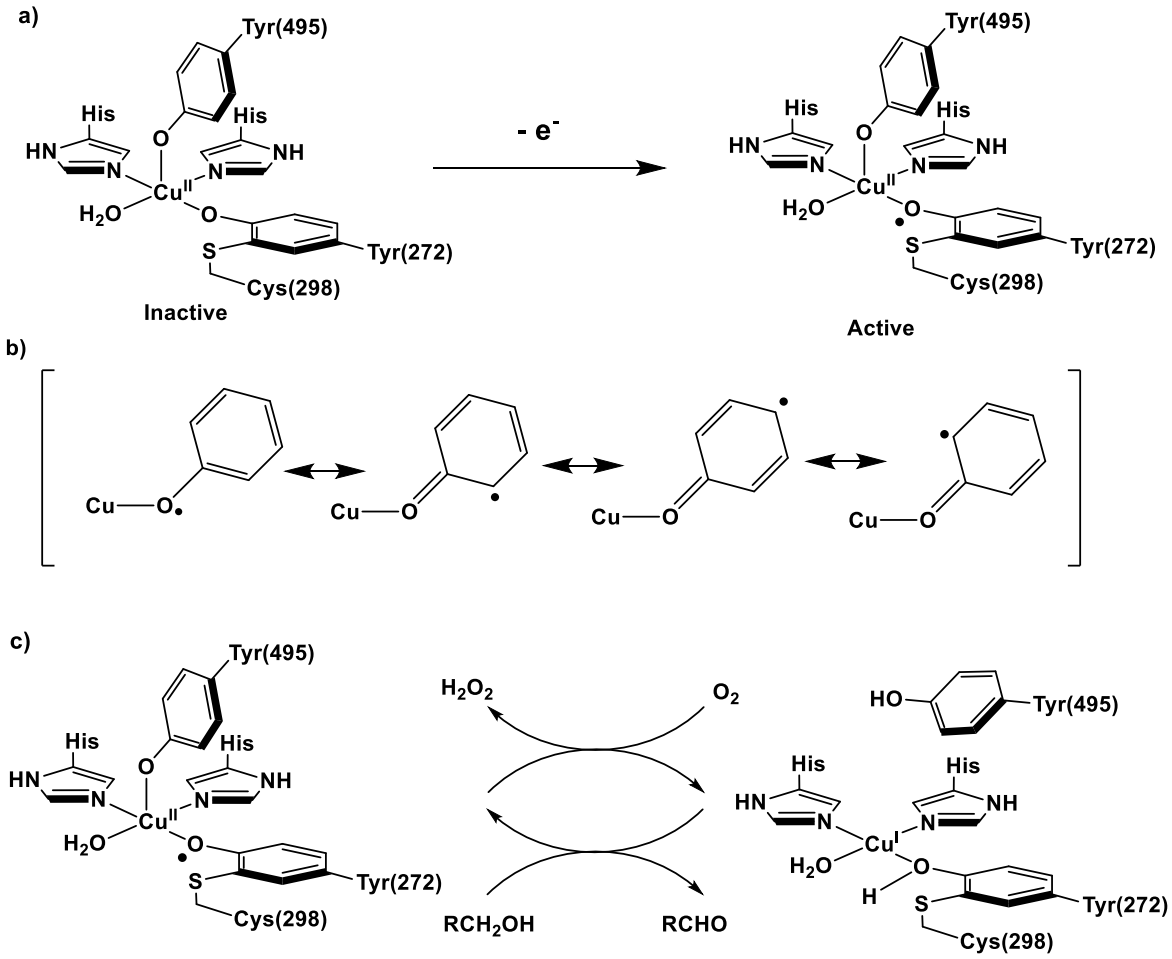

Scheme 1.16: a) The activation of galactose oxidase. b) The resonance structure of the activated form of galactose oxidase. c) Oxidation of galactose by galactose oxidase.

While the term ‘non-innocent redox ligand’ was originally introduced by Jørgensen in 1966, these complexes were mainly considered spectroscopic curiosities at the time. Their true potential as synthetically useful ligand scaffolds did not emerge in coordination chemistry until much later when their usefulness in catalysis became apparent. Presently, various families of redox-active ligands have been created and studied. Some examples of these types of ligands include quinones, diimines, bis(imino)pyridines, diphenylamines, polypyridines and dithiolenes.[74–78] Sulphur containing redox ligands particularly have received attention due to their resemblance to numerous biological systems and their ability to demonstrate intriguing redox activity by

coordinating to a variety of metals.[58,69,82–86] While sulphur is well known to be less electronegative than oxygen, it is better able to retain spin density which is advantageous when forming radical species. As such a large number of multi-dentate redox active S and Se ligands have been engineered and reported in the literature.[68,69,82–85,87]

One such example is the work of Paretzki *et al.* and their synthesis of an O,N,S redox active ligand. Refluxing a mixture of the ligand with nickel(II) chloride in the presence of triethylamine yielded the tetradentate bis-ligated species. Intriguingly, the ligand exhibits unpaired electrons delocalized on the two separate ligands. This complex is then able to undergo two subsequent one electron oxidations which are accompanied by structural changes in the complex and coordination of the two thioether pendants (**Scheme 1.17**). The initial oxidation removes one unpaired electron from one of the redox active ligands causing a change in geometry as the thioether arms now coordinate to the nickel centre forming the high spin nickel(II) complex. The next oxidation removes the second unpaired electron from the other ligand forming the doubly charged high spin cationic species demonstrating the ability of the ligand scaffold to contribute electrons to the oxidation process.[87] This example thus shows cooperativity between the redox-activity and hemilability of this ligand system.

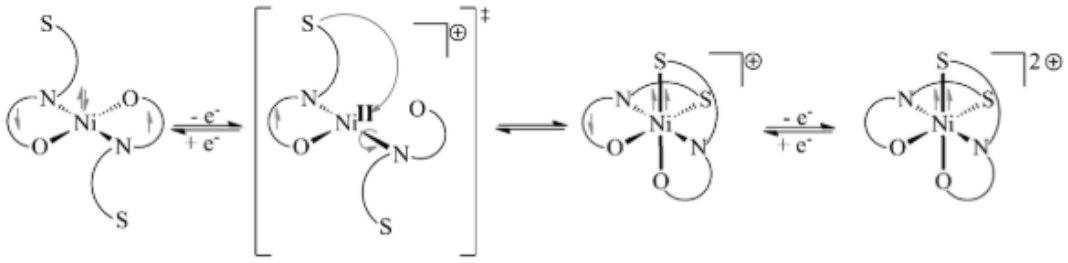

Scheme 1.17: Structural changes of Ni(II) O,N complex over two subsequent one electron oxidations.[87]

Heyduk *et al.* have recently developed a tridentate sulphur and nitrogen containing ligand which has been paired with tungsten to form bis-ligated tungsten(VI) complexes.[57] These complexes undergo two reversible reductions and two partially reversible oxidations. Heyduk and co-workers have been able to show the non-innocence of this ligand as oxidations of this d^0 tungsten complex are necessarily ligand-based.

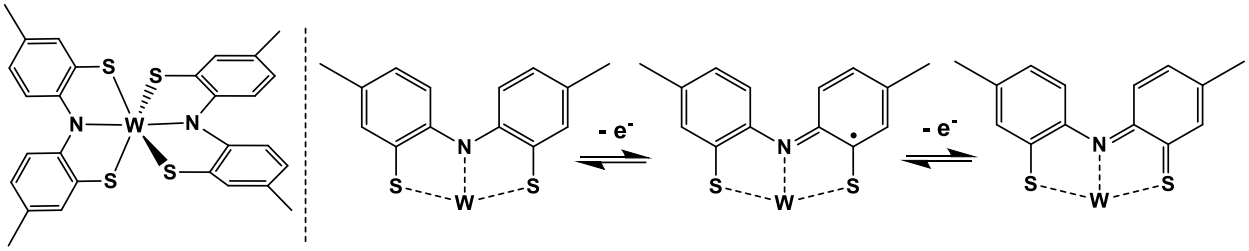

Scheme 1.18: Heyduk's tungsten SNS complex (left) and its non-innocent behaviour (right).

1.4. Introduction to Cobalt in Bifunctional Catalysis

Cobalt is the twenty-seventh element in the periodic table which has only one naturally occurring isotope of cobalt-59 and an electronic configuration of $[Ar]3d^74s^2$. It can exist in a range of oxidation states from -I to IV with I,II and III being the most common. Unlike other common transition metals like iron or nickel, cobalt does not exist in the Earth's crust as a native metal due to the oxygen in the atmosphere and the chlorine in the oceans both being abundant enough to prevent its formation. Despite this, cobalt is considered to be in medium abundance and exists in a number of mineral forms that are found in the same deposits as copper and nickel ores. Cobalt also serves an important role biologically and is an essential element to the metabolism of all animals. As mentioned above, cobalt makes up a key constituent of cobalamin, better known as vitamin B_{12}.[25,88] Bacteria in the stomachs of grazing animals convert cobalt salts ingested from plants into cobalamin which are then consumed further by

carnivores through predation. As such a minimal concentration of cobalt is essential in the soil for the well-being of animals in that ecosystem.

Cobalt has long been an attractive metal of choice for catalysis. Like all first-row transition metals, cobalt is significantly less toxic[89] than its second and third row counter-parts[90]. Additionally, due to its much higher abundance in the Earth's crust, it is significantly more economical to utilise cobalt in catalyst design than the much rarer (and more expensive) noble metals. The combination of these environmental and economic benefits makes cobalt an attractive option for the development of new catalysts. This is reflected in the number of examples of cobalt bifunctional catalysts that have been developed in recent years.

Hanson *et al.* developed a series of aliphatic PNP pincer ligands and have been able to pair them with a cobalt(II) metal centre, forming a series of cobalt PNP cationic complexes with a variety of auxiliary ligands. Of these, a complex containing an amine functionality in the PNP ligand with an alkyl auxiliary ligand was found to be effective for the hydrogenation of a variety of ketones under low temperature conditions with isolated yields ranging from moderate to high.[91,92] The authors suspect that the mechanism for this transformation is cooperative as the same reaction does not proceed when using the N-Me analogue under identical reaction conditions, again highlighting the importance of the 'NH effect' discussed in depth above.[91]

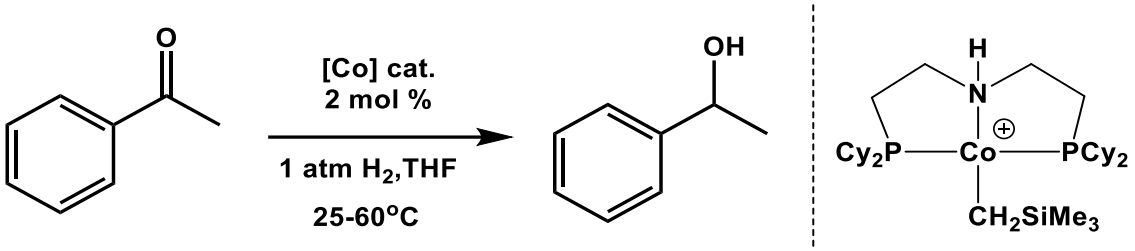

Scheme 1.19: Hydrogenation of ketones by Hanson's cobalt catalyst that is suspected to proceed through a bifunctional mechanism.

Additional work from the Kempe group in 2015 yielded another cobalt PNP complex that effects hydrogenation of a wide scope of ketones into their corresponding alcohols under similarly ambient conditions, albeit at a much higher hydrogen pressure then Hanson's example.[93] While this complex also proceeds through a bifunctional mechanism, it contains the pyridine-based ligands discussed in detail in Chapter 1.1.4 as thoroughly studied computationally by Wang *et al*.[94] In a noticeable difference however, the methylene substituents common on the terminal arms of this family of PNP pincer ligands have been replaced with amine functionalities. The increased basicity of these terminal arms makes the activation of dihydrogen substantially more efficient, improving the cooperation between ligand and metal.[93,94]

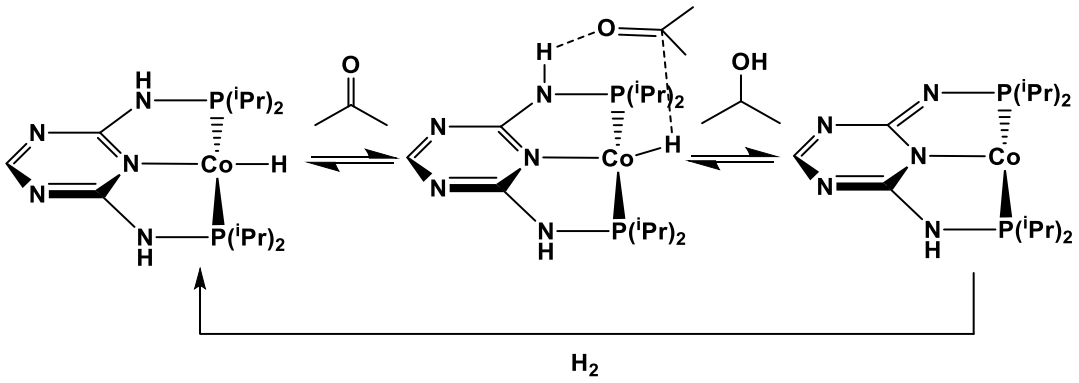

Scheme 1.20: Dehydrogenation of ketones by Kempe's Co PNP catalyst.

1.5. Scope of this Work

The work described in this thesis aims to continue the advancement of the field of bifunctional catalysis by exploring the reactivity of two newly designed SNS amido and thiolate donor ligands when paired with cobalt as the active metal centre. This will enable a comparison to a series of well-defined iron complexes that have been previously prepared and characterized in the Baker group as well as for a comparison of the behaviour between the two ligands themselves. The reactivity of the resulting complexes from the combination of these ligands and cobalt will also be explored. Specifically, **Chapter 2** introduces the synthesis and reactivity of a tridentate amido ligand that shows a strong preference for the formation of a bis-ligated cobalt(II) compound. The reactivity of this 19 e^- bis-amido complex is then directly contrasted to its iron analogue. **Chapter 3** highlights the complexes that have been formed with the SNS thiolate ligand. Electron-rich ancillary ligands promote selective oxidative addition of a C_{aryl}-S bond, forming a dianionic SNC ligand. Moreover, the SNS thiolate ligand undergoes imine coupling in the presence of cobalt, forming square planar $[Co(N_2S_2)]^-$. The reactivity and electrochemistry of this new complex are explored. This work is concluded in **Chapter 4** by a look to the future of bifunctional catalysis and new directions that our group will take with these novel ligands.

1.6. References

(1) Hunt, L. B. *Platin. Met. Rev.* **1984**, *28* (2), 76–83.

(2) Chakraborty, S.; Bhattacharya, P.; Dai, H.; Guan, H. *Acc. Chem. Res.* **2015**, *48* (7), 1995–2003.

(3) Morris, R. H. *Acc. Chem. Res.* **2015**, *48* (5), 1494–1502.

(4) Ivar van der Vlugt, J. *Eur. J. Inorg. Chem.* **2012**, 363–375.

(5) Khusnutdinova, J. R.; Milstein, D. *Angew. Chem. Int. Ed.* **2015**, *54*, 12236–12273.

(6) Omann, L.; Ko, C. D. F.; Klare, H. F. T.; Oestreich, M. *Acc. Chem. Res.* **2017**, *50*, 1258–1269.

(7) Gunanathan, C.; Milstein, D. *Chem. Rev.* **2014**, *114* (24), 12024–12087.

(8) Gordon, J. C.; Kubas, G. J. *Organometallics* **2010**, *29* (21), 4682–4701.

(9) Lubitz, W.; Ogata, H.; Rüdiger, O.; Reijerse, E. *Chem. Rev.* **2014**, *114* (8), 4081–4148.

(10) Kubas, G. J. *Chem. Rev.* **2007**, *107* (10), 4152–4205.

(11) Fontecilla-Camps, J. C.; Volbeda, A.; Cavazza, C.; Nicolet, Y. *Chem. Rev.* **2007**, *107* (10), 4273–4303.

(12) Nicolet, Y.; De Lacey, A. L.; Vernède, X.; Fernandez, V. M.; Hatchikian, E. C.; Fontecilla-Camps, J. C. *J. Am. Chem. Soc.* **2001**, *123* (8), 1596–1601.

(13) Fan, H. J.; Hall, M. B. *J. Am. Chem. Soc.* **2001**, *123* (16), 3828–3829.

(14) Barton, B. E.; Olsen, M. T.; Rauchfuss, T. B. *J. Am. Chem. Soc.* **2008**, *130*, 16834–16835.

(15) Silakov, A.; Wenk, B.; Reijerse, E.; Lubitz, W. *Phys. Chem. Chem. Phys.* **2009**, *11*, 6592–6599.

(16) Ogata, H.; Mizoguchi, Y.; Mizuno, N.; Miki, K.; Adachi, S. ichi; Yasuoka, N.; Yagi, T.; Yamauchi, O.; Hirota, S.; Higuchi, Y. *J. Am. Chem. Soc.* **2002**, *124* (39), 11628–11635.

(17) Lacey, A. L. De; Hatchikian, E. C.; Volbeda, A.; Frey, M.; Fontecilla-camps, J. C.; Fernandez, V. M. *J. Am. Chem. Soc.* **1997**, *119*, 7181–7189.

(18) Niu, S.; Thomson, L. M.; Hall, M. B. *J. Am. Chem. Soc.* **1999**, *121*, 4000–4007.

(19) Amara, P.; Volbeda, A.; Fontecilla-Camps, J. C.; Field, M. J. *J. Am. Chem. Soc.* **1999**, *121* (18), 4468–4477.

(20) Kovacs, J. A. *Chem. Rev.* **2004**, *104* (2), 825–848.

(21) Noguchi, T.; Hoshino, M.; Tsujimura, M.; Odaka, M.; Inoue, Y.; Endo, I. *Biochemistry* **1996**, *35* (51), 16777–16781.

(22) Mathé, C.; Mattioli, T. A.; Horner, O.; Lombard, M.; Latour, J. M.; Fontecave, M.; Nivière, V. *J. Am. Chem. Soc.* **2002**, *124* (18), 4966–4967.

(23) Serrano-plana, J.; Garcia-bosch, I.; Company, A.; Costas, M. *Acc. Chem. Res.*, **2015**, *48(8)*, 2397-2406

(24) Mobley, H. L.; Island, M. D.; Hausinger, R. P. *Microbiol. Rev.* **1995**, *59* (3), 451–480.

(25) Krautler, B. *Encyclopedia of Inorganic and Bioinorganic Chemistry*; Wiley and

Sons, Ltd., **2011**; Vol. 1, pp 1–22.

(26) Brown, K. L. *Chem. Rev.* **2005**, *105*, 2075–2149.

(27) Fryzuk, M. D.; MacNeil, P. A.; Rettig, S. J. *Organometallics* **1986**, *5* (12), 2469–2476.

(28) Fryzuk, M. D.; MacNeil, P. A.; Rettig, S. J. *J. Am. Chem. Soc.* **1987**, *109* (9), 2803–2812.

(29) Blum, Y.; Czarkle, D.; Rahamim, Y.; Shvo, Y. *Organometallics* **1985**, *4* (8), 1459–1461.

(30) Shvo, Y.; Czarkie, D.; Rahamim, Y.; Chodosh, D. F. *J. Am. Chem. Soc.* **1986**, *108* (23), 7400–7402.

(31) Ohkuma, T.; Ooka, H.; Hashiguchi, S.; Ikariya, T.; Noyori, R. *J. Am. Chem. Soc.* **1995**, *117* (9), 2675–2676.

(32) Doucet, H.; Ohkuma, T.; Murata, K.; Yokozawa, T.; Kozawa, M.; Katayama, E.; England, A. F.; Ikariya, T.; Noyori, R. *Angew. Chem. Int. Ed.* **1998**, *37*, 1703–1707.

(33) Noyori, R.; Ohkuma, T. *Angew. Chem. Int. Ed.* **2001**, *40* (1), 40–73.

(34) Dub, P. A.; Gordon, J. C. *Dalton Trans.* **2016**, *45* (16), 6756–6781.

(35) Dub, P. A.; Henson, N. J.; Martin, R. L.; Gordon, J. C. *J. Am. Chem. Soc.* **2014**, *136*, 3505–3521.

(36) Dub, P. A.; Scott, B. L.; Gordon, J. C. *J. Am. Chem. Soc.* **2017**, *139* (3), 1245–1260.

(37) Dub, P. A.; Gordon, J. C. *ACS Catal.* **2017**, *7*, 6635–6655.

(38) Blaquiere, N.; Diallo-Garcia, S.; Gorelsky, S. I.; Black, D. A.; Fagnou, K. *J. Am. Chem. Soc.* **2008**, *130* (43), 14034–14035.

(39) Staubitz, A.; Sloan, M. E.; Robertson, A. P. M.; Friedrich, A.; Schneider, S.; Gates, P. J.; Manners, I.; Schmedt auf der Guenne, J. *J. Am. Chem. Soc.* **2010**, *132*, 13332–13345.

(40) Baker, R. T.; Gordon, J. C.; Hamilton, C. W.; Henson, N. J.; Lin, P.; Maguire, S.; Murugesu, M.; Scott, B. L.; Smythe, N. C. *J. Am. Chem. Soc.* **2012** *134*, 5598-5609.

(41) Kalviri, H. A.; Gärtner, F.; Ye, G.; Korobkov, I.; Baker, R. T. *Chem. Sci.* **2015**, *6* (1), 618–624.

(42) Ruddy, A. J.; Kelly, C. M.; Crawford, S. M.; Wheaton, C. A.; Sydora, O. L.; Small, B. L.; Stradiotto, M.; Turculet, L. *Organometallics* **2013**, *32* (19), 5581–5588.

(43) Ruddy, A. J.; Sydora, O. L.; Small, B. L.; Stradiotto, M.; Turculet, L. *Chem. - Eur. J.* **2014**, *20*, 13918–13922.

(44) Moulton, C. J.; Shaw, B. L. *J. Chem. Soc. Dalton Trans.* **1975**, *0*, 1020–1024.

(45) Lagaditis, P. O.; Sues, P. E.; Sonnenberg, J. F.; Wan, K. Y.; Lough, A. J.; Morris, R. H. *J. Am. Chem. Soc.* **2014**, *136* (4), 1367–1380.

(46) Schmeier, T. J.; Dobereiner, G. E.; Crabtree, R. H.; Hazari, N. *J. Am. Chem. Soc.* **2011**, *133*, 9274–9277.

(47) Marziale, A. N.; Friedrich, A.; Klopsch, I.; Drees, M.; Celinski, V. R.; Gu, D.; Schneider, S. *J. Am. Chem. Soc.* **2013**, *135*, 13342–13355.

(48) Gunanathan, C.; Milstein, D. *Acc. Chem. Res.* **2011**, *44* (8), 588–602.

(49) Ben-ari, E.; Leitus, G.; Shimon, L. J. W.; Milstein, D.; Reho, V. *J. Am. Chem. Soc.* **2006**, *128*, 15390–15391.

(50) Zhang, J.; Leitus, G.; Ben-David, Y.; Milstein, D. *Angew. Chem. Int. Ed.* **2006**, *45* (7), 1113–1115.

(51) Gregor, L. C.; Chen, C.; Fafard, C. M.; Fan, L.; Guo, C.; Foxman, B. M.; Gusev, D. G.; Ozerov, O. V. *Dalton Trans.* **2010**, *39*, 3195–3202.

(52) Hahn, R.; Nakamura, A.; Tanaka, K.; Nakayama, Y. *Inorg. Chem.* **1995**, *34*, 6562–6564.

(53) Klerman, Y.; Ben-ari, E.; Diskin-posner, Y.; Leitus, G.; Shimon, L. J. W.; Ben-david, Y.; Milstein, D. *Dalton Trans.* **2008**, *0*, 3226–3234.

(54) Singh, P.; Singh, A. K. *Organometallics* **2010**, *29* (23), 6433–6442.

(55) Miecznikowski, J. R.; Lo, W.; Lynn, M. A.; Jain, S.; Keilich, L. C.; Kloczko, N. F.; O'Loughlin, B. E.; Dimarzio, A. P.; Foley, K. M.; Lisi, G. P.; et al. *Inorg. Chim. Acta* **2012**, *387*, 25–36.

(56) Harkins, S. B.; Peters, J. C. *J. Am. Chem. Soc.* **2004**, *126*, 2885–2893.

(57) Shaffer, D. W.; Szigethy, G.; Ziller, J. W.; Heyduk, A. F. *Inorg. Chem.* **2013**, *52* (4), 2110–2118.

(58) Schnödt, J.; Manzur, J.; García, A.; Hartenbach, I.; Su, C.; Fiedler, J.; Kaim, W. *Eur. J. Inorg. Chem.* **2011**, *2011* (9), 1436–1441.

(59) McGuinness, D. S.; Wasserscheid, P.; Keim, W.; Morgan, D.; Dixon, J. T.; Bollmann, A.; Maumela, H.; Hess, F.; Englert, U. *J. Am. Chem. Soc.* **2003**, *125*, 5272–5273.

(60) Misumi, Y.; Seino, H.; Mizobe, Y. *J. Am. Chem. Soc.* **2009**, *131* (41), 14636–14637.

(61) Sellmann, D.; Prakash, R.; Heinemann, F. W.; Moll, M.; Klimowicz, M. *Angew. Chem. Int. Ed.* **2004**, *43* (14), 1877–1880.

(62) Braunstein, P.; Naud, F. *Angew. Chem. Int. Ed.* **2001**, *40* (4), 680–699.

(63) Bassetti, M. *Eur. J. Inorg. Chem.* **2006**, *0* (22), 4473–4482.

(64) Ding, S.; Ghosh, P.; Darensbourg, M. Y.; Hall, M. B. *Proc. Nat. Acad. Sci.* 2017. pp E9775–E9782.

(65) Burrows, A. D. *Sci. Prog.* **2002**, *85*, 199–217.

(66) Gianneschi, N. C.; Bertin, P. A.; Nguyen, S. T.; Mirkin, C. A.; Zakharov, L. N.; Rheingold, A. L. *J. Am. Chem. Soc.* **2003**, *125*, 10508–10509.

(67) Oliveri, C. G.; Gianneschi, N. C.; Nguyen, S. T.; Mirkin, C. A.; Stern, C. L.; Wawrzak, Z.; Pink, M. *J. Am. Chem. Soc.* **2006**, *128* (50), 16286–16296.

(68) Schnödt, J.; Manzur, J.; García, A. M.; Hartenbach, I.; Su, C. Y.; Fiedler, J.; Kaim, W. *Eur. J. Inorg. Chem.* **2011**, *20* (9), 1436–1441.

(69) Bubrin, M.; Schweinfurth, D.; Ehret, F.; Záliš, S.; Kvapilová, H.; Fiedler, J.; Zeng, Q.; Hartl, F.; Kaim, W. *Organometallics* **2014**, *33* (18), 4973–4985.

(70) Huynh, H. V.; Yeo, C. H.; Chew, Y. X. *Organometallics* **2010**, *29* (6), 1479–1486.

(71) Bassetti, M.; Capone, A.; Salamone, M. *Organometallics* **2004**, *23* (2), 247–252.

(72) Hirotsu, M.; Santo, K.; Tanaka, Y.; Kinoshita, I. *Polyhedron* **2018**, *143*, 201–208.

(73) Hübner, R.; Weber, S.; Strobel, S.; Sarkar, B.; Záliš, S.; Kaim, W. *Organometallics* **2011**, *30*, 1414–1418.

(74) Broere, D. L. J.; Plessius, R.; Van Der Vlugt, J. I. *Chem. Soc. Rev.* **2015**, *44*, 6886–6915.

(75) Luca, O. R.; Crabtree, R. H. *Chem. Soc. Rev.* **2013**, *42*, 1440–1459.

(76) Chirik, P. J.; Wieghardt, K. *Science*. 2010, pp 794–795.

(77) Blanchard, S.; Derat, E.; Desage-El Murr, M.; Fensterbank, L.; Malacria, M.; Mouriès-Mansuy, V. *Eur. J. Inorg. Chem.* **2012**, *2012* (3), 376–389.

(78) Chirik, P. J. *Inorg. Chem.* **2011**, *50* (20), 9737–9740.

(79) Jazdzewski, B. A.; Tolman, W. B. *Coord. Chem. Rev.* **2000**, *200–202*, 633–685.

(80) Borman, C. D.; Saysell, C. G.; Sokolowski, A.; Twitchett, M. B.; Wright, C.; Sykes, A. G. *Coord. Chem. Rev.* **1999**, *190–192*, 771–779.

(81) Herebian, D.; Wieghardt, K. E.; Neese, F. *J. Am. Chem. Soc.* **2003**, *125*, 10997–11005.

(82) Ghosh, P.; Bill, E.; Weyhermüller, T.; Neese, F.; Wieghardt, K. *J. Am. Chem. Soc.* **2003**, *125*, 1293–1308.

(83) Roy, N.; Sproules, S.; Weyhermu, T.; Wieghardt, K. *Inorg. Chem.* **2009**, *48*, 3783–3791.

(84) Sproules, S.; Wieghardt, K. *Coord. Chem. Rev.* **2010**, *254*, 1358–1382.

(85) Presow, S. R.; Ghosh, M.; Bill, E.; Weyhermüller, T.; Wieghardt, K. *Inorg. Chim. Acta* **2011**, *374* (1), 226–239.

(86) Ye, S.; Sarkar, B.; Lissner, F.; Schleid, T.; Van Slageren, J.; Fiedler, J.; Kaim, W. *Angew. Chem. Int. Ed.* **2005**, *44*, 2103–2106.

(87) Paretzki, A.; Bubrin, M.; Fiedler, J.; Záliš, S.; Kaim, W. *Chem. Eur. J.* **2014**, *20* (18), 5414–5422.

(88) Brown, K. L. *Chem. Rev.* **2005**, *105* (6), 2075–2149.

(89) Leyssens, L.; Vinck, B.; Van Der Straeten, C.; Wuyts, F.; Maes, L. *Toxicology* **2017**, *387* (March), 43–56.

(90) Carneiro, M. L. B.; Lopes, C. A. P.; Miranda-Vilela, A. L.; Joanitti, G. A.; da Silva, I. C. R.; Mortari, M. R.; de Souza, A. R.; Báo, S. N. *Toxicol. Reports* **2015**, *2*, 1086–1100.

(91) Zhang, G.; Vasudevan, K. V.; Scott, B. L.; Hanson, S. K. *J. Am. Chem. Soc.* **2013**, *135* (23), 8668–8681.

(92) Zhang, G.; Hanson, S. K. *Org. Lett.* **2013**, *15* (3), 650–653.

(93) Rösler, S.; Obenauf, J.; Kempe, R. *J. Am. Chem. Soc.* **2015**, *137* (25), 7998–8001.

(94) Qu, S.; Dang, Y.; Song, C.; Wen, M.; Huang, K. W.; Wang, Z. X. *J. Am. Chem. Soc.* **2014**, *136*, 4974–4991.

Permissions for all schemes and figures have been granted and are available upon request.

Chapter 2: Cobalt Reactions with the SNS Amido Ligand

2.1. Introduction

In the field of bifunctional catalysis, the inclusion of a nitrogen donor group is often an important component in successful ligand design. Nitrogen donors have been shown to be essential in the activation of substrates in biological metalloenzymes such as [FeFe]-hydrogenases which rely on a pendant amine to assist in the activation of the dihydrogen bond.[1–4] In metal complexes this 'NH effect' has been identified as a crucial component in bifunctional mechanisms for the catalytic hydrogenation of ketones and imines,[5–8] dehydrogenation of amine-boranes,[9–11] hydrosilylation of aldehydes, ketones and esters,[12] and hydroboration of alkenes,[13] among other examples.

The success of some of the more effective bifunctional ligands is also due in part to the tridentate pincer design that allows for the tight metal binding of a variety of donors, including P,S,N and C.[14–16] To this end our group has developed an easily prepared tridentate SNS amido ligand, the anion of which contains a hard nitrogen donor, capable of enabling a bifunctional mechanism, as well as two soft -SMe thioether donors that are able to stabilize a range of metal oxidation states.[17–21] Moreover, the thioether arm that binds the metal in a six-membered ring can serve as a hemilabile ligand to provide an open site for substrate coordination.[22–24] This amine ligand shall hereby be referred to in short hand as $S^{Me}N^{H}S^{Me}$, with the superscript representing the groups connected to the respective donors on the ligand before deprotonation. A variety of tridentate sulfur-containing amine ligands have been reported in the literature such as $[S^{R}N^{H}S^{R}]$,[25] $[S^{H}N^{H}S^{H}]$,[26] $[O^{H}N^{H}S^{R}]$,[27,28] $[N^{R}N^{H}S^{H}]$,[29] and $[N^{H}S^{R}N^{H}]$[30] as presented in **Figure 2.1.**

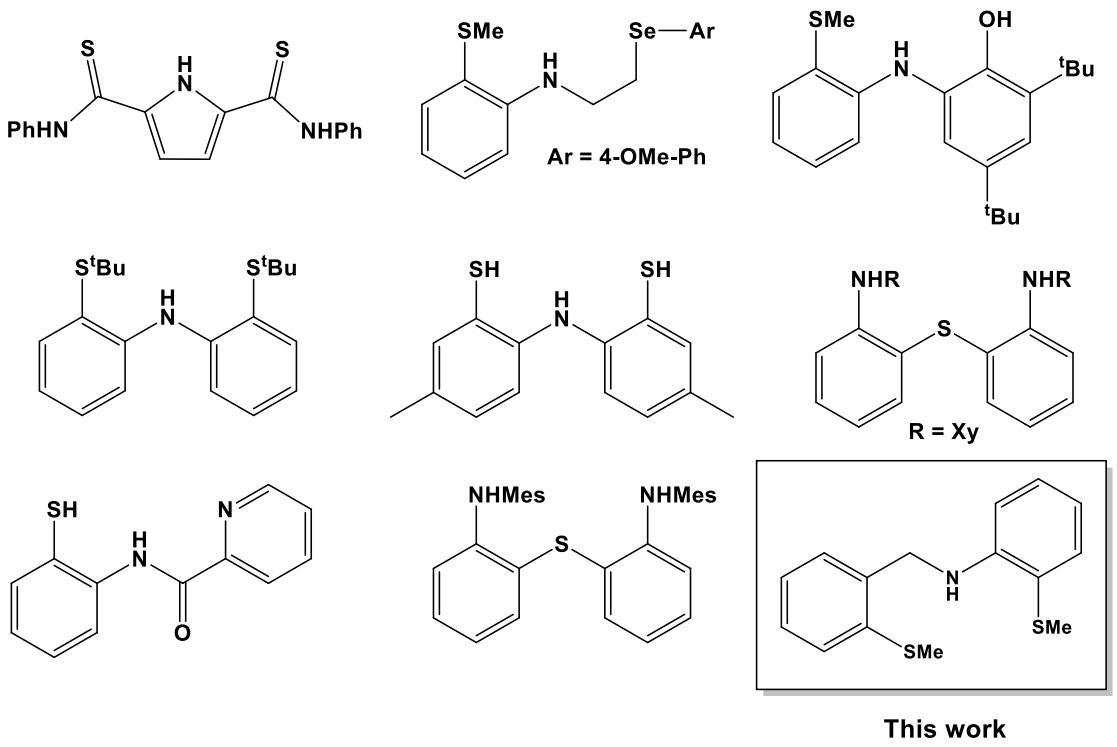

Figure 2.1: Sulfur-containing bifunctional amine ligands.

Our objective using this $S^{Me}N^{H}S^{Me}$ ligand is to prepare a series of cobalt SNS amido complexes and assess their activity as bifunctional catalysts. Previous work with iron showed that the ligand prefers to form a bis-ligated complex upon deprotonation as fully characterized elsewhere.[31] The hemilability of the thioether moiety in the six-membered ring resulting from coordination of the ligand was demonstrated in reactivity studies with strongly coordinating ligands such as 2,2'-bipyridine, 1,2-bis(dimethylphosphino)ethane and 2,6-dimethylphenyl isonitrile (henceforth referred to as Bipy, DMPE and CNAr respectively; **Scheme 2.1**).

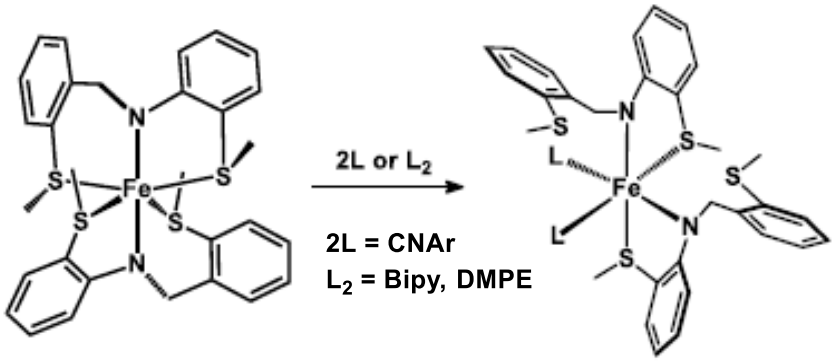

Scheme 2.1: Hemilability of the six-membered ring thioether arm in the iron complex $Fe(\kappa^3\text{-}S^{Me}NS^{Me})_2$.

Upon protonation with the Brønsted acid trifluoromethanesulfonimide ($HNTf_2$) one ligand is protonated, forming an iron(II) cation which showed a significant lengthening of the Fe-N_{amine} bond versus that of the Fe-N_{amido}. The implied weakening of this bond was confirmed when the protonated ligand was displaced by adding one equivalent of bis(2-diphenylphosphinoethyl)phenylphosphine) (triphos) forming the 16 electron iron cationic complex which has been fully characterized elsewhere (**Scheme 2.2**).[31] Preliminary investigation of the latter complex as a precatalyst for ammonia-borane dehydrogenation showed it to be a selective albeit sluggish catalyst. It showed better performance with dimethylamine-borane and formation of an Fe-hydride complex identified by ^{1}H NMR spectroscopy is suggestive of a bifunctional activation pathway.[31] This work with iron provides a good template for the behaviour that may be expected when this SNS ligand is paired with cobalt and a baseline for which the chemistry of the different metals can be compared.

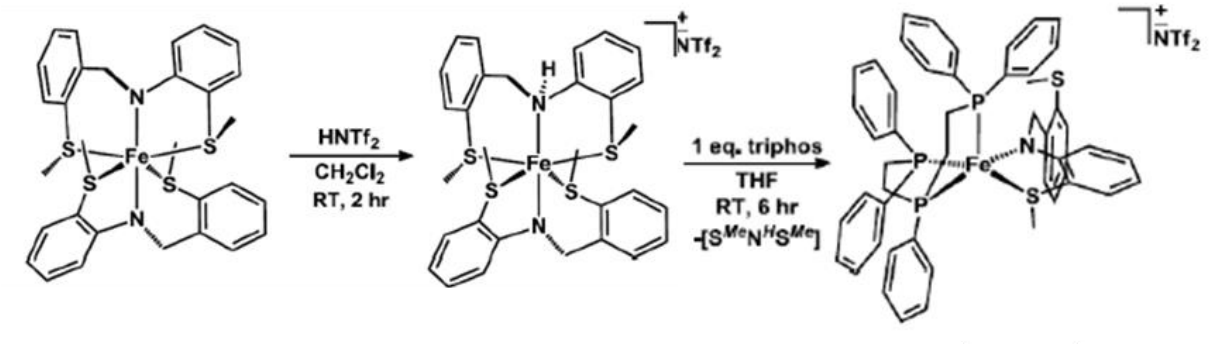

Scheme 2.2: Protonation and displacement of the $S^{Me}N^{H}S^{Me}$ ligand in the iron bis-amido complex.[31]

2.2. $S^{Me}N^{H}S^{Me}$ Ligand Synthesis

The synthesis of this amido SNS ligand has been designed to be accomplished in two steps using inexpensive and widely available starting materials to make our ligand more economically advantageous (**Scheme 2.3**). This is in contrast to the generally expensive and time-consuming synthesis of previously reported sulfur-containing amine ligands.[20,21,25,26,30,32] Formation of the $S^{Me}N^{H}S^{Me}$ ligand is accomplished by the condensation of 2-(methylthio)benzaldehyde and 2-(methyl-thio)aniline in dry ethanol which is stirred at room temperature under nitrogen for 18 h. The resulting yellow powder (2-(2-methylthiobenzylidene) methylthioaniline) was then reduced with excess ammonia-borane to form the final product, 2-(2-methylthiobenzyl)methylthioaniline, in excellent yields.

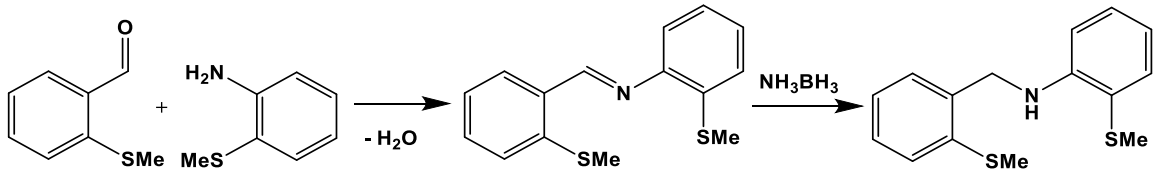

Scheme 2.3: The synthesis of $S^{Me}N^{H}S^{Me}$

Formation of the ligand was confirmed using ^{1}H NMR spectroscopy, the spectrum of which is shown below (**Figure 2.2**), while further characterization such as ^{13}C NMR, UV/Vis, IR spectroscopy and elemental analysis are reported elsewhere.[31] The ^{1}H NMR spectrum reveals resonances for all seventeen protons on the ligand with the most noticeable being two large resonances at 2 ppm which are identifiable as the two different thiomethyl groups. The two-proton doublet at 4.5 ppm corresponds to the benzylic protons next to the nitrogen atom while the broad one proton singlet at 5.5 ppm is the amine proton. The remaining resonances in the aromatic region correspond to the eight different protons on the aromatic rings of the ligand.

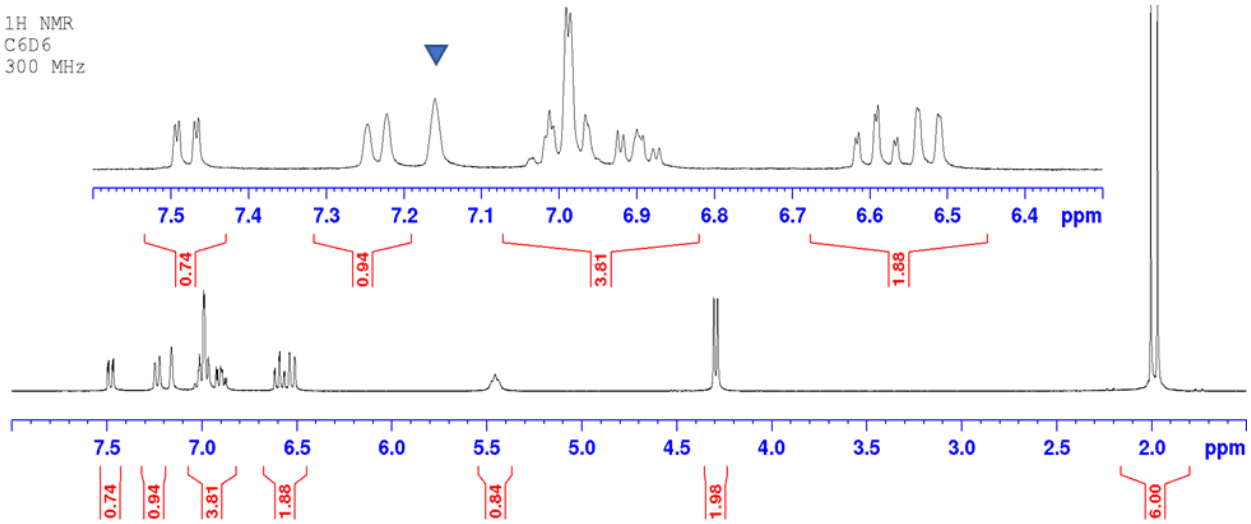

Figure 2.2: ^{1}H NMR spectrum of $S^{Me}N^{H}S^{Me}$ in C_6D_6 (blue triangle).

2.3. Formation of Co(II) Bis-Amido Complex [Co(κ^3-$S^{Me}NS^{Me}$)$_2$], 2-1

2.3.1. Synthesis of **2-1** from $CoCl(PPh_3)_3$

A cobalt(I) complex was targeted as a desirable starting material due to its diamagnetism which would make characterization using ^{1}H NMR spectroscopy much more straightforward. To such end, the tris-triphenylphosphine cobalt(I) chloride

complex was prepared according to methods reported in the literature (a detailed description of this prep. can be seen in the experimental section below).[33]

The $S^{Me}N^{H}S^{Me}$ ligand and one equivalent of base (lithium trimethylsilylamide or potassium *tert*-butoxide) were combined as solids and dissolved in THF to form a clear yellow solution as the ligand was deprotonated forming the lithium/potassium SNS salt. The dropwise addition of this solution into a green suspension of $CoCl(PPh_3)_3$ caused a rapid change in colour to a reddish-purple which upon removal of solvent yielded a bright purple powder. After filtration of LiCl and rinsing with a substantial amount of diethyl ether (DEE) to remove triphenylphosphine and the conjugate acid the yield was calculated to be 47%. The ^{1}H NMR spectrum revealed a series of paramagnetically shifted SNS ligand resonances ranging from 112 to -48 ppm consistent with loss of all three PPh_3 ligands. Crystals suitable for single-crystal X-ray diffraction were grown by layering a saturated THF solution with hexanes and the surprising molecular structure revealed that the formed species was a 19 e^- pseudooctahedral cobalt(II) bis-amido complex, **2-1** (**Scheme 2.4**). A more detailed description of the characterization of **2-1** is discussed below. It is hypothesized that the formation of cobalt(II) from cobalt(I) was facilitated by a disproportionation reaction between cobalt atoms that would explain the poor observed yield.

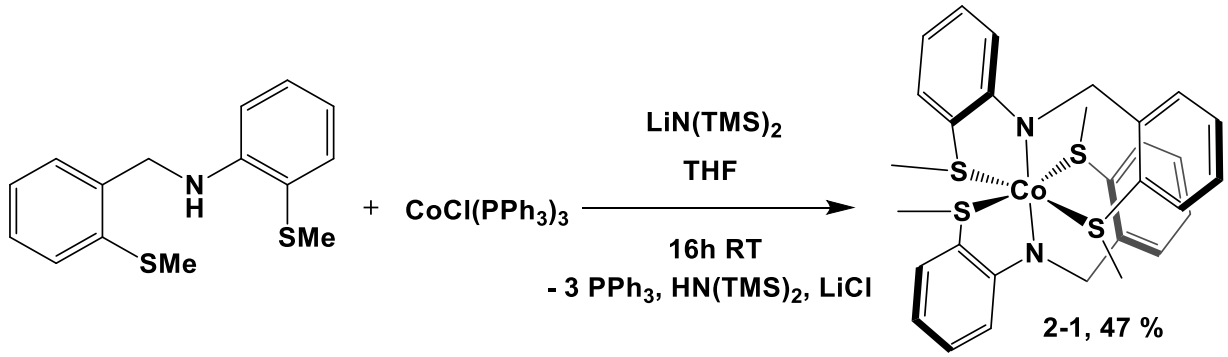

Scheme 2.4: Synthesis of **2-1** from $CoCl(PPh_3)_3$.

2.3.2. Synthesis of **2-1** from Cobalt(II) Chloride

In an attempt to improve the yields of **2-1**, we employed a cobalt(II) starting material, cobalt(II) chloride. Two equivalents of $S^{Me}N^{H}S^{Me}$ and $LiN(TMS)_2$ were combined as solids with the cobalt(II) chloride and addition of THF gave a yellow solution with a blue suspension that transitioned rapidly to the purple colour of **2-1**. Upon removal of LiCl by filtration, the purple solution was dried and washed extensively with DEE to remove $HN(TMS)_2$ affording **2-1** in 84% yield.

2.3.3. Synthesis of **2-1** from Cobalt(II) Bis[bis(trimethylsilyl)amide]

In an attempt to avoid the extensive DEE wash from the above salt metathesis route, we prepared the $Co[N(SiMe_3)_2]_2$ according to previously published methods.[34] This starting material has the advantage of containing a base suitably strong enough to deprotonate the $S^{Me}N^{H}S^{Me}$ ligand as well as being quite soluble in DEE. This second factor allows for the reaction to be performed in DEE causing precipitation of the bis-amido product once formed while the conjugate acid and any excess ligand remain in solution. Isolation of the purple powder was then accomplished by filtration and a single rinse yielding spectroscopically pure product in excess of 92% yield. This is a significant improvement over the initial yield of 47% and also produces a much cleaner product.

2.3.4. Synthesis of **2-1** from Cobalt(III) Acetylacetonate, $Co(acac)_3$

In order to extend our Co SNS chemistry to trivalent cobalt we started with the Co(III) starting material, $Co(acac)_3$. Amazingly however, addition of one equivalent each of $S^{Me}N^{H}S^{Me}$ and $LiN(TMS)_2$ to $Co(acac)_3$ in deuterated benzene resulted in the colour transitioning from a blue-green to the characteristic purple of the bis-amido complex. This transformation was confirmed by appearance of the bis-amido resonances in the ^1H NMR spectrum. The reduction from cobalt(III) to cobalt(II) is hypothesized to be facilitated by the base in solution acting as a reducing agent as there is no other obvious electron source in the reaction vessel. The formation of the same complex from such a wide range of starting materials in different oxidation states is a testament to the apparent thermodynamic stability of complex **2-1**.

2.4. Characterization of $Co(\kappa^3\text{-}S^{Me}NS^{Me})_2$, 2-1

The complex $Co(\kappa^3\text{-}S^{Me}NS^{Me})_2$ has been characterized using ^1H NMR spectroscopy, single-crystal X-ray diffraction and cyclic voltammetry. The molecular structure of **2-1** exhibits distorted meridional binding of the two ($\kappa^3\text{-}S^{Me}NS^{Me}$) amido ligands to the cobalt(II) centre with an average S-Co-S bond angle of 166.24(3)^o in a pseudooctahedral geometry with *trans* amido groups (N-Co-N = 176.46(9)^o, **Figure 2.3**). This structure is analogous to the previously reported bis-amido iron complex $Fe(\kappa^3\text{-}S^{Me}NS^{Me})_2$ with bond distances similar to the 2.5389(7) Å for the 5-membered Fe-S bond, 2.7156(7) Å for the 6-membered Fe-S bond and 2.015(2) Å for the amido Fe-N bond.[31] Specifically, the longer thioether Co-S bond in the six-membered ring has an average bond distance of 2.6754(7) Å versus the five-membered ring which has an

average bond distance of 2.4752(7) Å. This suggests that the former will more easily dissociate from the metal. The average Co-S bond distance of 2.5753(7) Å is also noticeably longer than other thioether-cobalt bond distances that have been reported in the literature.[35–37] The average Co-N bond distance of 1.971(2) Å, however, is within the range of reported distances for cobalt(II) amido complexes.[36,38,39]

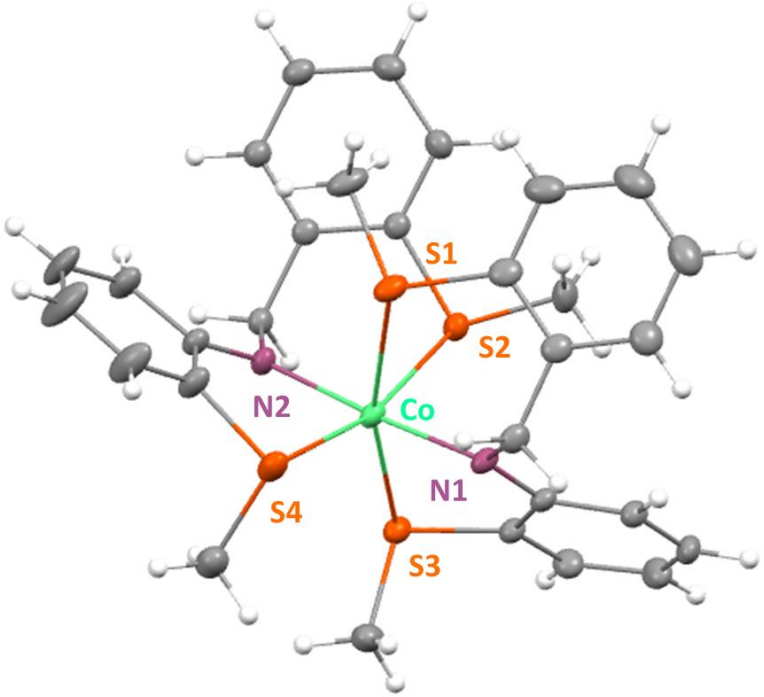

Bond	Distance
Co – S1	2.6481(7) Å
Co – S3	2.4723(7) Å
Co – N1	1.967(2) Å
Co – S2	2.478(7) Å
Co – S4	2.7027(7) Å
Co – N2	1.974 (2) Å
Bonds	**Angle**
N1-Co-N2	176.46(9)°
S1-Co-S3	165.41(3)°
S2-Co-S4	167.06(3)°
N1-Co-S3	82.49(6)°
N1-Co-S1	85.36(6)°
N2-Co-S2	83.02(6)°
N2-Co-S4	85.84(6)°

Figure 2.3: Molecular structure of Co(κ^3-$S^{Me}NS^{Me}$)$_2$ (**2-1**) with selected bond distances and angles.

The ^{1}H NMR spectrum of **2-1** reveals a number of broad paramagnetic resonances from 112 to -48 ppm consistent with a cobalt(II) centre (**Figure 2.4**). The spectrum shows only one set of resonances for the coordinated amido ligand reflecting the apparent mirror plane symmetry (containing S1-Co-S2) enabled by rapid flexing of the six-membered rings on the NMR time scale. A total of thirteen of the expected sixteen protons can be accounted for in the spectrum. Efforts to locate the missing three

resonances by extending the spectral range have been unsuccessful so it is likely the remaining signals have been broadened to the point where they are indistinguishable from the baseline. The two resonances at 112 ppm and 49 ppm can be assigned to the two inequivalent thiomethyl groups from their 3H integrations and the sharp 1H resonances are likely due to the four six-membered ring aromatic protons that are farthest from the unpaired electron. As the ortho substitution of the N and S donors in the five-membered ring are reminiscent of redox-active catechol-type ligands, the SOMO may have significant spin density in this ring, making definitive assignment of the remaining 1H signals impossible without sophisticated computational methods.

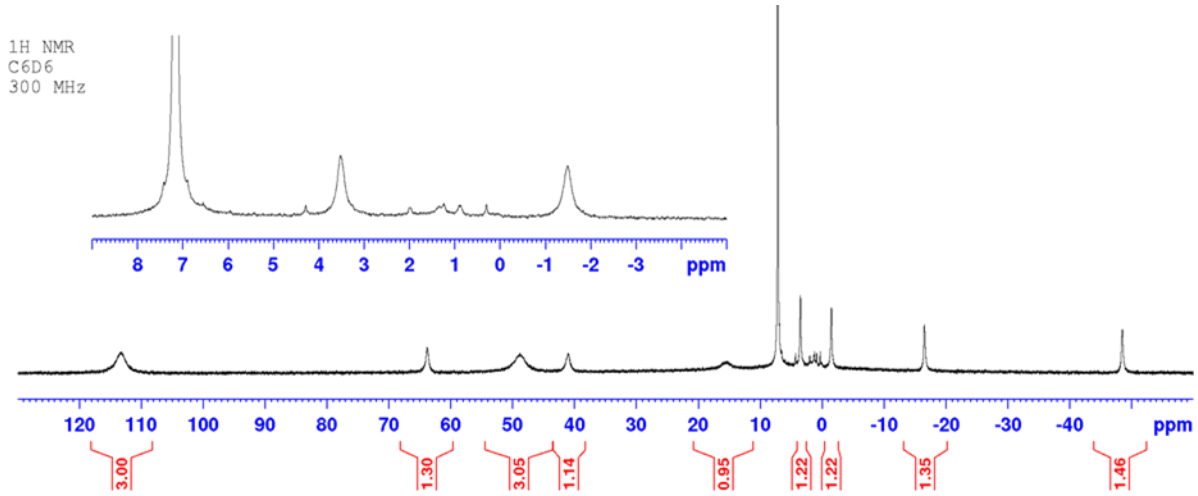

Figure 2.4: ^{1}H NMR spectrum of Co(κ^3-S^{Me}NS^{Me})$_2$, **2-1**.

Given the potential redox activity of this species, cyclic voltammetry experiments were performed by Andrea Mulas of the Bucher group at ENS Lyon in France. Acquisition of this data was challenging due to the extreme water-sensitivity of **2-1**. At the low concentrations that CV experiments are performed, the purple colour was observed to rapidly transition to yellow. As a result, the solvent was dried extensively with activated alumina before a suitable CV curve was acquired (**Figure 2.5**).

From this curve we can observe two oxidations occurring at approximately -250 mV and 400 mV to the reference silver electrode. The first of these curves corresponds to the oxidation of the metal from Co(II) to Co(III) and appears by the peak separation to be reversible. Repeated cycles, however, resulted in a steady intensity decrease of this wave suggesting that the oxidation is only quasi-reversible. This result suggests that the oxidation potential of **2-1** is on par with the reduction potential of cationic silver in THF (-240 mV vs. Ag/Ag^+ in DCM),[40] which could allow for access to the Co(III) species when used as a chemical oxidant. The second of these two oxidations at 400 mV is clearly irreversible as can be seen from the unsymmetrical shape of the curve. This oxidation may be the result of an electron being pulled from the ligand instead of the metal, spurring additional reactivity and rendering the oxidation irreversible. No reduction from Co(II) to Co(I) was observed.

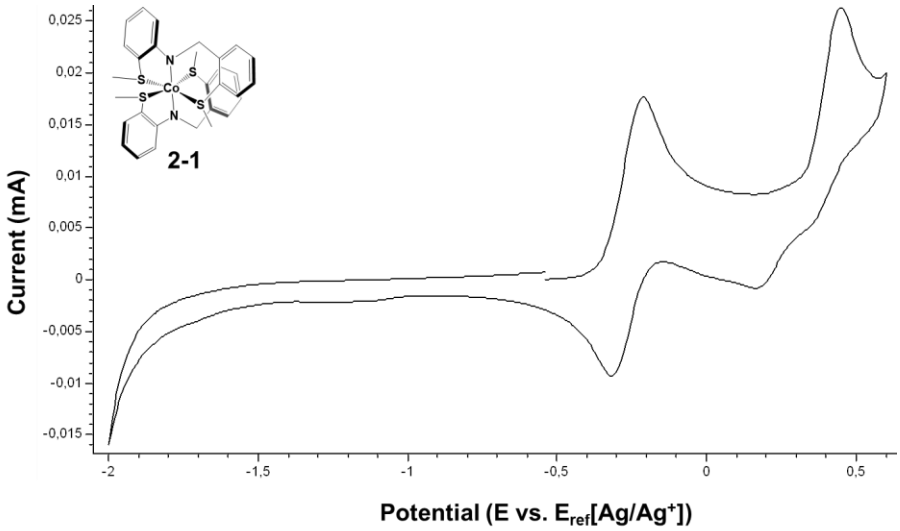

Figure 2.5: Cyclic voltammetry curve for $Co(\kappa^3\text{-}S^{Me}NS^{Me})_2$ (**2-1**) in dry DCM. Performed at 5 mM with tetrabutylammonium hexafluorophosphate (0.1 M), 100 mV/s.

Samples of **2-1** were also sent to the Université de Montréal for elemental analysis. However, after two attempts the resulting calculated weight % values had unacceptable levels of error compared to the theoretical weight % values, even after accounting for possible water contamination.

2.5. Reactivity of Co(κ^3-$S^{Me}NS^{Me}$)$_2$, 2-1

2.5.1. Probing for Hemilability of Thioether Arm

In order to explore the hemilability of the six-membered ring thioether arm, **2-1** was treated with a variety of neutral donor ligands. As noted above, dissociation of the six-membered thioether arms of the d^6 iron(II) bis-amido complex allowed for coordination of Bipy, DMPE and CNAr ligands. Similar reactions of these ligands with **2-1** did not prove to be so simple. No visible colour change was detected upon addition of one equivalent of Bipy to the purple solution of **2-1**, even after stirring for 16 h. While the ^{1}H NMR spectrum revealed a broadening of both the $S^{Me}NS^{Me}$ and Bipy resonances (**Figure 2.6**) suggestive of rapid exchange, no significant colour change was noted at low temperatures and attempts to isolate a product at low temperature only gave **2-1**. This is in stark contrast to the iron analogue which readily dissociates two thioether arms to accept the bidentate ligand, a transformation that is accompanied by a distinct colour change from yellow to red-brown. The apparent reduced hemilability of the thioether arms with cobalt is surprising considering that both complexes had considerably elongated cobalt-sulphur bond distances in their six-membered rings.

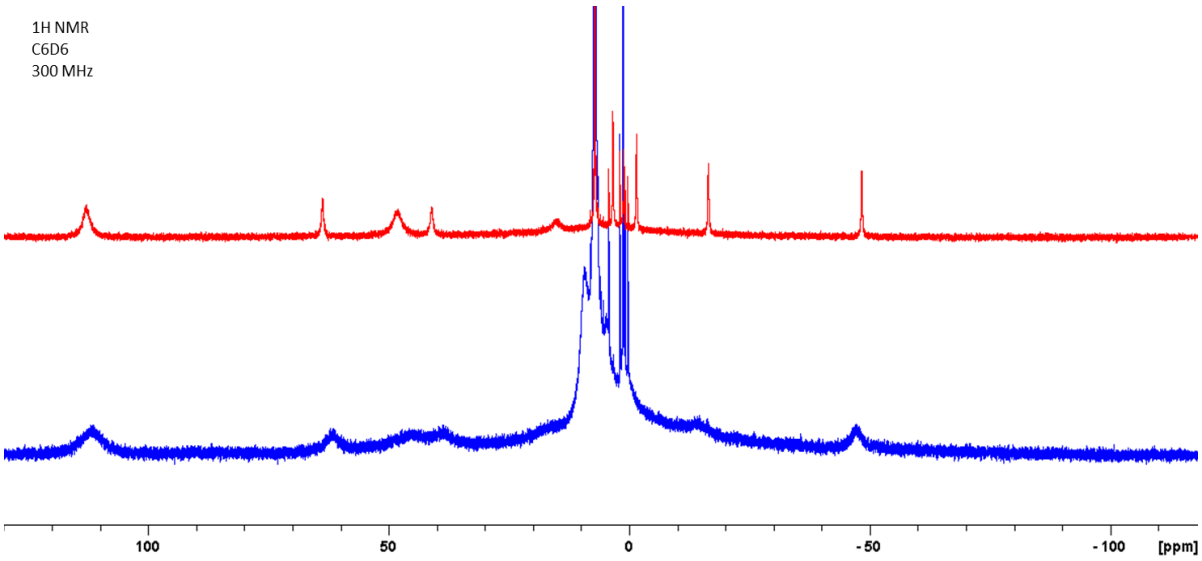

Figure 2.6: ^{1}H NMR spectrum of **2-1** (red) and **2-1** with one equivalent of Bipy (blue).

In contrast, addition of two equivalents of CNAr to **2-1** caused an instantaneous colour change from purple to an opaque dark-brown. The ^{1}H NMR spectrum of this reaction after 15 min showed a new product being formed and after 16 h all starting material had been consumed (**Figure 2.7**, purple). However, both the high number of resonances in the ^{1}H NMR spectrum and multiple signals integrating to non-integer values suggests that at least two different complexes are being formed. Surprisingly, after 15 min the characteristic resonances for the protonated SNS amine ligand also began to appear suggesting that the reaction is not limited to the simple displacement of the thioether arms by the isocyanides as originally anticipated. As traces of water could be ruled out by control experiments, one possibility is intermolecular deprotonation of the benzylic C-H bond by the amido N giving a coordinated imine in one complex and a coordinated amine in the other. A similar amine to imine conversion has been observed previously during the selective C^{aryl}-S bond activation in $[Fe(S^{Me}NS^{Me})(PMe_3)_3]^+$.[41] Alternatively, the Co centre of a second complex could perform a hydrogen atom abstraction from the benzylic CH_2 group forming a coordinated imine and Co(III)-H.

Subsequent N-H reductive elimination could then yield the free $S^{Me}N^{H}S^{Me}$ ligand and a diamagnetic Co(I) complex. H-atom abstraction has been documented previously for cobalt(II) complexes including systems with PNP and SNS pincer ligands[42–45] Formation of a cobalt(I) complex could also explain the appearance of resonances in the diamagnetic region (δ 6.5-5 and 3.5-2.5) not accounted for by the protonated ligand. Attempts to isolate individual products from this reaction have proven unsuccessful thus far due to similar solubilities in a range of solvents.

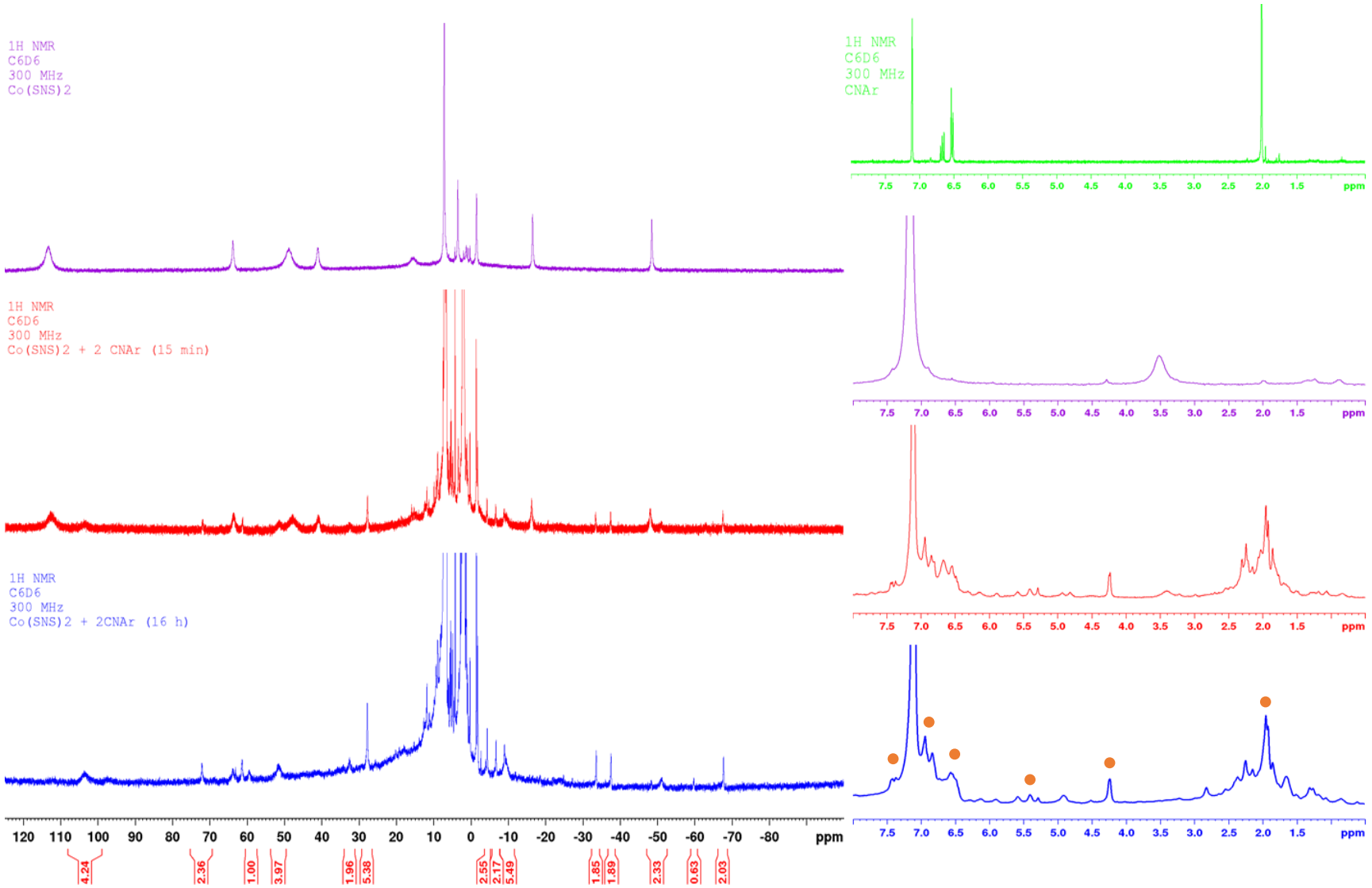

Figure 2.7: ^{1}H NMR spectra of **2-1** (purple), **2-1** with 2 equiv. of CNAr after 15 min (red) and the same reaction after 16 h (blue). $S^{Me}N^{H}S^{Me}$ denoted by orange circles. Free CNAr (green) is shown for comparison.

Addition of one equivalent of DMPE to a solution of **2-1** in deuterated benzene initially gave no colour change. Inspection of the ^{31}P NMR spectrum 15 min after addition showed two singlets due to coordinated DMPE along with a broad resonance at -50 ppm where free DMPE appears (**Figure 2.8**). After 16 h, the solution became dark-brown and the free DMPE resonance has became a sharp singlet while multiple broad signals were observed in the range of 19 to 50 ppm, none of which integrate well with each other. The four resonances at 105, 65, 28 and -53 ppm in the ^{1}H NMR spectrum after 15 min indicate the formation of a new paramagnetic complex, presumably from DMPE coordination (**Figure 2.9**, blue). On closer inspection of the diamagnetic region, however, the reaction is very clearly accompanied by the formation of both free $S^{Me}N^{H}S^{Me}$ ligand and diamagnetic Co-DMPE products. After 16 h, all resonances now appear in the diamagnetic region (**Figure 2.9**, red). Attempts to isolate the initial product by rapid removal of solvent or by trying to precipitate the complex in the freezer were not successful.

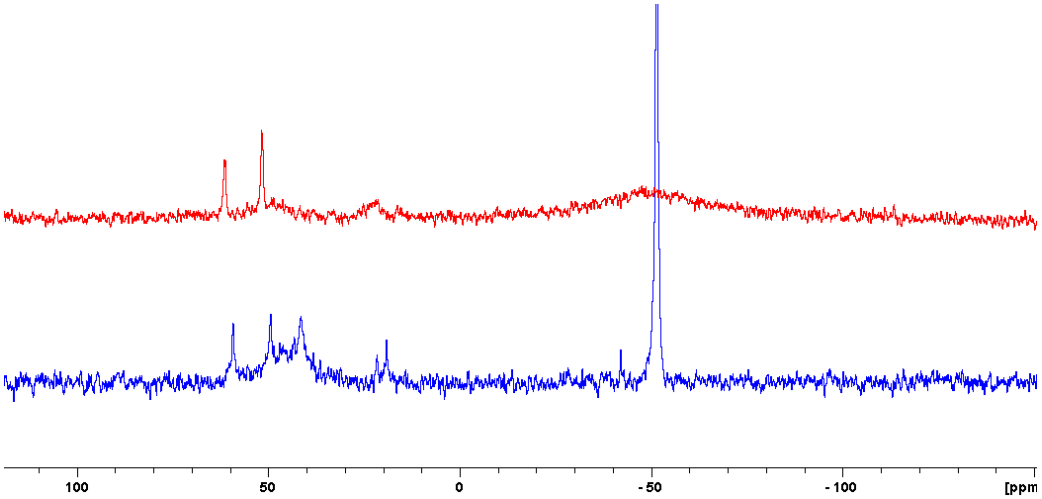

Figure 2.8: $^{31}P\{^{1}H\}$ NMR spectrum of **2-1,** 15 min after addition of DMPE (red) and the same reaction after 16 h (blue).

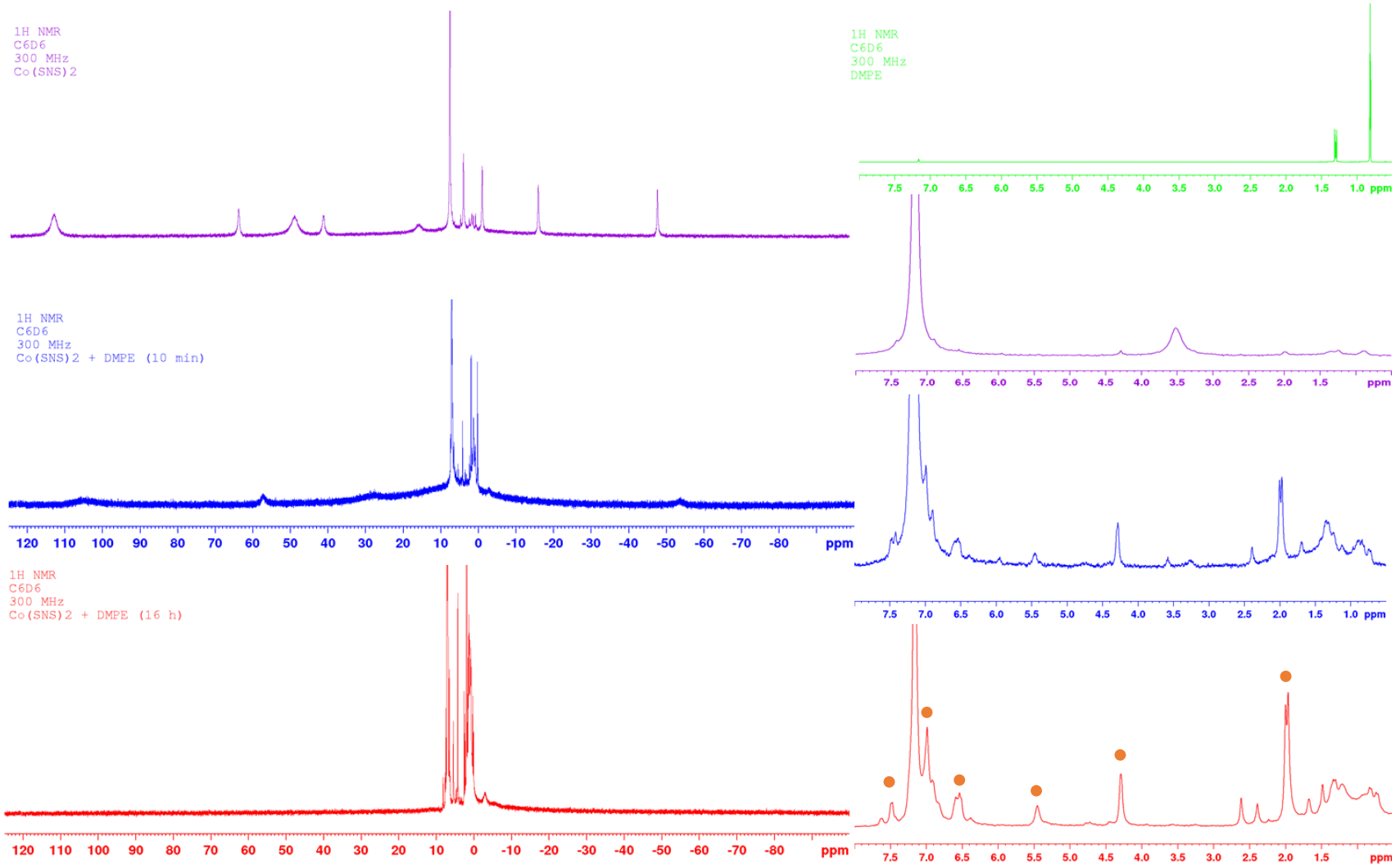

Figure 2.9: ^{1}H NMR spectra of **2-1** (purple), **2-1** and DMPE after 15 min (blue) and the same reaction mixture after 16 h (red). $S^{Me}N^{H}S^{Me}$ denoted by orange circles. Free DMPE (green) is shown for comparison.

The above results clearly demonstrate that the behaviour of the cobalt bis-amido complex is in stark contrast to that of its iron analogue. While the SNS amido ligand in the iron complex clearly exhibits hemilabile behaviour, binding a variety of ancillary ligands, the cobalt analogue seems to react reversibly with Bipy and undergoes redox reactions in the presences of CNAr or DMPE.

2.5.2. Ligand Removal by Protonation

In general, late metal amidos are strong bases and can thus be protonated without a change in the metal's oxidation state. In the context of the iron bis-amido species, mono-protonation was accompanied by the expected elongation of the iron-nitrogen bond length in the protonated ligand from 2.015(2) to 2.2763(15) Å, indicating a weaker association to the metal. This led to an effective technique for the removal of one equivalent of ligand to form the mono-ligated species for applications in catalysis as noted above.[31] In one example, the strongly coordinating tridentate ligand bis(2-diphenylphosphinoethyl)phenyl phosphine (triphos) displaced the protonated SNS ligand, forming the cationic 16e$^-$ complex [Fe(κ^2-S^{Me}NS^{Me})(κ^3-triphos)](NTf$_2$) which was characterized by single-crystal X-ray diffraction (**Scheme 2.2**).

Following the same rationale, **2-1** was treated with one equivalent of HNTf$_2$ dropwise in C_6D_6 transforming the purple solution to a green product which precipitated out of solution. The green solid is hypothesized to be the monoprotonated cationic salt [Co(κ^3-S^{Me}NS^{Me})(κ^3-S^{Me}N^{H}S^{Me})](NTf$_2$), **2-2**, although attempts to grow crystals suitable for single-crystal X-ray diffraction have been unsuccessful. On dissolution in CD_3CN for NMR studies, the green solid afforded a blue solution.

The ^{1}H NMR spectrum of this blue solution revealed a paramagnetic product that exhibits similar chemical shifts to that of **2-1** as well as resonances of the free $S^{Me}N^{H}S^{Me}$ ligand in the diamagnetic region (**Figure 2.10**). Integration of the paramagnetically shifted signals accounts for twelve of the sixteen protons present on the SNS ligand suggesting that the remaining four resonances are either hidden under the diamagnetic signals or, like **2-1**, are broadened into the baseline. The resonances at 97 and 52 ppm can be identified as the thiomethyl protons from their 3H integrations while the 2H resonance at 35 ppm can be identified as equivalent benzylic protons in the proposed $[Co(S^{Me}NS^{Me})(MeCN)_n](NTf_2)$ complex **2-3**. We were unable to determine the value of n in the formula of complex **2-3** due to its lack of solubility in other deuterated NMR solvents (C_6D_6, toluene-d_8, THF-d_8, CD_2Cl_2, $CDCl_3$). Attempts to grow crystals suitable for single-crystal X-ray diffraction were also unsuccessful.

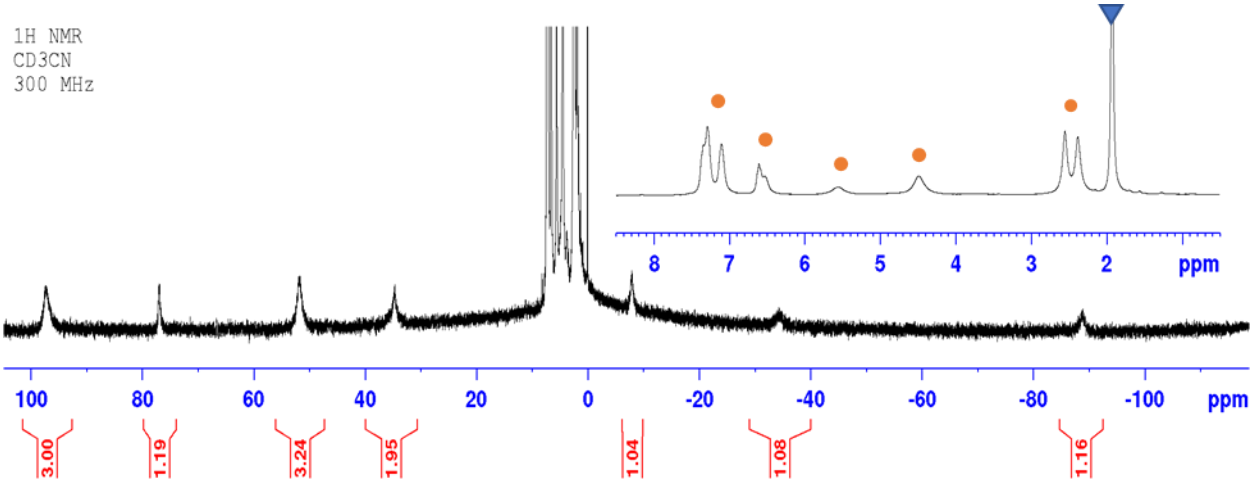

Figure 2.10: ^{1}H NMR spectrum of $[Co(\kappa^{3}\text{-}S^{Me}NS^{Me})(CD_3CN)_n](NTf_2)$, **2-3,** with $S^{Me}N^{H}S^{Me}$ (orange circles) in CD_3CN (residual peak blue triangle).

The ability of acetonitrile to displace the protonated SNS ligand opens the door to the possibility of attaching a number of ancillary ligands to the cobalt, forming a number of new mono-ligated complexes which may be suitable for catalysis studies. Following this line of reasoning, two equivalents of triphenylphosphine (PPh_3) were added dropwise to a blue acetonitrile solution of **2-3** causing no obvious colour change to the solution. The ^1H NMR spectrum of this solution appeared identical to that of the acetonitrile complex with the added resonances of free PPh_3 in the diamagnetic region, demonstrating that acetonitrile was not being displaced by the triphenylphosphine. To encourage coordination of the PPh_3, the acetonitrile was removed *in vacuo* slowly causing the formation of a green solid. The ^1H NMR spectrum of this complex in C_6D_6 showed new paramagnetically-shifted resonances that support the coordination of at least one PPh_3 ligand to the metal (**Figure 2.11**). Specifically, the multi-proton resonances at 95 and 15 ppm are consistent with the ortho and meta protons (each 6H) of PPh_3 and there are more than two 3H resonances (cf. 3H resonance of the PPh_3 para protons). Further work is needed, however, to ensure that all the paramagnetically-shifted resonances are due to a single complex. The ^{31}P NMR spectrum shows only a broad signal for free PPh_3 as ^{31}P NMR resonances are rarely observed for paramagnetic phosphine complexes. Efforts to acquire an accurate crystal structure are currently underway.

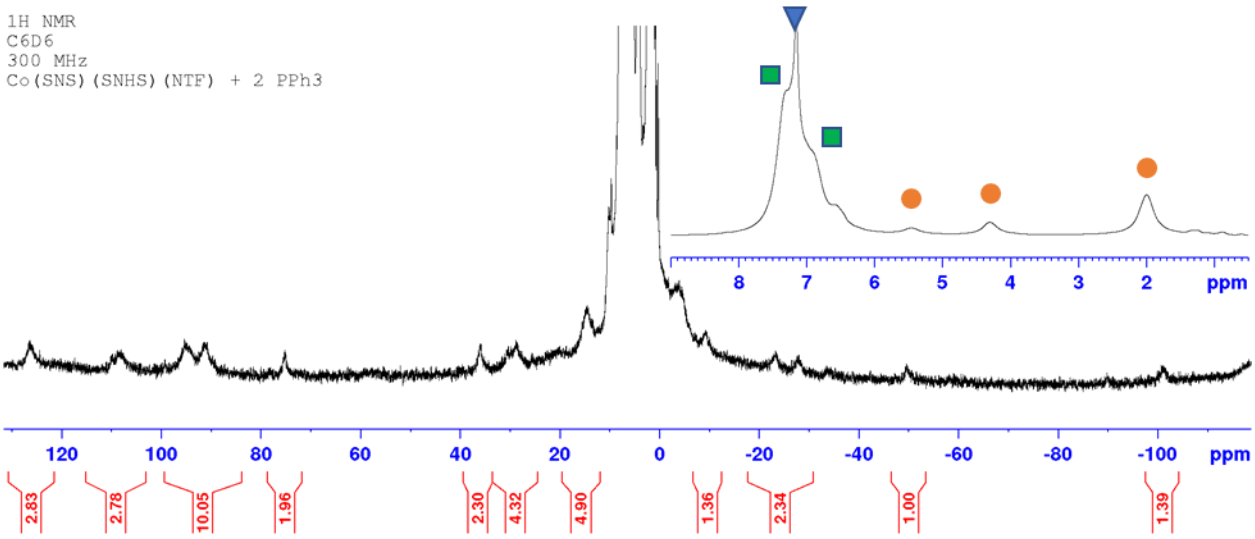

Figure 2.11: ^{1}H NMR spectrum of **2-3** with two equivalents of PPh_3 in C_6D_6 (blue triangle). $S^{Me}N^{H}S^{Me}$ (orange circles) and free PPh_3 (green squares) are also highlighted.

In an attempt to grow crystals to characterize this complex by single crystal X-ray diffraction, a saturated solution of the green complex in benzene was layered with hexanes. This caused the formation of orange-yellow crystals over a period of two days. When analyzed, these crystals were revealed to be the di-cationic pseudooctahedral species $[Co(\kappa^3\text{-}S^{Me}N^{H}S^{Me})_2](NTf_2)_2$ (**2-4**) with two equivalents of protonated SNS ligand coordinated to the metal (**Figure 2.12**). Interestingly, the SNS amine ligands in this species are coordinated *facially* to Co in contrast to the Co bis-amido complex and the Fe amido-amine cation in which they were always bound meridionally. Following protonation, the Co-N bond has lengthened from 1.967(2) Å to 2.1236(2) Å corresponding to the expected weakening of the bond. The thioether Co-S bond in the five-membered ring remains relatively unchanged going from 2.4723(7) Å to 2.4837(5) Å while that bond in the six-membered ring has contracted from 2.6481(7) Å to 2.5892(6) Å. Elongation of the Co-N bond reinforces the hypothesis that a strong enough donor would be able to displace the SNS amine ligand. This di-cationic species

may be a suitable pathway for future students to access mono-ligated SNS cobalt complexes by protonating both ligands, replacing one with an ancillary ligand and then deprotonating the SNS ligand which remains on the metal.

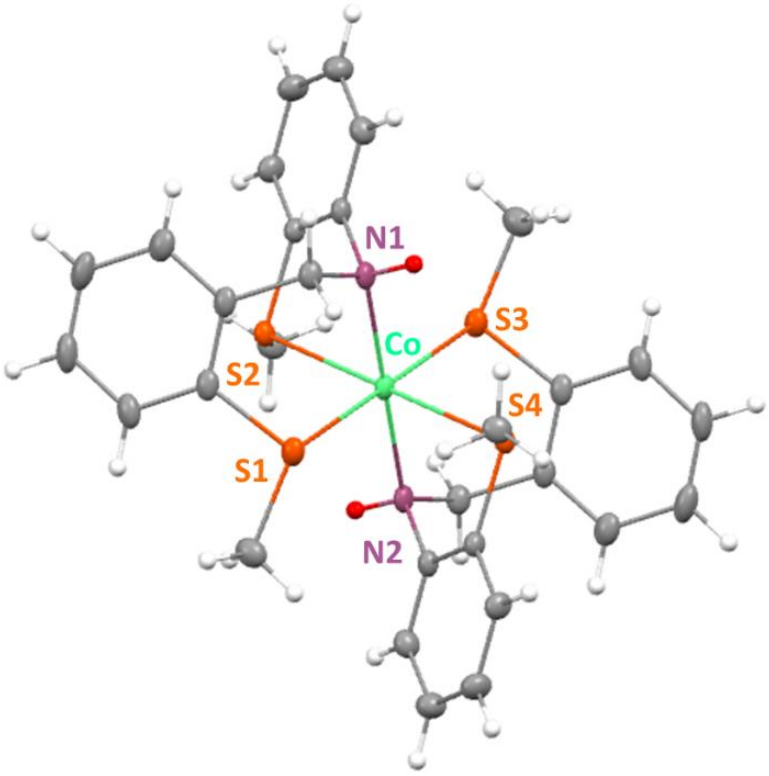

Bond	Distance
Co – S1	2.5892(6) Å
Co – S2	2.4837(5) Å
Co – N1	2.1236(2) Å
Co – S3	2.5892(6) Å
Co – S4	2.4837(5) Å
Co – N2	2.1236(2) Å
Bonds	**Angle**
N1-Co-N2	180.00°
S1-Co-S3	180.00°
S2-Co-S4	180.00°
N1-Co-S3	85.26(5)°
N1-Co-S1	94.75(5)°
N2-Co-S2	99.93(5)°
N2-Co-S4	80.07(5)°

Figure 2.12: Molecular structure of $[Co(\kappa^3\text{-}S^{Me}N^{H}S^{Me})_2](NTf_2)_2$, **2-4,** with selected bond distances and angles. Anions omitted for clarity and H atoms from protonation highlighted in red.

In an attempt to form a Co(II) mono-amido SNS complex with a hard donor ligand, the blue acetonitrile solution of **2-3** was treated dropwise with one equivalent of Bipy, again causing no immediate colour change. After stirring overnight, however, the solution had transitioned from blue to a lighter turquoise. The ^{1}H NMR spectrum revealed the formation of new paramagnetically-shifted resonances and free protonated SNS ligand, confirming formation of the new product, $[Co(\kappa^3\text{-}S^{Me}NS^{Me})(Bipy)](NTf_2)$, **2-5** (**Scheme 2.5**, **Figure 2.13**).

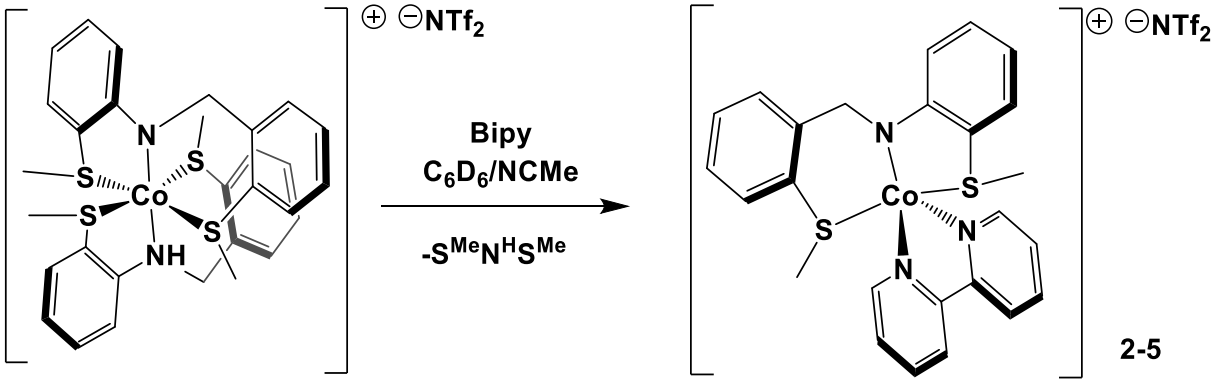

Scheme 2.5: Synthesis and proposed structure of [Co(κ^3-S^{Me}NS^{Me})(Bipy)](NTf$_2$), **2-5**.

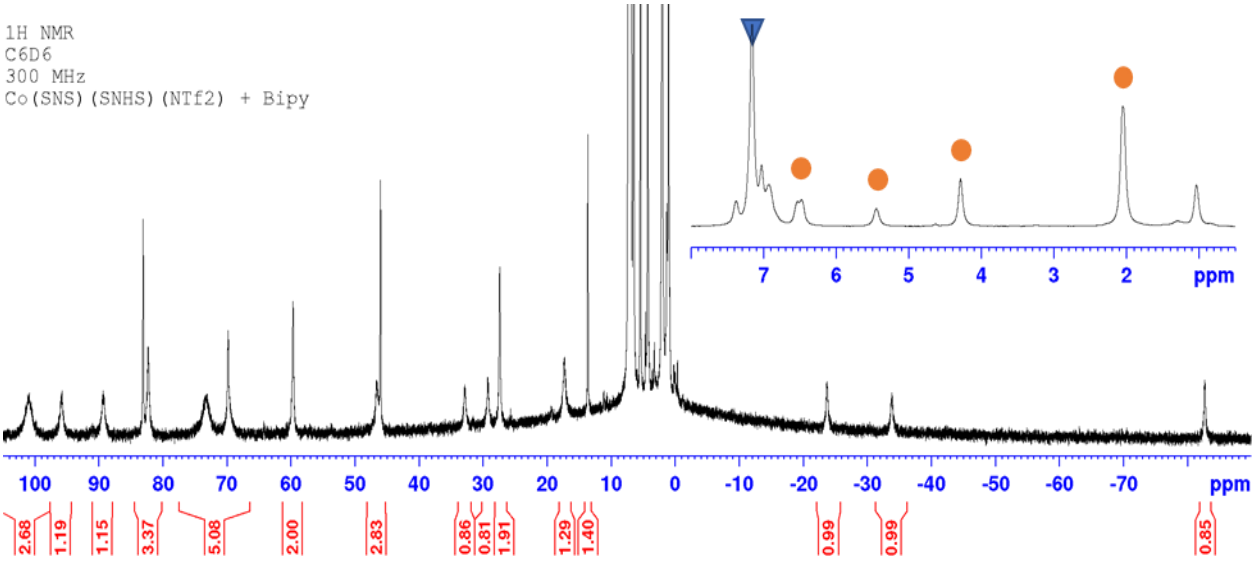

Figure 2.13: ^{1}H NMR spectrum of [Co(κ^3-S^{Me}NS^{Me})(Bipy)](NTf$_2$), **2-5** in C$_6$D$_6$ (blue triangle). S^{Me}N^{H}S^{Me} (orange circles) also highlighted.

The thiomethyl 3H resonances are seen at δ 101 and 73 ppm as these both integrate to approximately three protons and the presence of four 2H resonances suggest a 17e$^-$ trigonal bipyramidal structure with an effective mirror plane, again due to the rapid flexing of the six-membered ring on the NMR time scale.

2.5.3. Dehydrogenation of Amine-Boranes Catalyzed by Cobalt-$S^{Me}NS^{Me}$ Complexes

In order to probe the potential bifunctional reactivity of the Co bis-amido complex and its mono-amido derivatives, a series of experiments were performed to assess their activity for the catalytic dehydrogenation of ammonia-borane (AB). Purple **2-1** and twenty equiv. of AB were combined in an NMR tube and upon addition of THF instantly formed a black solution. Upon heating this solution at 60 ^{o}C for 2.5 h some hydrogen evolution was observed, accompanied by precipitation of a black solid. The ^{11}B NMR spectrum of the reaction mixture revealed almost no consumption of the AB, but some amino-and imino-borane oligomers were observed.[41] It is apparent that **2-1** is quite unstable in such a highly reducing environment.

In order to further stabilize the complex under these reaction conditions, the same experiment was performed with **2-1** and one equiv. of DMPE per Co. Addition of DMPE dissolved in THF to an NMR tube containing **2-1** and AB as solids caused the instant formation of a golden-brown solution accompanied by vigorous hydrogen evolution. Heating the NMR tube to 60 ^{o}C for 2.5 h resulted in additional hydrogen formation along with an off-white precipitate shown previously to be poly(aminoborane).

The ^{11}B NMR spectrum of the soluble products (**Figure 2.14**) showed nearly complete conversion of AB evidenced by the sharp quartet at -24 ppm. Borazine is detectable by the doublet at 29 ppm along with cross-linked borazine as the shoulder at 25 ppm. The series of overlapping signals from -10 to -14 ppm results from the formation of aminoborane oligomers, with each resonance presumably representing a different chain length. The BH_3 on the chain terminus can be identified from the

shoulder at -25 ppm due to its very similar chemical shift to AB. Interestingly, there seems to be no trace of any BH signal around -5 ppm, which is highly unusual since the formation of aminoborane oligomers is almost always accompanied by the formation of cyclic branched BH-containing products in these dehydrogenation reactions.[46] The final resonance of note is the complex signal at -40 ppm. Decoupling this signal from the neighbouring protons simplifies the resonance into what appears to be a pair of doublets with chemical shifts similar enough to overlap. The coupling constants of these two doublets are 58 and 54 Hz, which along with the chemical shift suggests that they result from a DMPE-borane complex, either DMPE●BH_3 or DMPE●$2BH_3$. This behaviour was also observed with the Fe(S^{Me}NS) and Fe(S^{Me}NC) DMPE catalyst precursors.[41] The colour of the solution at this time was still a golden brown suggesting that some of the catalyst resting state species was still intact, despite the ongoing consumption of DMPE. It is likely that with more time, the reaction could have reached completion.

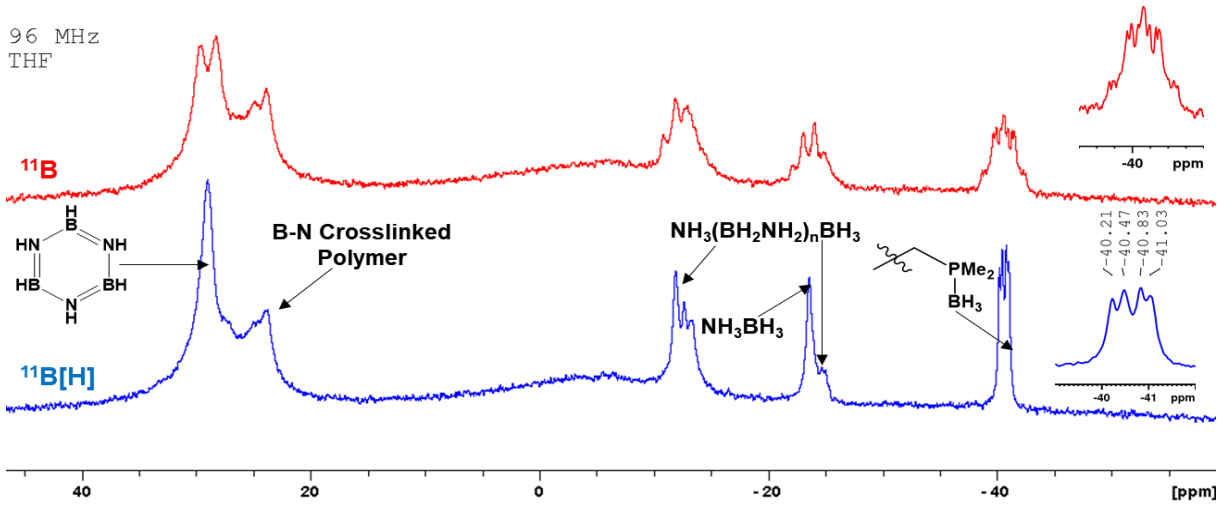

Figure 2.14: ^{11}B (red) and ^{11}B{H} (blue) NMR spectra of the catalytic dehydrogenation of AB using 5 mol% of **2-1** and 1 equiv. of DMPE at 60 ^{o}C for 2.5 h.

The ^{31}P NMR spectrum of the reaction mixture reveals several broad resonances between 70 and -50 ppm which suggest the formation of a diamagnetic Co(I) species, since coordinated phosphorus resonances are typically difficult to detect in paramagnetic compounds. The two resonances at 8.6 and 0.7 ppm correspond to P-B complexes while the resonance at -47.6 ppm is due to a dangling κ^1-DMPE. The other P must be coordinated to either BH_3 or the metal. What appears to be a small amount of free DMPE at -48 ppm is also visible (**Figure 2.15**). The presence of the resonance at 8.6 along with that at -41 ppm in the ^{11}B NMR spectrum demonstrate that Co-DMPE catalysts formed in situ are also unstable under the highly reducing reaction conditions, going on to form DMPE-borane species which presumably deactivates the catalyst. While this behaviour is similar to that of the Fe(S^{Me}NS) and (S^{Me}NC) precatalysts, this was not the case with the dehydrogenation of AB using the cationic Fe($S^{Me}NS^{Me}$)(triphos) amido complex. The NMR spectra of these reactions showed no sign of triphos consumption, indicating a stable catalyst resting state.[41]

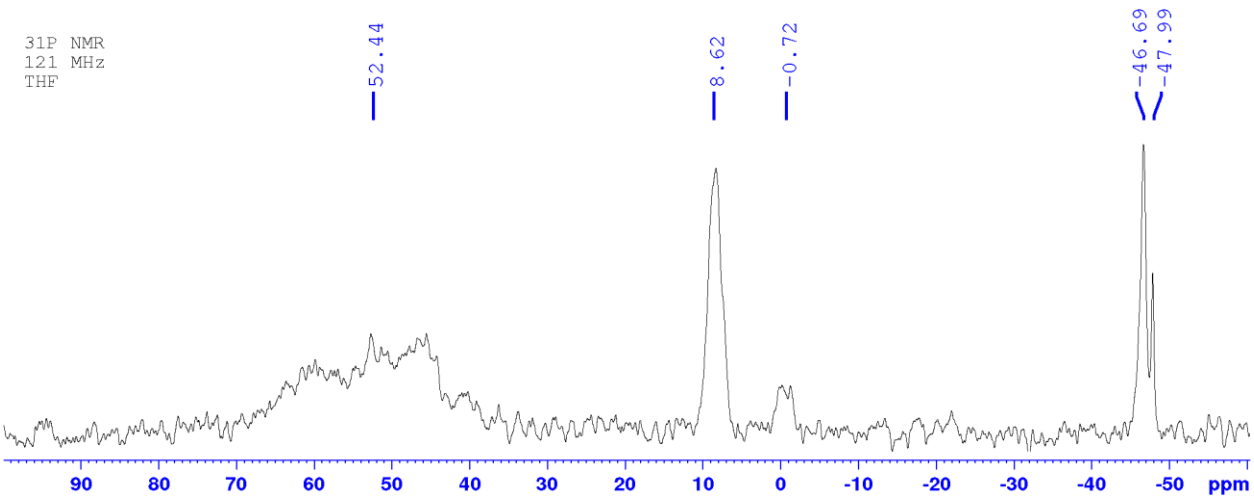

Figure 2.15: ^{31}P NMR spectrum of the catalytic dehydrogenation of ammonia-borane using 5 mol% **2-1** in the presence of 1 equiv. of DMPE after heating at 60 ^{o}C for 2.5 h.

Previous work showed that moving to methylamine-borane (MeAB) from AB as a substrate for dehydrogenation did not result in the formation of a DMPE-borane complex when using the Fe(S^{Me}NC)(DMPE) precatalyst.[41] Using this rationale, the dehydrogenation experiment was repeated with MeAB and the **2-1** DMPE precatalyst. The ^{11}B NMR spectrum showed that after 2.5 h of heating at 60 ^{o}C, a significant amount of MeAB still remained in solution. The reaction was allowed to continue for an additional 22 h during which time the MeAB was completely consumed. The ^{11}B NMR spectrum (**Figure 2.16**) reveals that using the MeAB did greatly reduce DMPE consumption as the P-B resonances at -41 ppm are much smaller than those resulting from AB. The two resonances are doublets with coupling constants similar to those observed with AB, but now one is distinctly larger, making it easier to visualize how they overlap.

Another exciting feature of the ^{11}B NMR spectrum is the remarkably high selectivity of the catalyst. The vast majority of the soluble products are in the form of 1,3,5-trimethylborazine (doublet at 31 ppm) or in the methylaminoborane trimer (triplet at -7 ppm) (**Figure 2.16**). This kind of selectivity is unprecedented in amine-borane dehydrogenation as usually there is a significant amount of methylaminoborane oligomer formation.[46] But as can be seen from the sharpness and lack of shoulders around the base of the triplet, almost none of these are being produced. There are additional unassigned resonances at 23, 21 and -20 ppm. While at first glance the signal at -20 could be assigned to MeAB, it is far too broad although some line width reduction on proton decoupling is apparent. In contrast, the two resonances at 21 and 23 ppm are not affected by proton decoupling.

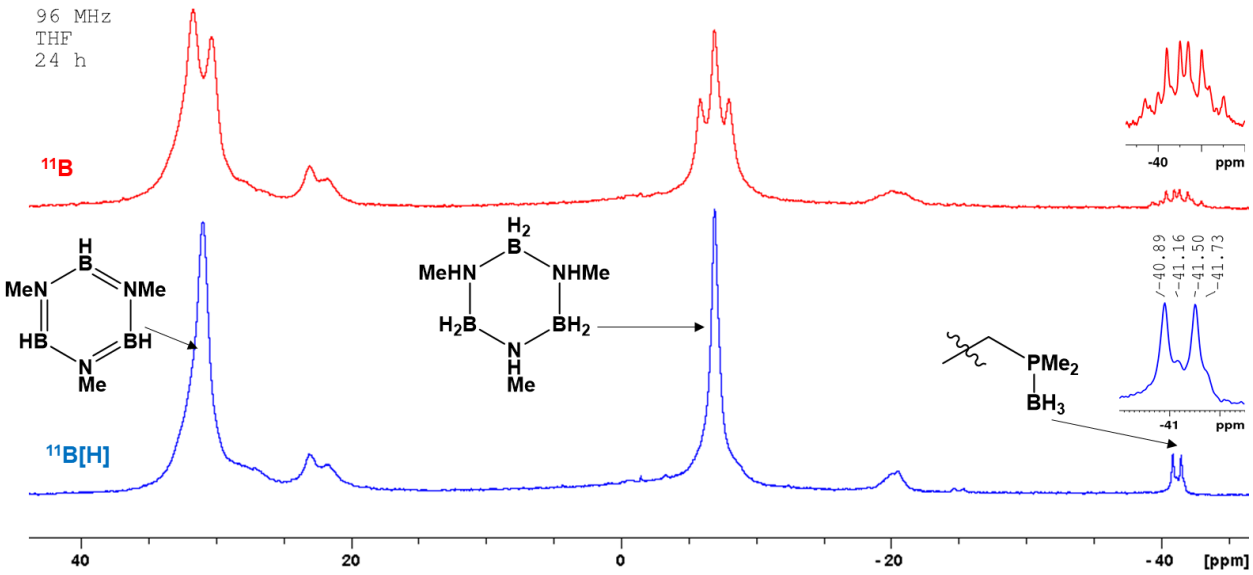

Figure 2.16: ^{11}B (red) and ^{11}B{H} (blue) NMR spectra of the catalytic dehydrogenation of MeAB using 5 mol% of **2-1** and 1 equiv. of DMPE heating at 60 ^{o}C for 24 h.

The ^{31}P NMR spectrum resembles the one acquired using AB as a substrate. Broad resonances between 70 and 40 ppm imply DMPE-Co species while free DMPE can be seen at -48 ppm. Most important however is the DMPE-borane resonance at -7.8 ppm. It is significantly smaller than its counterpart in the spectrum acquired using AB, reinforcing the catalyst resting-state's improved stability under these conditions. In line with these results, the solution after 24 h still maintained its golden-brown colouration, implying that the resting state was still alive and could presumably continue reacting should more substrate be added.

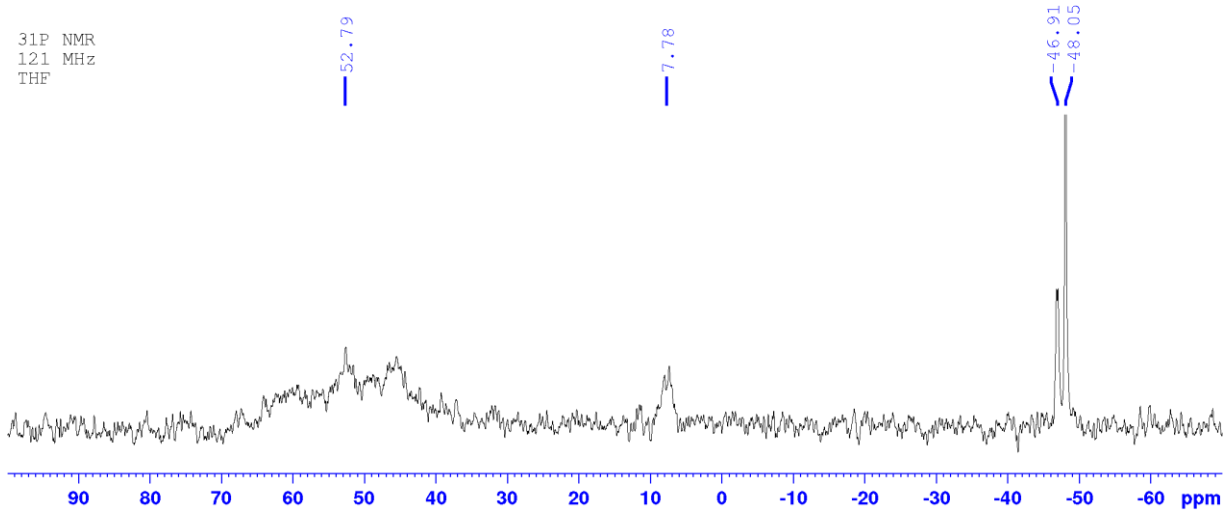

Figure 2.17: ^{31}P NMR spectrum of the catalytic dehydrogenation of MeAB using 5 mol% **2-1** in the presence of 1 equiv. of DMPE after heating at 60 ^{o}C for 24 h.

To the best of our knowledge, the only other nitrogen-containing cobalt species utilised for catalytic AB dehydrogenation is the 18e$^-$ trigonal bipyramidal cobalt(I) hydride species, (κ^4-N($CH_2CH_2PPh_2$)$_3$)CoH, prepared by Rossin *et al.*[47] This species was able to produce 1 equiv. of H_2 per equiv. of AB over the course of 48 h along with long-chain poly(aminoboranes). H_2 evolution was only observed when heating at 55 ^{o}C however, showing it to be less active than our catalyst.

It is possible that the mechanism for this reaction can proceed either through a Co(I)/Co(III) catalytic cycle or through a Co(I) bifunctional catalytic cycle. In the Co(I)/Co(III) cycle, after generation of a Co(I) active species, AB would coordinate to the metal through η^2 coordination of the BH_3 end of the AB. The B-H bond could then be activated *via* oxidative addition, forming a boryl ligand and a cobalt hydride. Beta-hydride elimination then releases the BH_2NH_2 monomer and reductive elimination of the two hydride ligands releases H_2, regenerating the active species (**Scheme 2.6 a)**). While this behaviour has been observed with cobalt group member rhodium,[46] it is less

likely to occur with the first-row transition metal. A concerted bifunctional mechanism where the B-H bond is activated by cobalt and the N-H bond is activated by the amido SNS ligand, is more likely (**Scheme 2.6 b)**). As the slow step is likely to be the B-H activation in route a) and H_2 loss in route b) the observation of a hydride signal at -14.4 ppm in the ^{1}H NMR spectrum after MeAB dehydrogenation (**Figure S1, Appendix**) is more consistent with a bifunctional mechanism.

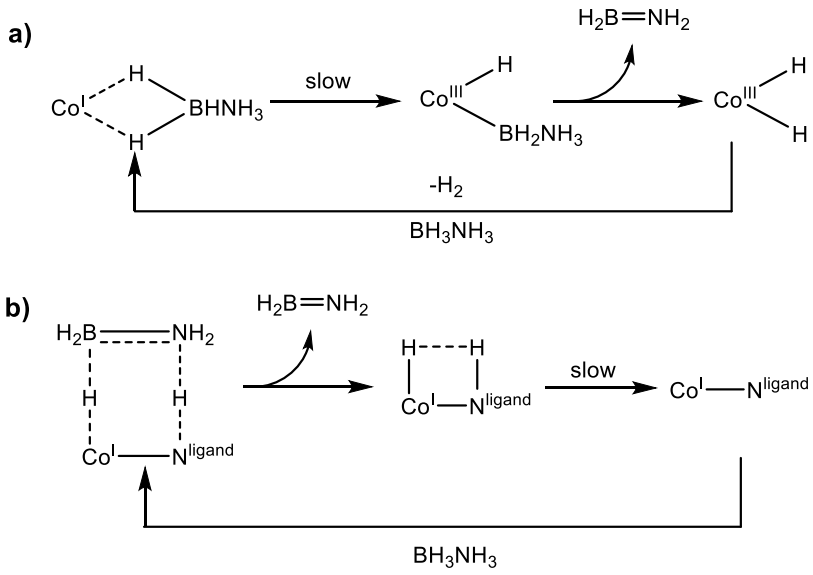

Scheme 2.6: Possible mechanisms for AB dehydrogenation.

Following formation of the BH_2NH_2 monomer, the cobalt-hydride species is also suspected to catalyze the polymerization of these monomers (**Scheme 2.7**). DFT studies of the POP iridium hydride catalyst by Bhunya *et al.* suggest that after Ir-H coordination to the BH_2 end of the aminoborane monomer frees up the nitrogen lone pair for attack on a second monomer.[48] Formation of this new B-N bond again releases the adjacent nitrogen lone pair for attack on a third monomer, etc. The very low activation barrier (3.3 kcal/mol) makes polymerization kinetically favorable compared to

the formation of cyclic chains, although polymer growth is limited by the number of BH_2NH_2 monomers generated in solution, which is the slower of the two reactions.

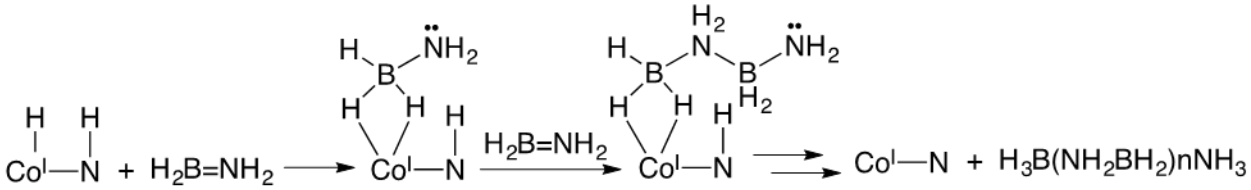

Scheme 2.7: Possible aminoborane polymerization pathway.

What remains to be seen is why, when substituting AB for MeAB, the selectivity suddenly switches to cyclic products. The cyclohexane analogue, 1,3,5-methylcyclo-triborazane, is the result of trimerization of BH_2NHMe in solution, which may suggest that the additional steric interaction from the methyl group may disfavour the approach of the monomer towards the metal, preventing polymerization. Such a small steric interaction from the relatively small methyl group, however, cannot completely account for the lack of oligomers since oligomerization has been observed with MeAB for a number of other catalysts.[41] In our case there may be a role for the proximate Co-NH that could prevent chain growth before it even gets started in the case of MeAB but not AB. Further study is required to better understand the selectivity that has been observed using the Co SNS DMPE catalyst.

2.6. Conclusions

In conclusion, we showed that reactions of our anionic amido ligand with mono-, di- and even tri-valent cobalt precursors all led to the formation of the pseudo-octahedral $19e^-$ cobalt(II) bis-amido complex, **2-1**. Electrochemical studies confirmed the extreme water sensitivity of **2-1** but persistent efforts by our collaborators eventually

identified a quasi-reversible oxidation to the Co(III) d^6 cation. The use of cationic silver in THF may be a suitable oxidant for future students to access this presumably diamagnetic complex that may be less water-sensitive if the cationic charge reduces the basicity of the amido N.

As the molecular structure of **2-1** showed similar Co-S bond elongation in the six-membered rings, we expected to obtain ligand adducts in a similar manner to those for the Fe analog. Instead we found that Bipy was unreactive and phosphines and π-acceptor isocyanide ligands induced redox processes that were accompanied by loss of the protonated $S^{Me}N^{H}S^{Me}$ ligand. In order to more cleanly effect the loss of one protonated ligand we were able to isolate the Co amido-amine cation, **2-2** as a poorly soluble green solid that upon dissolution in acetonitrile afforded the blue Co amido complex as an acetonitrile adduct, **2-3**. Although we were able to substitute the acetonitrile with PPh_3, attempted recrystallization gave ligand redistribution, revealing the unprecedented molecular structure of di-protonated $[Co(S^{Me}N^{H}S^{Me})_2](NTf_2)_2$, **2-4**, in which both SNS ligands are now facially coordinated to cobalt. In spite of further efforts, only with the hard ligand Bipy were we able to isolate a mono-amido product, namely $[Co(S^{Me}NS^{Me})(Bipy)](NTf_2)$, **2-5**.

Probing the ability of **2-1** as a precatalyst for AB dehydrogenation revealed that it is unstable under these reducing conditions. Performing the catalysis in the presence of one equivalent on DMPE resulted in better activity but poor selectivity as a mixture of cyclics and polymers were observed. Moreover, formation of DMPE-borane was indicative of catalyst decomposition. Changing the substrate to MeAB showed a

decrease in reactivity but a much more selective reaction which suddenly favour the formation of almost only cyclic compounds, with less catalyst decomposition.

The fundamental differences observed here between iron and cobalt SNS amido complexes have introduced cobalt's role in the "oxidation state roulette" referred to in the title of this thesis. In the next Chapter we compare the chemistry and reactivity of the Co SNS amido complexes with their SNS thiolate counterparts.

2.7. Experimental

2.7.1. General Considerations

All experiments were conducted under nitrogen using an MBraun glovebox unless otherwise stated. All solvents were deoxygenated/dried by purging with nitrogen on a column of activated alumina using a J. C. Meyer solvent purification system. Deuterated benzene was prepared by purging with nitrogen then letting the liquid stand over activated alumina overnight. Deuterated acetonitrile was prepared by purging with nitrogen and then refluxing over CaH_2 overnight which was followed by distillation of the solvent the next day. All solvents were stored over activated 4 Å molecular sieves. Glassware was always oven-dried for at least 4 h at 150 ^{o}C before shipping into the glovebox. The following chemicals were purchased and used as is from the following suppliers: 2-(methylthio)benzaldehyde (Aldrich, 90%), 2-methylthioaniline (Alfa Aesar, 98%), ammonia-borane (Aldrich, 90%), dimethylamine-borane (Aldrich, 97%), bipyridine (Aldrich, 98%), 2,6-methylphenyl isonitrile (Aldrich, 96%), 1,2-bis(dimethylphosphino)-ethane (Strem, 98%), triphenylphosphine (Oakwood, 99%) trifluoromethanesulfon-amide (Alfa Aesar, 96%). ^{1}H, ^{11}B, ^{19}F, ^{31}P NMR spectra were all collected on a 300 MHz

Bruker Avance or Avance II instrument. Proton spectra were referenced against the residual solvent signal, boron spectra were referenced against the borazine signal at 29 ppm or the 1,3,5-methylborazine signal at 31 ppm and phosphorus was referenced against an external H_3PO_4 standard at 0 ppm. Single-crystal X-ray diffraction studies were performed by Dr. Bulat Gabidullin at the University of Ottawa or Dr. Thierry Maris at the Université de Montréal.

2.7.2. Synthesis of $S^{Me}N^{H}S^{Me}$

2-(methylthio)benzaldehyde (1.7 mL, 13.14 mmol) and 2-(methylthio)aniline (1.8 mL, 14.45 mmol) were added to a 100 mL round bottom Schlenk flask followed by the addition of 20 mL of dry ethanol. The resulting brown solution was shipped out of the glovebox and refluxed under nitrogen for 18 h. After this the reaction mixture was cooled in a freezer at -35 ^{o}C overnight which caused the precipitation of a yellow solid: 2-(2-methylthiobenzylidene) methylthioaniline. This product was filtered with cold ethanol and dried *in vacuo* before shipping into the glovebox. Yield: 3.30 g, 92% based on 2-(methyl)thiobenzaldehyde. No further workup was required. ^{1}H NMR (300 MHz, C6D6 at 25 ^{o}C) δ 1.88 (s, 3H, S–Me), 2.02 (s, 3H, S–Me), 6.84-7.01 (m, 7H, Ar–H), 8.41 (d, 1H, Ar–H), 9.02 (s, 1H, N=C–H). 13C NMR (101 MHz, C6D6) δ 14.54 (CH3), 16.71 (CH3), 117.90 (Ar–C), 125.03 (Ar–C), 125.38 (Ar–C), 125.84 (Ar–C), 126.64 (Ar–C), 127.97 (Ar–C), 129.61 (Ar–C), 131.49 (Ar–C), 135.05 (Ar–C), 135.29 (Ar–C), 141.12 (Ar–C), 150.14 (Ar–C), 157.62 (N=C).

The yellow powder was used directly in the second step without any further purification. 2-(2-methylthiobenzylidene) methylthioaniline (2 g, 7.32 mmol) was added to a 100 mL ampoule with four equivalents of ammonia-borane (0.9 g, 58.56 mmol) and

a stir bar. 20 mL of THF was added to form a bight yellow solution with a suspension of ammonia-borane. The ampoule was sealed and removed from the glovebox to be heated in an oil bath at 65 ^{o}C for 20 h. The next day the colour had disappeared and a white suspension was visible. THF was removed using vacuum and the residue was purified using column chromatography (hexanes: ethyl acetate, 4:1) to afford an off-white solid. Yield 1.71 g, 84 % based on 2-(2-methylthiobenzylidene) methylthioaniline. ^{1}H NMR (300 MHz, C_6D_6 at 25 ^{o}C) δ 1.96 (s, 3H, S–Me), 2.00 (s, 3H, S–Me), 4.29 (d, 2H, 3*J* = 5.9 Hz, –CH2), 5.46 (t, 1H, 3*J* = 5.9 Hz, N–H), 6.53 (dd, 1H, Ar–H), 6.59 (td, 1H, Ar–H), 6.89 (m, 1H, Ar–H), 6.99 (m, 3H, Ar–H), 7.23 (dq, 1H, Ar–H), 7.48 (dd, 1H, Ar–H). ^{13}C NMR (101 MHz, C_6D_6) δ 15.36 (CH_3), 18.13 (CH_3), 46.12 (N–C), 110.94 (Ar–C), 117.67 (Ar–C), 120.32 (Ar–C), 125.29 (Ar–C), 125.99 (Ar–C), 127.88 (Ar–C), 127.94 (Ar–C), 130.04 (Ar–C), 134.89 (Ar–C), 137.24 (Ar–C), 137.51 (Ar–C), 148.71 (Ar–C).

2.7.3. Synthesis of Tris(triphenylphosphine) Cobalt Chloride (Improved synthesis from literature report)[33]

Anhydrous cobalt(II) chloride (1.65 g, 12.7 mmol) was added to a 500 mL two-necked round bottom Schlenk flask with a large stir bar. Triphenylphosphine (10.0 g, 38.1 mmol, 3 equiv.) was ground into a fine powder and combined with the cobalt chloride. Zinc powder (3.0 g, 46 mmol, excess) was added to a solid addition funnel which was attached to one neck of the round bottom flask. The flask was then sealed with a stopper and shipped out of the glovebox to the Schlenk line. On the line, the stopper was replaced under positive nitrogen pressure with a septum and dried ethanol was added *via* cannula transfer with stirring. This resulted in an electric blue solution with suspended PPh_3. This was stirred vigorously at 35 ^{o}C for one hour under positive

nitrogen pressure vented into an oil bubbler. After one hour, the solid addition funnel was tipped, adding the zinc to the reaction mixture which was removed from the oil bath and allowed to stir vigorously for 3 h or until the PPh_3 was no longer visible. This gradually caused precipitation of a green solid from the blue solution. Aqueous HCl (6 M, 150 mL) was deoxygenated by nitrogen purge and added through canula transfer, quenching the reaction and forming hydrogen gas. The mixture was stirred for an additional hour or until gas ceased evolving. The green powder was then stable when exposed to air and recovered by filtration using a 30 mL frit with suction. The solid was then washed with distilled water (100 mL), ethanol (99%, 100 mL) and hexanes (100 mL) (solvents were not deoxygenated). The green powder was dried *in vacuo,* shipped into the glovebox overnight and stored in the freezer to avoid thermal decomposition. Yield 6.2 g, 56 % based on cobalt chloride. ^{1}H NMR (300 MHz C_6D_6 at 25^{o}C) δ 9.98 (br s, 6H, Ph-H, ortho/meta), 2.72 (br s, 6H, Ph-H, ortho/meta) and 0.72 (br s, 3H, Ph-H, para).

2.7.4. Synthesis of Cobalt Bis(trimethylsilylimide) (Improved synthesis from literature report) [34]

Anhydrous cobalt(II) chloride (1.30 g, 10 mmol) was weighed out and put into a round-bottom Schlenk flask charged with a magnetic stir bar. Lithium bis(trimethylsilyl)-amide (3.30 g, 20 mmol, 2 equiv.) was weighed out separately and dissolved in 20 mL of THF to form a colourless solution. This solution was added dropwise over the course of five minutes to the blue powder while stirring vigorously, causing a gradual colour change to an olive green. After the addition was complete the solution was left to stir for 16 h at 50 ^{o}C. The next day the THF was removed *in vacuo* from the green solution

yielding a green gel that was then dissolved in DEE and filtered through Celite using a medium porosity frit. This filtration caught a grey solid (LiCl) while the green filtrate was dried to a green crystalline powder of $Co(N(SiMe_3)_2)_2$. Yield: 3.69 g, 92%. ^1H NMR (300 MHz, C_6D_6 at 25 ^oC) δ -17.0 (br ,16H, Si-CH_3).

2.7.5. Synthesis of $Co(\kappa^3\text{-}S^{Me}NS^{Me})_2$, **2-1**

Cobalt(II) bis(trimethylsilylimide) (364 mg, 0.8 mmol) and $S^{Me}N^HS^{Me}$ (453 mg, 1.6 mmol, 2 equiv.) were combined as solids in a vial. The vial was charged with a stir bar and DEE, instantly forming a purple solution. After, stirring overnight at room temperature a purple solid precipitated and the solution was stored at -35 ^oC overnight to maximize precipitation. The cold suspension was then passed through Celite using a medium porosity frit, catching the purple solid which was then washed with 15 mL of DEE in three equal portions. The purple solid was then extracted with DCM, filtered and the solvent removed *in vacuo* yielding a bright purple powder which was used without further purification. Yield 475 mg, 92 %. Crystals suitable for single-crystal X-ray diffraction were grown from a saturated solution of THF layered with hexanes at -30 ^oC. ^1H NMR (300 MHz, C_6D_6 at 25 ^oC) δ 113.43 (br s, 3H, SCH_3), 63.69 (br s, 1H), 48.73 (br s, 3H, SCH_3), 41.04 (br s, 1H), 15.57 (br s, 1H), 3.64 (br s, 1H), -1.42 (br s, 1H), -16.58 (br s, 1H), and -48.73 (br s, 1H).

2.7.6. Probing Hemilability of **2-1** with Bipy or CNAr

$Co(\kappa^3\text{-}S^{Me}NS^{Me})_2$, **2-1**, (5 mg, 0.008 mmol) was weighed out in a vial and dissolved in C_6D_6 to form a purple solution. In a separate vial, the ancillary ligand Bipy (1.3 mg, 0.008 mmol, 1 equiv.) or CNAr (2 mg, 0.016 mmol, 2 equiv.) was weighed out

and dissolved in C_6D_6 to both form clear solutions. These clear solutions were then added dropwise to the stirring purple solution which resulted in no colour change in the case of Bipy and the colour transitioning to a dark brown in the case of CNAr. Samples of each solution were transferred into NMR tubes for ^{1}H NMR analysis.

2.7.7. Probing Hemilability of **2-1** with DMPE

$Co(\kappa^3\text{-}S^{Me}NS^{Me})_2$, **2-1**, (9 mg, 0.015 mmol) was weighed out in a vial and dissolved in C_6D_6 to form a purple solution. In a separate vial, DMPE (2.5 µL, 0.015 mmol, 1 equiv.) was measured out using a microsyringe and dissolved in C_6D_6 already present in a separate vial. This clear solution was then added to the purple solution dropwise with stirring initially with no colour change. A sample of the solution was added to an NMR tube to monitor the reaction. The colour transitioned from purple to dark-brown over the course of 16h.

2.7.8. Protonation of $Co(\kappa^3\text{-}S^{Me}NS^{Me})_2$, **2-1**

$Co(\kappa^3\text{-}S^{Me}NS^{Me})_2$, **2-1**, (30 mg, 0.05 mmol) was weighed out in a vial and dissolved in C_6D_6 to form a purple solution. In a separate vial, triflimde ($HNTf_2$, 14 mg, 0.05 mmol, 1 equiv.) was weighed out and dissolved in C_6D_6 to form a colourless solution. This solution was then added dropwise to the purple solution with stirring which caused the gradual transition to a green solution with green solid forming on the side. Upon completing the addition of the second solution, the green suspension was allowed to stir for 5 min after which CD_3CN (0.5 mL, excess) was added causing the solid to instantly dissolve and form a blue solution. A sample was extracted for analysis by NMR. ^{1}H NMR (300 MHz, CD_3CN at 25 ^{o}C) δ 97.40 (br s, 3H, SCH_3), 77.00 (br s, 1H,

Ar-H), 51.87 (br s, 3H, SCH_3), 34.80 (br s, 2H, CH_2), 3.75 (br s, 1H, Ar-H), -7.80 (br s, 1H, Ar-H), -34.51 (br s, 1H, Ar-H), -88.73 and (br s, 1H, Ar-H). ^{19}F NMR (282.4 MHZ, CD_3CN at 25 ^oC) δ -80.27 (s, $^-N(SO_2CF_3)_2$).

In a third vial, Bipy (8 mg, 0.05 mmol, 1 equiv.) was weighed out and dissolved in C_6D_6 forming a colourless solution which was then added dropwise to the blue solution. This initially caused no colour change but stirring overnight resulted in a transition to a lighter turquoise colour. A sample of the solution was extracted into an NMR tube for analysis. ^1H NMR (300 MHz, C_6D_6 at 25 ^oC) δ 100.99 (br s, 3H, SCH_3), 95.83 (br s, 1H, Ar-H), 89.33 (br s, 1H, Ar-H), 83.11 (s, 1H, Ar-H), 82.34 (br s, 2H), 73.27 (br s, 3H, SCH_3), 69.87 (br s, 2H, CH_2), 59.71 (br s, 2H, Bipy-H), 46.63 (br s, 1H, Ar-H), 46.02 (s, 2H, Bipy-H), 32.90 (br s, 1H, Ar-H), 29.35 (br s, Ar-H), 27.42 (br s, 2H, Bipy-H), 17.34 (br s, 1H, Ar-H), 13.66 (br s, 1H, Ar-H), -23.70 (br s, 1H), -33.80 (br s, 1H) and -82.6 (br s,1H). ^{19}F NMR (300 MHz, C_6D_6 at 25 ^oC) δ -79.26 (s, $^-N(SO_2CF_3)_2$).

2.7.9. Catalyzed Dehydrogenation of Ammonia-Borane

In an NMR tube, purple **2-1** (5 mg, 0.008 mmol) and colourless ammonia-borane (5 mg, 0.16 mmol, 20 equiv.) were weighed out as solids and 0.5 mL of THF (dried over activated alumina) was added, instantly forming a black solution. The NMR tube was sealed and heated to 60 ^oC in an oil bath and left for 2.5 h during which a black precipitate crashed out of solution and some hydrogen evolution was observed. After 2.5 h, ^{11}B and ^{11}B {H} NMR spectra were acquired to monitor the progress of the reaction.

For experiments performed in the presence of DMPE, purple **2-1** (5 mg, 0.008 mmol) and colourless ammonia-borane (5 mg, 0.16 mmol, 20 equiv.) or methylamine-borane (7.4 mg, 0.16 mmol, 20 equiv.) were weighed out as solids in an NMR tube. In a separate vial, 0.5 mL of THF was measured out and DMPE (1.3 µL, 0.008 mmol, 1 equiv.) was added. After quickly stirring, this solution was added to the NMR tube containing the solids causing the instant formation of a brown solution with significant hydrogen evolution being observed. The NMR tube was sealed and heated at 60 ^{o}C in an oil bath for 2.5 h during which a white precipitate gradually formed at the bottom of the NMR tube. Hydrogen evolution was observed for most of the heating time. After 2.5 h, ^{11}B, ^{11}B{H} and ^{31}P NMR spectra were acquired.

2.8. References

(1) Gordon, J. C.; Kubas, G. J. *Organometallics* **2010**, *29* (21), 4682–4701.

(2) Lubitz, W.; Ogata, H.; Rüdiger, O.; Reijerse, E. *Chem. Rev.* **2014**, *114* (8), 4081–4148.

(3) Kubas, G. J. *Chem. Rev.* **2007**, *107* (10), 4152–4205.

(4) Fontecilla-Camps, J. C.; Volbeda, A.; Cavazza, C.; Nicolet, Y. *Chem. Rev.* **2007**, *107* (10), 4273–4303.

(5) Doucet, H.; Ohkuma, T.; Murata, K.; Yokozawa, T.; Kozawa, M.; Katayama, E.; England, A. F.; Ikariya, T.; Noyori, R. *Angew. Chem. - Int. Ed.* **1998**, *37* (12), 1703–1707.

(6) Dub, P. A.; Gordon, J. C. *Dalton Trans.* **2016**, *45* (16), 6756–6781.

(7) Ohkuma, T.; Ooka, H.; Hashiguchi, S.; Ikariya, T.; Noyori, R. *J. Am. Chem. Soc.* **1995**, *117* (9), 2675–2676.

(8) Zhang, G.; Vasudevan, K. V.; Scott, B. L.; Hanson, S. K. *J. Am. Chem. Soc.* **2013**, *135*, 8668–8681.

(9) Blaquiere, N.; Diallo-Garcia, S.; Gorelsky, S. I.; Black, D. A.; Fagnou, K. *J. Am. Chem. Soc.* **2008**, *130* (43), 14034–14035.

(10) Baker, R. T.; Gordon, J. C.; Hamilton, C. W.; Henson, N. J.; Lin, P.; Maguire, S.; Murugesu, M.; Scott, B. L.; Smythe, N. C. *J. Am. Chem. Soc.* **2012**.

(11) Marziale, A. N.; Friedrich, A.; Klopsch, I.; Drees, M.; Celinski, V. R.; Schmedt Auf Der Günne, J.; Schneider, S. *J. Am. Chem. Soc.* **2013**, *135* (36), 13342–13355.

(12) Ruddy, A. J.; Kelly, C. M.; Crawford, S. M.; Wheaton, C. A.; Sydora, O. L.; Small, B. L.; Stradiotto, M.; Turculet, L. *Organometallics* **2013**, *32* (19), 5581–5588.

(13) Ruddy, A. J.; Sydora, O. L.; Small, B. L.; Stradiotto, M.; Turculet, L. *Chem. - Eur. J.* **2014**, *20*, 13918–13922.

(14) Gunanathan, C.; Milstein, D. *Acc. Chem. Res.* **2011**, *44* (8), 588–602.

(15) Gunanathan, C.; Milstein, D. *Chem. Rev.* **2014**, *114* (24), 12024–12087.

(16) Werkmeister, S.; Junge, K.; Beller, M. *Org. Process Res. Dev.* **2014**, *18* (2), 289–302.

(17) Sellmann, D.; Prakash, R.; Heinemann, F. W.; Moll, M.; Klimowicz, M. *Angew. Chem. - Int. Ed.* **2004**, *43* (14), 1877–1880.

(18) Hirotsu, M.; Santo, K.; Tanaka, Y.; Kinoshita, I. *Polyhedron* **2018**, *143*, 201–208.

(19) Roy, N.; Sproules, S.; Weyhermu, T.; Wieghardt, K. *Inorg. Chem.* **2009**, *48*, 3783–3791.

(20) Singh, P.; Singh, A. K. *Organometallics* **2010**, *29* (23), 6433–6442.

(21) Miecznikowski, J. R.; Lo, W.; Lynn, M. A.; Jain, S.; Keilich, L. C.; Kloczko, N. F.; O'Loughlin, B. E.; Dimarzio, A. P.; Foley, K. M.; Lisi, G. P.; et al. *Inorg. Chim. Acta* **2012**, *387*, 25–36.

(22) Bassetti, M. *Eur. J. Inorg. Chem.* **2006**, *0* (22), 4473–4482.

(23) Bassetti, M.; Capone, A.; Salamone, M. *Organometallics* **2004**, *23* (2), 247–252.

(24) Braunstein, P.; Naud, F. *Angew. Chem. - Int. Ed.* **2001**, *40* (4), 680–699.

(25) Koizumi, T. A.; Teratani, T.; Okamoto, K.; Yamamoto, T.; Shimoi, Y.; Kanbara, T. *Inorg. Chim. Acta* **2010**, *363* (11), 2474–2480.

(26) Shaffer, D. W.; Szigethy, G.; Ziller, J. W.; Heyduk, A. F. *Inorg. Chem.* **2013**, *52* (4), 2110–2118.

(27) Ye, S.; Sarkar, B.; Lissner, F.; Schleid, T.; Van Slageren, J.; Fiedler, J.; Kaim, W. *Angew. Chem. - Int. Ed.* **2005**, *44*, 2103–2106.

(28) Hübner, R.; Weber, S.; Strobel, S.; Sarkar, B.; Záliš, S.; Kaim, W. *Organometallics* **2011**, *30*, 1414–1418.

(29) Noveron, J. C.; Olmstead, M. M.; Mascharak, P. K. *Inorg. Chem.* **1998**, *37* (6), 1138–1139.

(30) Xiao, J.; Deng, L. *Organometallics* **2012**, *31* (1), 428–434.

(31) Das, U. K.; Daifuku, S. L.; Iannuzzi, T. E.; Gorelsky, S. I.; Korobkov, I.; Gabidullin, B.; Neidig, M. L.; Baker, R.T.. *Inorg. Chem.* **2017**, *56* (22), 13766–13776.

(32) McGuinness, D. S.; Wasserscheid, P.; Keim, W.; Morgan, D.; Dixon, J. T.; Bollmann, A.; Maumela, H.; Hess, F.; Englert, U. *J. Am. Chem. Soc.* **2003**, *125* (18), 5272–5273.

(33) Aresta, M.; Rossi, M.; Sacco, A. *Inorg. Chim. Acta* **1969**, *3* (2), 227–231.

(34) Bryan, A. M.; Long, G. J.; Grandjean, F.; Power, P. P. *Inorg. Chem.* **2013**, *52*, 12152–12160.

(35) Grant, G. J.; Shoup, S. S.; Hadden, C. E.; VanDerveer, D. G. *Inorg. Chim. Acta* **1998**, *274* (2), 192–200.

(36) Singh, A. K.; Mukherjee, R. *J. Chem. Soc. Dalton Trans.* **2008**, *0* (2), 260–270.

(37) Sharrad, C. A.; Cavigliasso, G. E.; Stranger, R.; Gahan, L. R. *J. Chem. Soc. Dalton Trans.* **2004**, *4* (8), 1166–1172.

(38) Cowley, R. E.; Bontchev, R. P.; Sorrell, J.; Sarracino, O.; Feng, Y.; Wang, H.; Smith, J. M. *J. Am. Chem. Soc.* **2007**, *129*, 2424–2425.

(39) Whited, M. T.; Rivard, E.; Peters, J. C. *Chem. Commun.* **2006**, *0*, 1613–1615.

(40) Connelly, N. G.; Geiger, W. E. *Chem. Rev.* **1996**, *96* (2), 877–910.

(41) Das, U.K. *Iron Chemistry of Hemilabile SNS Ligands: Synthesis, Reactivity, and Catalytic Applications,* Ph.D. Dissertation, University of Ottawa, ON, **2018**.

(42) Komarsamy, L. *Application of cobalt complexes containing SNS ligands as catalysts for biomimetic paraffin* activation. M.Sc. Dissertation, University of KwaZulu-Natal, Durban, South Africa, **2012**.

(43) Naicker, D.; Friedrich, H. B.; Omondi, B. *RSC Adv.* **2015**, *5* (77), 63123–63129.

(44) Hu, L.; Chen, H. *ACS Catal.* **2017**, *7* (1), 285–292.

(45) Estes, D. P. *Transition Metal Hydrides that Mediate Catalytic Hydrogen Atom Transfers,* Ph.D. Dissertation, Columbia University, New York, USA, **2014**.

(46) Johnson, H. C.; Hooper, T. N.; Weller, A. S. *The Catalytic Dehydrocoupling of Amine-Boranes and Phosphine-Boranes,* In E. Fernandez, A. Whiting (Eds.) *Synthesis and Application of Organoboron Compounds*; **2015**; pp 153–216.

(47) Todisco, S.; Luconi, L.; Giambastiani, G.; Rossin, A.; Peruzzini, M.; Golub, I. E.; Filippov, O. A.; Belkova, N. V.; Shubina, E. S. *Inorg. Chem.* **2017**, *56* (8), 4296–4307.

(48) Bhunya, S.; Malakar, T.; Paul, A. *Chem. Comm..* **2014**, *50* (44), 5919–5922.

Chapter 3: Cobalt Reactions with the SNS Thiolate Ligand

3.1. Introduction

Many ligands envisioned for the purposes of bifunctional catalysis have been designed with a nitrogen donor group acting as a proton acceptor due to its strong Brønsted basicity. While this has resulted in a number of successful ligand systems, sulphur in the form of its thiolate functionality also has a reactive lone pair that can serve as a Brønsted base for bifunctional substrate activation. Sulphur is in fact much more prevalent in metalloenzyme chemistry and is well known to be important in the bifunctional activation of substrates in [FeNi]-hydrogenases,[1–5] nitrile hydratases,[6–8] superoxide reductases[9–11] and cysteine dioxygenases.[12,13] All of these systems contain a combination of thiolate and N-donor groups which are responsible for catalyzing many biologically important transformations. Additionally, thiolates typically form stronger bonds to metals than other sulphur functional groups and can serve as terminal or bridging ligands allowing them to form mononuclear or multinuclear compounds. As such, incorporation of thiolate moieties into bifunctional ligand design can be advantageous towards the development of ligands which aim to mimic the reactivity that is observed in nature.

A number of thiolate and nitrogen containing pincer ligands have already been developed for the purposes of bifunctional catalysis. Some examples of the variety of ligands that exist are [$O^{-}NS^{-}$],[14] [$S^{-}N^{R}S^{-}$],[15] [$S^{-}N^{-}S^{-}$],[16] [$N^{R}N^{R}S^{-}$],[17] [$N^{R}N^{-}S^{-}$],[18] [$N^{R}C^{-}S^{-}$][19] and [$S^{R}NS^{-}$][20] which are illustrated in **Figure 3.1** below. These ligands have been paired to a variety of transition metals including nickel, iron, chromium and tungsten to name a

few. Despite their prevalence throughout the literature, few studies of the bifunctional reactivity of thiolate-containing complexes have been carried out.

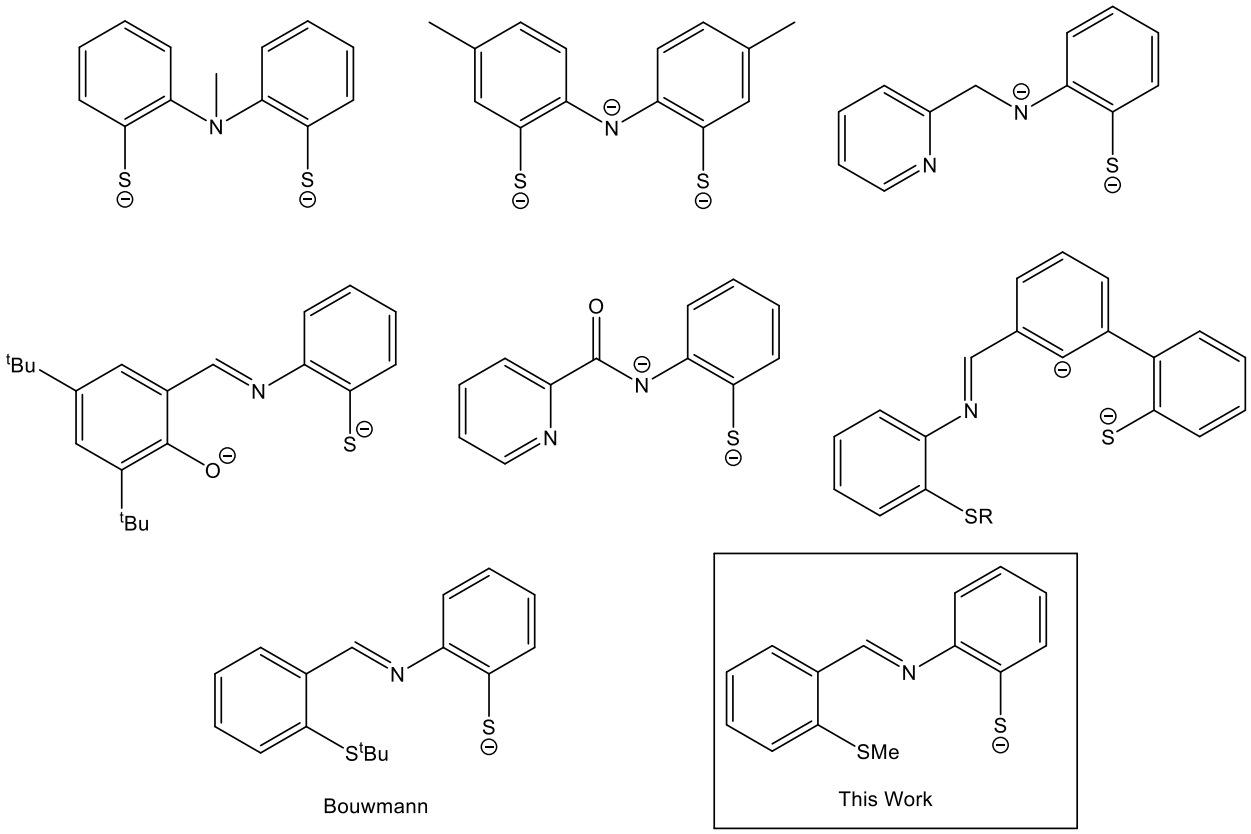

Figure 3.1: Nitrogen-containing bifunctional thiolate ligands.

Sellmann *et al.* in 2004 produced a pentadentate [$S^-S^RN^RS^RS^-$] ligand which formed a thiolate-bridged dinuclear ruthenium(III) complex. This species was capable of catalytically splitting dihydrogen *via* a bifunctional mechanism where the thiolate moiety was acting as a proton acceptor.[21] The Heyduk group in 2018 also demonstrated the non-innocence of their [$S^-N^-S^-$] ligand by synthesizing a series of nickel SNS complexes which are interrelated through one-electron transfer reactions. The ability to transform from one species to another has been proven and work is ongoing to try to enable these transformations to occur in a closed catalytic cycle, although the high calculated energy

barrier for hydrogen-atom transfer may present an obstacle in regenerating the active species.[22] Examples of catalysis with thioether-containing species are much more common such as the transfer hydrogenation of ketones by mononuclear ruthenium complexes bearing an [$S^RN^RS^R$] tridentate ligand.[23] Another chromium complex using an aliphatic [$S^RN^HS^R$] ligand has been shown to efficiently trimerize ethylene to 1-hexene at elevated temperature and pressure.[24] Finally, some ruthenium compounds containing a [$N^-S^RN^-$] ligand are catalytically active towards the hydrogenation of benzonitrile to benzylamine.[25]

The ligand system designed by Bouwman *et al.* consists of a thiolate and imine donor as well as a thioether arm containing a *tert*-butyl group (**Figure 3.1**). Reaction of this ligand with nickel(II) tetrafluoroborate resulted in cleavage of the *tert*-butyl-sulphur bond and formation of a dinuclear [S^-NS^-] Ni(II) species.[20] Our group has set out to improve upon this design by developing a more stable version of this ligand where the *tert*-butyl group is replaced with a methyl substituent which is less likely to be cleaved from the sulphur atom due to the inferior stability of a methyl carbocation compared to the tertbutyl carbocation. This novel tridentate SNS ligand, like the amido ligand above, contains a complementary combination of a hard nitrogen donor and soft thiolate donor, both of which have an available lone electron pair to act as proton acceptors in a bifunctional catalytic cycle. The ligand also contains a thioether arm that is capable of stabilizing a range of metal oxidation states[14,19,21,23,26] and which is also potentially hemilabile, allowing for a free site for substrate coordination.[27–29] This ligand shall be referred to by the shorthand $S^{Me}N^HS$ with the superscript representing the groups on the three donor atoms prior to deprotonation.

Our objective using this new $S^{Me}N^{H}S$ ligand is to prepare a series of cobalt SNS complexes and explore their reactivity towards bifunctional catalysis. Previous work with iron has shown a very diverse range of behaviour that can be expected for this ligand. Upon addition of $S^{Me}N^{H}S$ to iron(II) triflate in the presence of base, a trinuclear iron complex bearing four of these ligands is formed with the four thiolate moieties bridging the three iron centres. Further treatment of this complex with a variety of donor ligands produced a series of mono- and dinuclear iron complexes which have been fully characterized elsewhere.[30] Specifically, treatment of the trinuclear species with diphenylmethylphosphine ($PMePh_2$) and 2,6-dimethylphenyl isonitrile (CNAr) resulted in the formation of thiolate-bridged dinuclear species (**Scheme 3.1**). While the addition of trimethylphosphite ($P(OMe)_3$) in acetonitrile also resulted in an analogous dinuclear complex, changing the solvent to dichloromethane had the surprising effect of creating a mononuclear SNS iron(II) cationic complex. Adding deprotonated $S^{Me}N^{H}S$ to iron(II) triflate that had been ligated with trimethylphosphine (PMe_3) also formed a mono-ligated species to which a number of ancillary ligands could be applied.

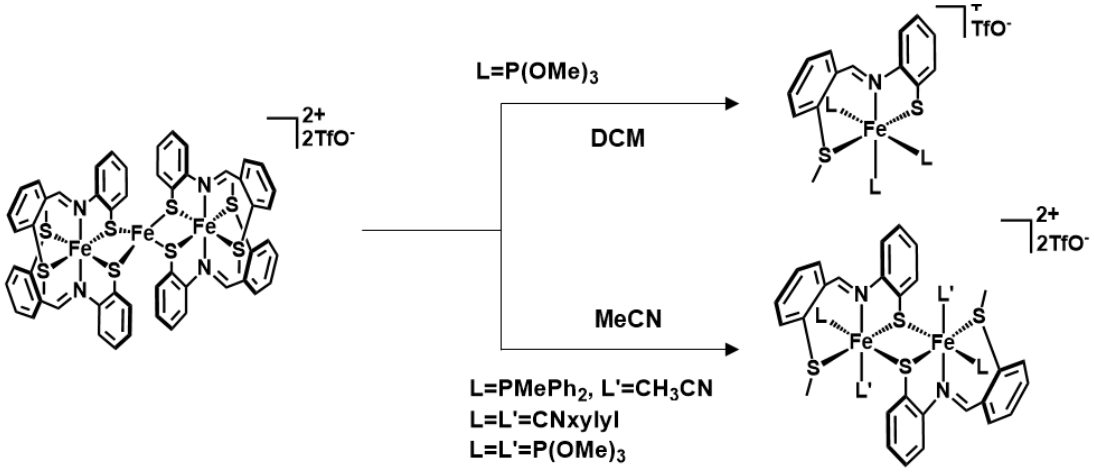

Scheme 3.1: Formation of tri-, di- and mononuclear iron thiolate SNS complexes.

The most remarkable observation from this PMe_3 species, however, was that upon heating at 60 ^oC in THF thermolysis occurs, cleaving the C^{aryl}-S^{Me} bond and forming an iron(II) species with a new SNC ligand (**Scheme 3.2**). The mechanism of this transformation is unknown but is suspected to occur by a radical mechanism due to the change in oxidation state from iron(II) to iron(III). However, attempts to trap the •SMe radical have proven unsuccessful and the theoretical by-product, dimethyl disulphide, has not been detected in solution. Both the SNS and SNC species were examined for activity towards amine-borane dehydrogenation as a means to test if these ligands were bifunctionally active. The majority of these complexes showed no catalytic reactivity and decomposed immediately in the presence of ammonia-borane but SNS and SNC complexes containing DMPE as an ancillary ligand did show mild catalytic activity at elevated temperature with the appearance of a hydride signal in the ^1H NMR spectrum suggestive of a bifunctional mechanism.[31]

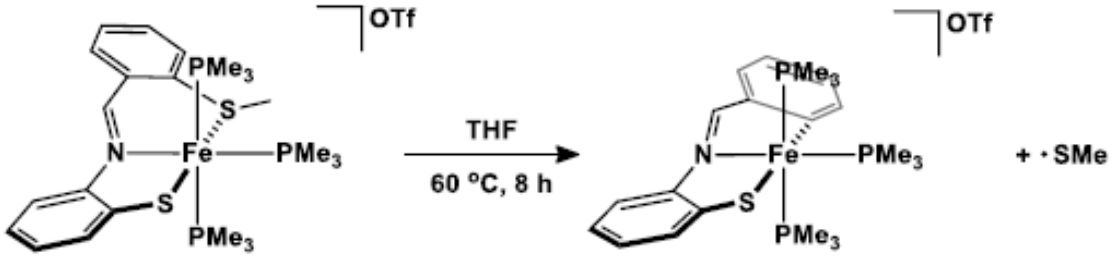

Scheme 3.2: Formation of new $(SNC)^{2-}$ ligand by C-S bond activation.

During the course of preparing these compounds, it was observed that treatment of low-coordinate iron complexes such as $Fe(N(SiMe_3)_2)_2$ with the $S^{Me}N^HS$ ligand afforded another new ligand through the imine coupling of two of the SNS ligands forming an iron(II) N_2S_2 complex (**Scheme 3.3**). Single crystal X-ray diffraction and

NMR studies revealed that this complex exists as a thiolate-bridged dimeric species as a solid but a monomer with one thioether arm coordinated in solution. In this new species, a new bond has formed between the imine groups of the two SNS ligands creating a new di-amido unit. This complex in solution was shown to be an effective precatalyst towards the selective hydroboration of a wide scope of aldehydes with high product yields using 0.1 mol % catalyst loading. The precatalyst was reactive only for the hydroboration of aldehydes as when the reaction was attempted with ketones, very low yields were achieved. Even with high catalyst loading (10 mol%) and at elevated temperatures less than 10% of the corresponding borate ester of acetophenone was detected after 16 h.[32]

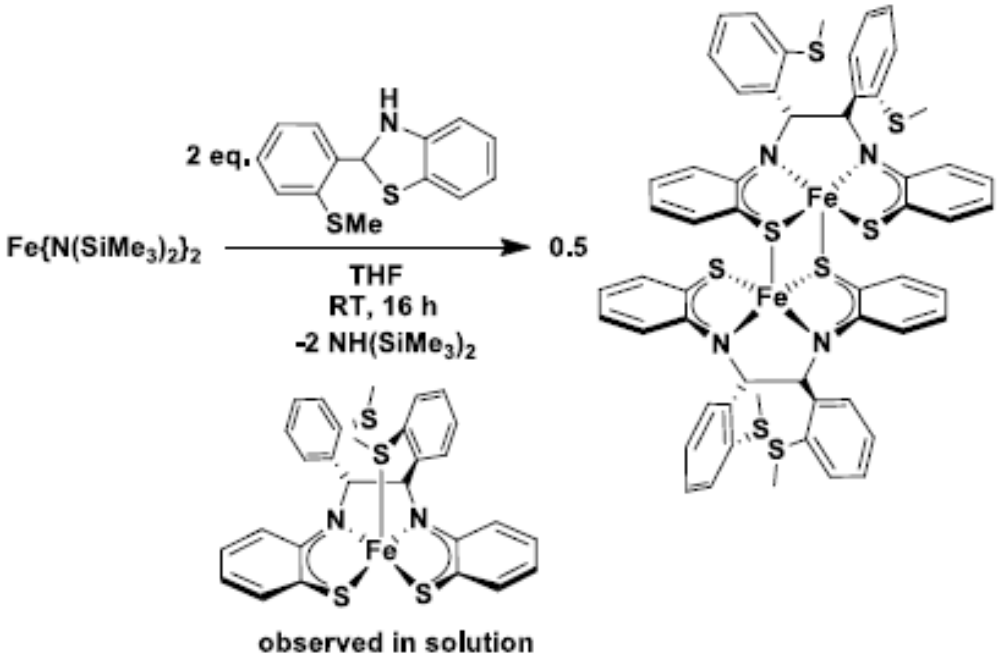

Scheme 3.3: Formation of the $(N_2S_2)^{2-}$ ligand by imine C-C coupling.

This body of work provides a good point of comparison to be able to contrast the effects that iron and cobalt have on the SNS thiolate ligands behaviour. This chapter

aims to explore if it is possible to synthesize analogous cobalt SNS complexes and to see if these species show any superior catalytic behaviour over their iron counterparts.

3.2. $S^{Me}N^{H}S$ Ligand Synthesis

The synthesis of the thiolate SNS ligand can be accomplished in a single-step reaction using inexpensive and readily available starting materials. This is in contrast to the generally expensive and time-consuming syntheses of previously reported imine-containing thiolate ligands.[14,15,17–19] The formation of $S^{Me}N^{H}S$ is accomplished by the condensation of 2-(methylthio)benzaldehyde and 2-aminothiophenol (**Scheme 3.4**).

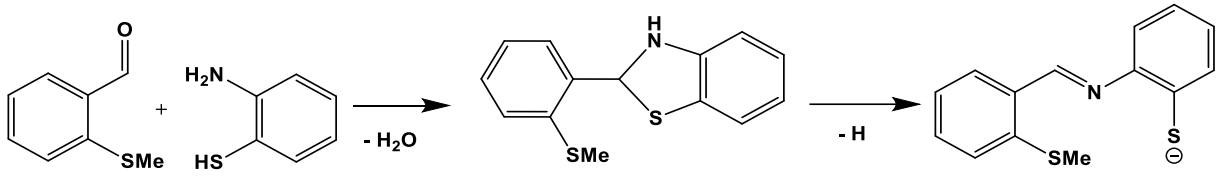

Scheme 3.4: The synthesis of $S^{Me}N^{H}S$

The two liquids were combined in dry ethanol under nitrogen to form a pale-yellow solution which was stirred at room temperature overnight after which the colour transitioned to an off-white suspension as the product precipitated out of solution. The product was collected by filtration and washed with cold ethanol and dried under vacuum to yield an off-white powder, 2-(2-methylthiophenyl)benzothiazolidine [$S^{Me}N^{H}S$]. ^{1}H NMR spectroscopy reveals that the ligand exists in a closed-ring structure as can be seen from the absence of a strong imine signal which would be expected in the range of 8-9 ppm (**Figure 3.2**). This is further supported by the presence of an amine resonance observed at 3.4 ppm and the strong N-H stretch observed at 3339 cm^{-1} in the infrared spectrum. The thiomethyl group can be identified as the three-proton resonance at 2 ppm while the remaining eight protons can be assigned to the complex resonances

attributed to the aromatic ring protons. Unlike the S$^{t\text{Bu}}$ analogue from the work of Bouwman, no ring-opened isomer is in solution.

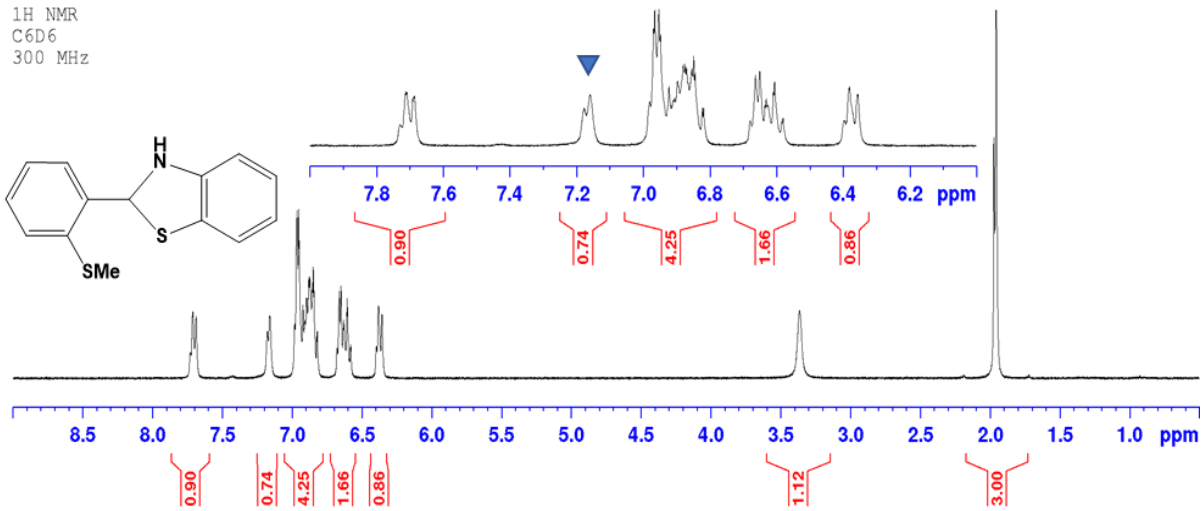

Figure 3.2: ^{1}H NMR spectrum of S^{Me}N^{H}S in C_6D_6 (blue triangle).

On deprotonation, however, the ring-opened form predominates, as demonstrated by the molecular structure of the thiolate-bridged dimeric lithium complex (**3-1**) determined by X-ray diffraction (**Figure 3.3**).[33] Note that both the thiolate S and imine N are coordinated to lithium while the thioether is not.

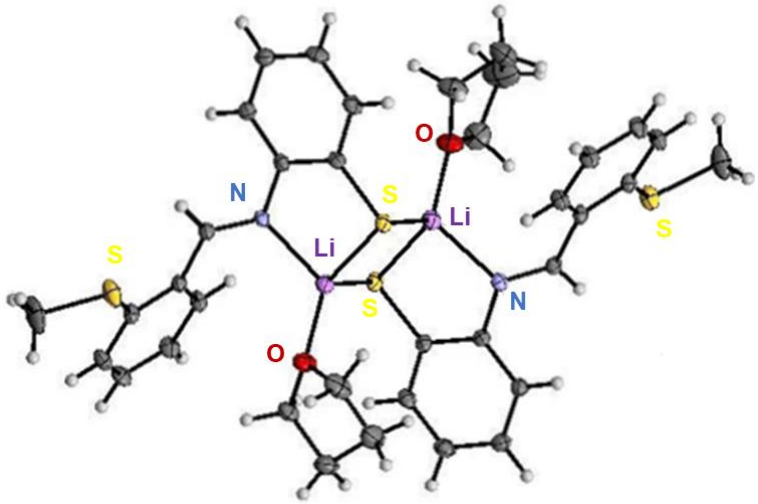

Figure 3.3: Molecular structure of **3-1**, {Li_2(S^{Me}NS)$_2$(THF)$_2$}.[33]

3.3. Formation of a New Cobalt SNC Complex, 3-2

3.3.1. Synthesis and Characterization

Given the tendency of the thiolate SNS ligand to form multinuclear complexes with iron, a strongly coordinating ancillary ligand was added to the cobalt reaction mixture to prevent addition of a second equivalent of the $S^{Me}N^{H}S$ ligand. Tris(triphenyl-phosphine) cobalt chloride, $S^{Me}N^{H}S$ and potassium *tert*-butoxide were first combined as solids in a vial. Benzene was added causing the solids to dissolve and shortly after the red KSNS salt to precipitate from the brown solution. One equivalent of 1,2-bis(diethylphosphino)ethane (DEPE) in benzene was then added to the solids causing an instant colour change to a black-brown with the red suspension of the $(SNS)^-$ salt. To try and increase the solubility of the SNS salt, the solution was heated at 70 ^oC overnight giving a blue-black solution with a brown suspension. Filtering the mixture through Celite removed the precipitated KCl and brown solid and removal of solvent from the blue-black filtrate and extensive washing with hexanes yielded a few milligrams of a black-blue flaky solid.

Crystals suitable for single crystal X-ray diffraction were grown from a saturated solution of THF layered with hexanes. The molecular structure (**Figure 3.4**) revealed this species to be Co(SNC)(SMe)(DEPE) (**3-2**) resulting from oxidative addition of the C^{aryl}-S^{Me} bond, forming the SNC ligand that had been observed previously with iron.[31] But while iron proceeded through a one electron mechanism giving an Fe(III) SNC product, cobalt undergoes a formal two-electron oxidative addition to the Co(III) product. This important difference is most likely due to iron's inability to access the Fe(IV) oxidation state with the soft donor phosphine and thiolate ligands.

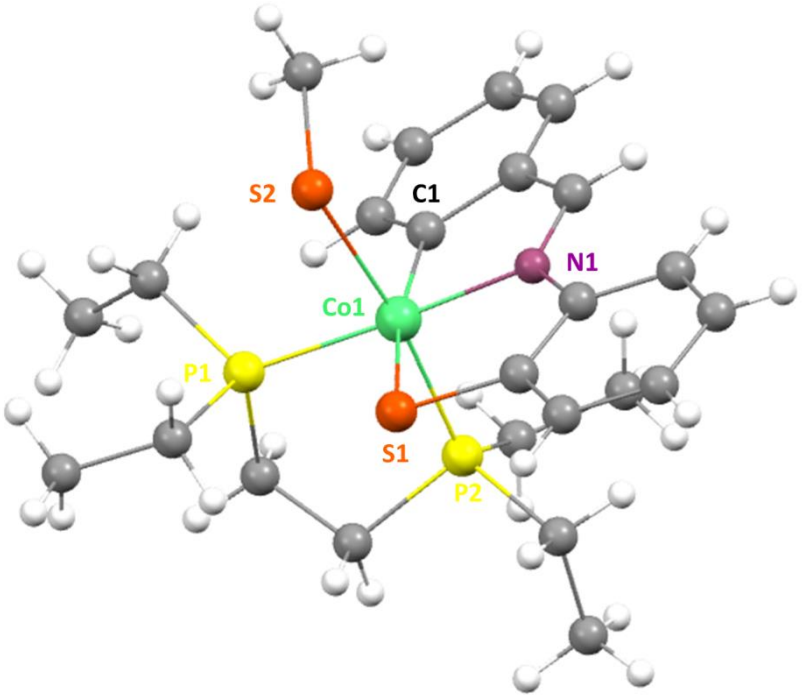

Bond	Distance
Co – S1	2.314(5) Å
Co – S2	2.306(4) Å
Co – N1	1.957(1) Å
Co – C1	1.945(1) Å
Co – P1	2.186(5) Å
Co – P2	2.224(4) Å
Bonds	**Angle**
N1-Co-S1	85.49(3)°
N1-Co-S2	90.89(3) °
N1-Co-C1	83.35(5)°
N1-Co-P1	176.10(4) °
N1-Co-P2	96.04(3)°
S2-Co-P1	85.32(2) °
S2-Co-P2	172.41(2) °

Figure 3.4: Molecular structure of Co(SNC)(SMe)(DEPE) (**3-2**) with selected bond lengths and angles.

The new 18e$^-$ Co(III) complex is in a pseudooctahedral geometry and contains the meridional tridentate SNC ligand, bidentate DEPE bis(phosphine) and SMe positioned *trans* to P. The dianionic SNC ligand is planar, in contrast to the more flexible SNS thiolate ligand. The Co-S bond distances are nearly identical to the methyl- (2.306(4) Å) and aryl-thiolate ligands (2.314(5) Å) and noticeably longer than the Fe-S bond distance (2.2319(6) Å) in the analogous Fe(SNC)$(PMe_3)_3$ complex.[31] The Co-N bond distance was found to be 1.957(1) Å in the cobalt SNC complex while the same bonds was 1.972(2) Å in the iron species. In contrast, the Co-C bond distance (1.945(1) Å) is shorter than the analogous Fe-C distance (1.976(2) Å).

In order to further study the reactivity of this SNC complex, a larger quantity of sample was required. However, attempts to scale up the reaction afforded instead the imine-coupled $[Co(N_2S_2)]^-$ anion which is discussed further in section 3.4. This curious result was reproduced multiple times at varying amounts of starting material as monitored by NMR spectroscopy. Attempts using different solvents, excess DEPE and alternate bis(phosphine) ligands were also unsuccessful.

In order to try and prevent this imine-coupling from occurring a number of different strategies were employed with various ancillary ligands. Initially it was thought that the coordinated PPh_3 in the starting material was perhaps making the metal too electron rich, so the phosphines were replaced with the more weakly donating trimethylphosphite. This was unsuccessful however, since after addition of deprotonated thiolate SNS formation of the N_2S_2 was detected in the ^1H NMR spectrum. Monodentate phosphorus ligands therefore seemed to be displaced from the metal too easily so bidentate phosphines such as DMPE and DEPE were then employed. The rational being that the bidentate phosphines would be much harder to displace, preventing two SNS ligands from coordinating to the metal. Addition of one equivalent of thiolate ligand to $CoCl(DEPE)_2$ yielded a black solution which when dried resulted in a dark-blue powder with the DMPE analogue giving a similar result. The ^1H NMR spectrum revealed a number of products being produced, one of which was the N_2S_2 causing the blue colouration. Using bulkier starting materials such as $Co(N(TMS)_2)(IPr)$ or $Co(N(TMS)_2)(SIPr)$ was hypothesized to discourage two SNS ligands from being able to coordinate to the metal, but this was equally unsuccessful. Crystals grown from solution revealed that the NHC's were being displaced from the metal and forming **3-3** with a

bis-NHC cationic cobalt species as the counter-ion. This frustrating result demonstrates the apparently high thermodynamic favourability of this N_2S_2 species.

3.4. Formation of the Imine-Coupled $[Co(N_2S_2)]^-$ Anion, 3-3

3.4.1. Synthesis and Characterization

Based on attempts to synthesize a mono-ligated cobalt thiolate species it was frequently observed that the combination of base, $S^{Me}N^{H}S$ and cobalt in THF resulted in the formation of a vibrant navy-blue solution which was characteristic of an imine-coupled N_2S_2 cobalt complex. While formation of this species resulted from a number of different starting materials and reaction conditions, the synthesis was most successful using cobalt(II) chloride as a starting material (**Scheme 3.5**). Cobalt(II) chloride, two equivalents of $S^{Me}N^{H}S$ and four equivalents of lithium bis(trimethylsilyl)amide were all combined in THF forming a red solution consistent with the colour of the SNS salt. Stirring this reaction initially caused a colour change to brown and then to a navy-blue overnight. Concentrating the solution under vacuum and diluting with toluene caused a colour change to indigo and the precipitation of LiCl which was removed by filtration. Removal of toluene yielded an indigo solid while washing with hexanes removed most of the conjugate acid, excess base and ligand. This indigo solution was dissolved once again in THF regaining the navy-blue colour and the solution was stored in the freezer to initiate crystallization of the complex.

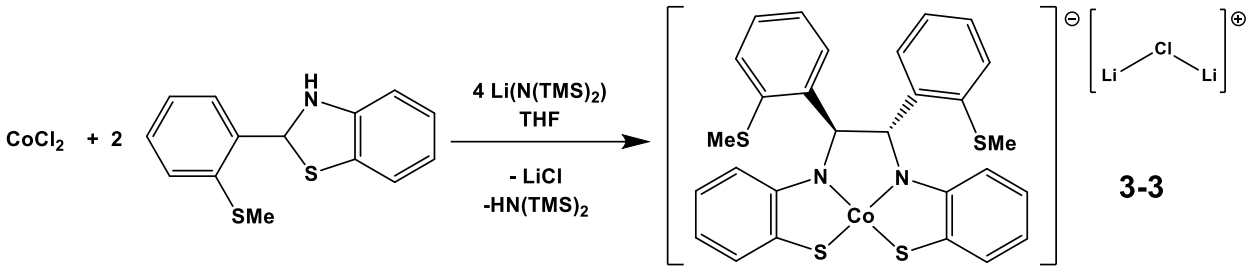

Scheme 3.5: Synthesis of [Co(N_2S_2)][Li_2 (μ-Cl)], (**3-3**).

Crystals suitable for single crystal X-ray diffraction were grown from a saturated solution of THF by cooling at -35 ^oC. The molecular structure confirms the formation of the imine-coupled N_2S_2 ligand bound to what at first appears to be a $14e^-$ cobalt(III) metal centre in a square-planar geometry (**Figure 3.5**). This structure is identical to the structure that was acquired by previous group member Dr. Cassandra Hayes. Unlike its neutral iron analogue, this cobalt species exists as an anion and does not dimerize through a thiolate-bridge in the solid phase.[32] Despite this difference, the two structures exhibit very similar bond distances. Specifically, the Fe(N_2S_2) species has average bond distances of 1.855(2) and 2.205(7) Å for the iron-nitrogen and iron-sulphur bonds respectively while the Co(N_2S_2) anion has average bond lengths of 1.817(2) and 2.168(8) Å for those corresponding bonds. The imine bridge in the iron species also has a bond length of 1.537(4) Å compared to 1.548(3) Å in the cobalt complex. Sproules and Wieghardt have also prepared an S- and N-donor ligand which also forms a very similar imine-coupled N_2S_2 ligand in the presence of cobalt with the only difference being that the dangling phenyl arms do not have a thioether group. This analogous complex has extremely similar bond lengths of 1.816(2) and 2.138(6) Å for the Co-N and Co-S bond respectively.[34] While both of these thiolate-cobalt distances are slightly

shorter than other Co-S distances reported in the literature[35–38] they are still consistent with a cobalt-thiolate bond distance.

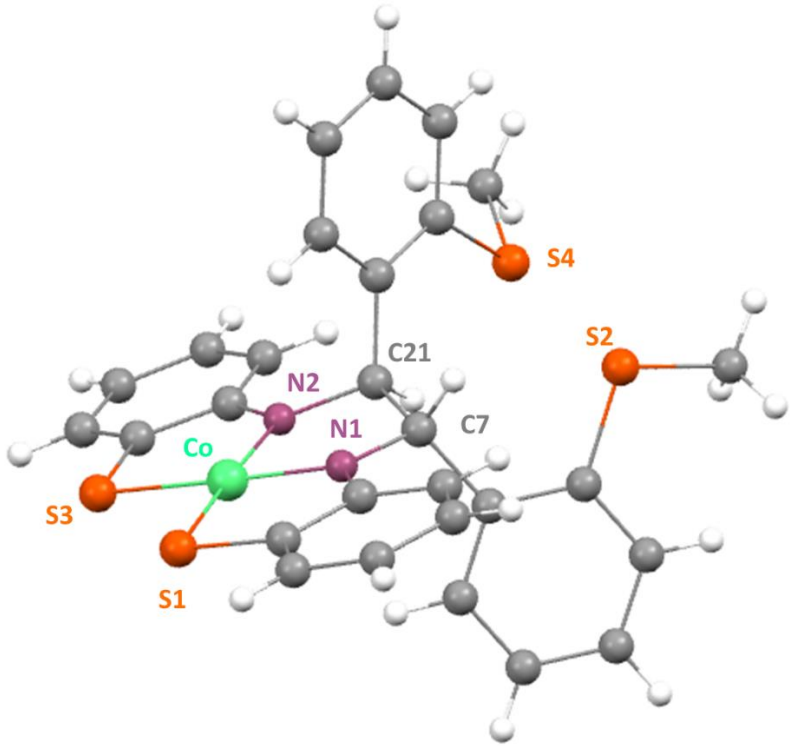

Bond	Distance
Co – S1	2.1668(8) Å
Co – S3	2.1693(8) Å
Co – N1	1.812(2) Å
Co – N2	1.821(2) Å
C7 – C21	1.548(3) Å
Bonds	**Angle**
N1-Co-N2	85.49(8)°
S1-Co-S3	96.83(3) °
N1-Co-S1	88.78(6)°
N1-Co-S3	174.27(6) °
N2-Co-S3	88.93(6)°
N2-Co-S1	174.13(6) °
N1-C7-C21	107.60(2) °
N2-C21-C7	107.02(2) °

Figure 3.5: Molecular structure of $[Co(N_2S_2)][Li_2(\mu\text{-}Cl)]$ (**3-3**) with selected bond distances and angles. Cation omitted for clarity.

The ^{1}H NMR spectrum of $[Co(N_2S_2)]^-$ shows a series of paramagnetic resonances ranging from 14 to -104 ppm which is unexpected for a diamagnetic cobalt(III) species (**Figure 3.6**). The resonance corresponding to the two dangling thiomethyl groups can be easily identified as the resonance at δ 2.96 from the integration equalling six protons. The remaining eight resonances all integrate to two protons apiece but the broadening and unpredictable chemical shifts of the paramagnetic signals makes assignment difficult. In total, twenty-two of the expected twenty-four protons can be accounted for. Efforts to locate the remaining two resonances by extending the spectral range have proven unsuccessful. This likely

means that the missing resonances have been broadened to the extent they are indistinguishable from the baseline.

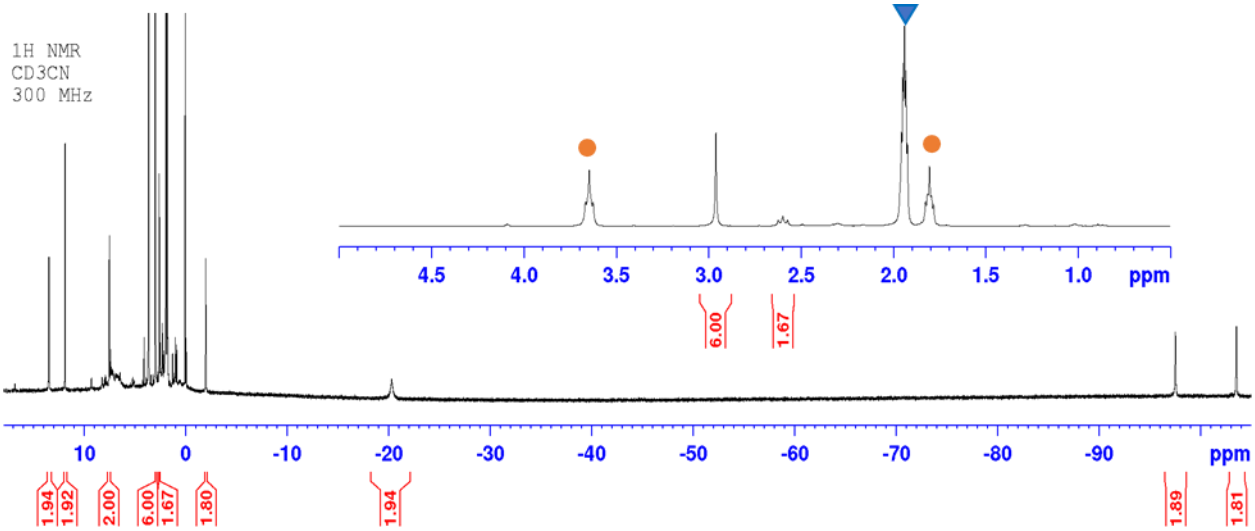

Figure 3.6: ^{1}H NMR spectrum of [Co(N_2S_2)][Li_2 (μ-Cl)] (**3-3**) in CD_3CN (blue triangle). Residual solvent THF (orange circles).

The structure derived from single crystal X-ray diffraction is puzzling since at first glance it suggests a 14e$^-$ square planar cobalt(III) species with four X donors, which would presumably be unstable due to its low electron count. An octahedral geometry would be much more reasonable as a six-coordinate species would have a closed d shell with a d^6 Co(III). Additionally, the presence of paramagnetically shifted signals in the ^{1}H NMR spectrum suggests the presence of unpaired electrons which would also not be the case for a diamagnetic Co(III) species. To investigate the electronic structure of this complex further, DFT calculations were carried out by Adiran de Aguirre in the Maseras group from the Institut Català s'Investigació Química at the B3LYP-D3 level of theory. These calculations revealed that the complex actually exists as a Co(I) species instead of the Co(III) that could be interpreted from **Figure 3.5**. The calculations found

that similar to the iron analogue, there are two unpaired electrons in the system. The singly-occupied molecular orbitals of these two electrons are illustrated in **Figure 3.7**.

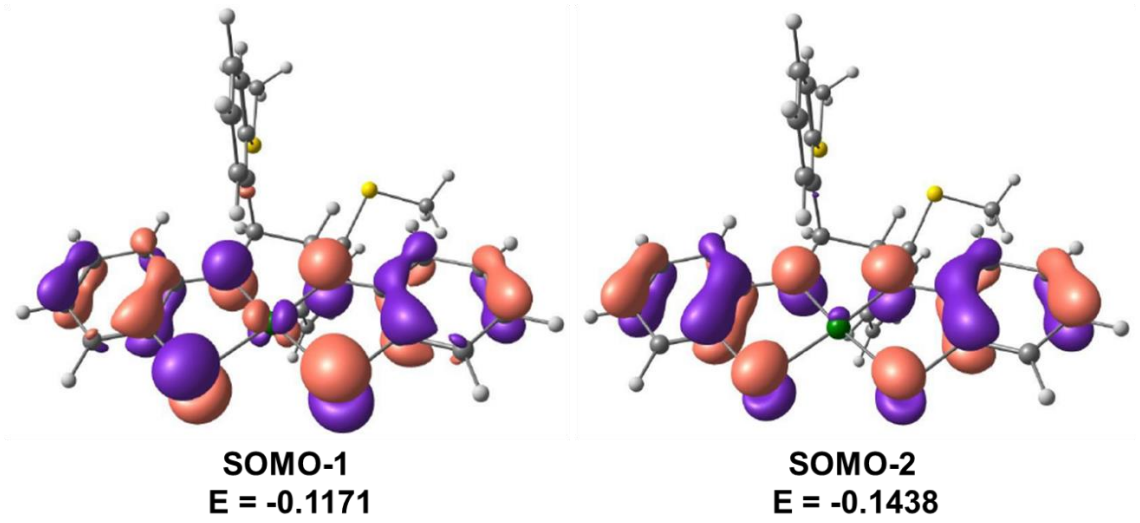

Figure 3.7: Singly occupied molecular orbitals of **3-3**.

As can be seen from both SOMO-1 and SOMO-2, there is a very large contribution from the ligand into both molecular orbitals with comparatively much less contribution coming from the metal. SOMO-1 does have noticeably more contribution coming from the metal compared to SOMO-2 but still has a much larger contribution coming from the nitrogen and sulphur atoms. With the electron density much more localized on the ligand instead of the metal, it is reasonable to conclude that the two unpaired electrons are delocalized in the ligand structure demonstrating the non-innocence of this ligand. This is in contrast to the iron species which had a much larger contribution to the molecular orbital from the metal, suggesting that the two unpaired electrons were located on the metal instead of the ligand. Having cobalt in its first oxidation state rationalizes the observed square planar geometry as a $16e^-$ square planar species is much more conceivable than a $14e^-$ one. The two unpaired electrons also explain the paramagnetism that was observed in the ^1H NMR spectrum which

would be unexpected for both Co(III) and Co(I) species. Strangely, however, both radicals are of the same spin making the ground state of this species a triplet. This is in stark contrast to the analogous iron(II) complex in which the electrons on the ligand are of opposite spin and the unpaired spins are metal centered (**Figure 3.8**).

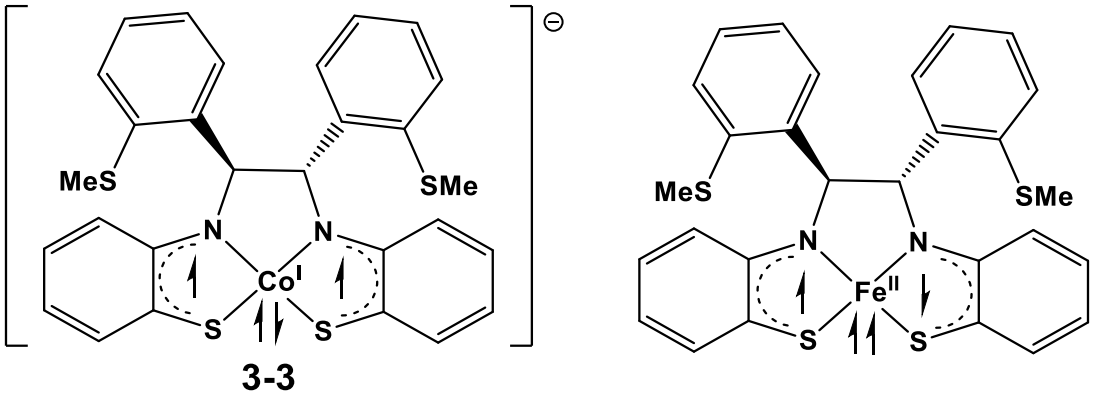

Figure 3.8: Lewis structures of the cobalt(I) N_2S_2 anion (**3-3**) and the analogous neutral iron(II) N_2S_2 complex.

The formation of this imine—coupled species demonstrates the non-innocence of this SNS ligand. Instead of four X-donors coordinated to the metal centre, it is more accurate to think of the N_2S_2 ligand as dianionic with the charges delocalized throughout the nitrogen-sulphur metallacycle as shown in **Figure 3.9**. This electronic representation is supported by shortening of the aryl carbon-nitrogen bond between the SNC and N_2S_2 ligands. In the SNC complex in which the nitrogen-carbon atoms share a single bond, the bond length is 1.4185(16) Å long. The corresponding bond in the N_2S_2 complex is 1.381(3) Å. This slight difference is presumably due to the increased double-bond character that is predicted from the resonance structures in **Figure 3.9**, however the two ligands do have important differences so not all of this bond shortening may be attributable to this factor.

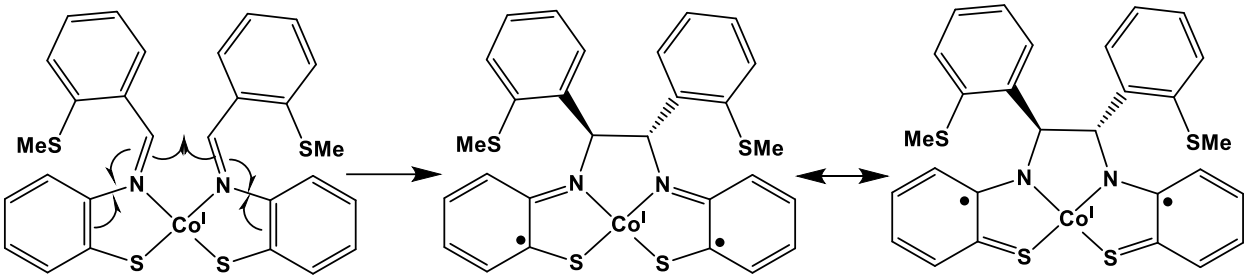

Figure 3.9: Lewis representation of the cobalt(I) N_2S_2 (**3-3**) resonance structure.

To examine the characteristics of the unpaired electrons in this complex the electron paramagnetic resonances spectrum (EPR) was collected by the group of Dr. Christophe Bucher from ENS Lyon in France. Three EPR spectra are shown in **Figure 3.10**; the initial cobalt(I) sample (in blue) shows some lines suggesting that some oxidation of the sample had taken place during shipping. The spectrum in red represents the completely oxidized cobalt(II) complex which clearly contains eight distinct lines, consistent with an electron coupling to the quadrupolar cobalt nucleus. Due to the very clear coupling pattern, it is likely that this spectrum is the result of the unpaired electron on the cobalt, which, due to its close proximity to the metal, would experience a stronger coupling to the nucleus. Finally, the spectrum in orange is the result of the subsequent back-reduction of the cobalt(II) complex and as such is representative of the pure cobalt(I) species. It lacks the lines present in the blue spectrum which resulted from cobalt(II) contamination. The broad, unresolved signals in this spectrum are indicative of the delocalization of the two unpaired electrons preventing the appearance of a highly resolved coupling pattern due to the constantly changing electronic environment from the electrons resonating throughout the ligand.

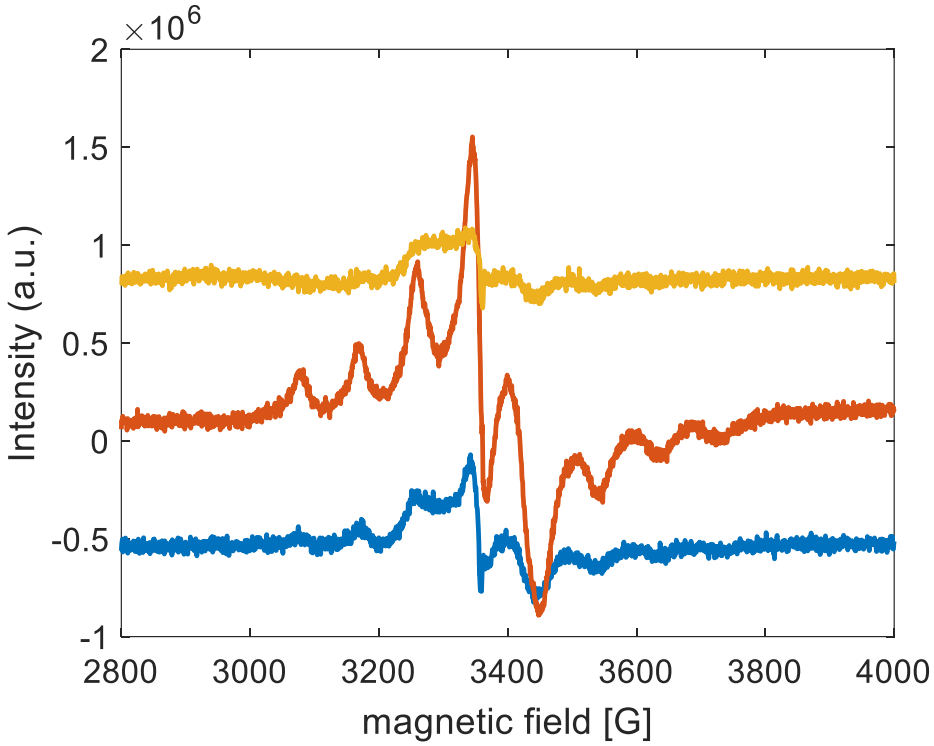

Figure 3.10: EPR spectrum of [Co(N_2S_2)][Li_2 (μ-Cl)] (**3-3**) in THF under nitrogen at -269 ^oC. Initial sample (blue), after oxidation at -300 mV (red) and after subsequent back-reduction at -800 mV (orange).

Given the non-innocent behaviour observed for this ligand from the DFT studies, cyclic voltammetry experiments were also performed by Prof. Bucher's group to explore the redox behaviour of this complex (**Figure 3.11**). From this experiment we can observe two reversible oxidations and one reversible reduction. The first oxidation occurring at approximately -550 mV to the reference silver electrode corresponds to the oxidation of the metal from Co(I) to Co(II) while the second oxidation at approximately 0 mV with respect to silver corresponds to the oxidation from Co(II) to Co(III). Another oxidation is also visible at higher potentials where an electron is being pulled from the ligand instead of the metal, spurring additional reactivity and rendering this oxidation irreversible. A stable, reversible reduction from Co(I) to Co(0) can finally be observed at approximately -1.7 V.

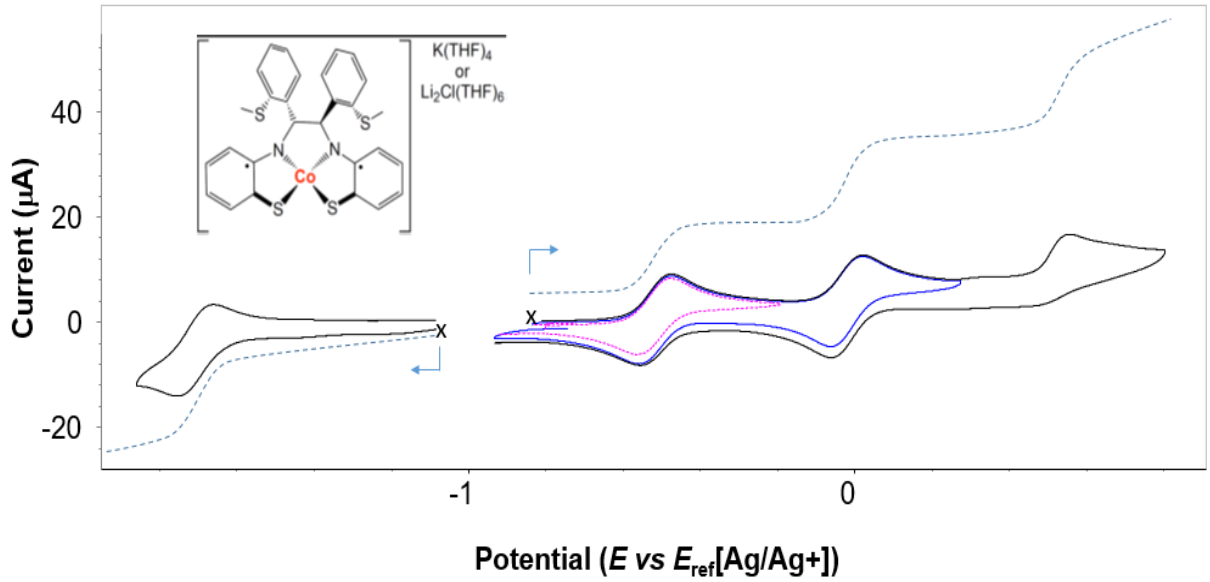

Figure 3.11: Cyclic voltammetry curve for [Co(N_2S_2)][Li_2 (μ-Cl)] (**3-3**) in THF. Performed at 1 mM with tetrabutylammonium hexafluorophosphate (0.1 M), 100 mV/s.

The above mentioned DFT study reveals that the Co(0) and Co(II) species exist as doublet ground states suggesting that the newly unpaired electron in both cases is of the opposite spin as the unpaired electrons on the N_2S_2 ligand. The Co(III) species interestingly was found to be an open-shell singlet implying that one electron on the metal is being promoted to a higher energy level and that these two unpaired electrons are now both the opposite spin of those found on the ligand (**Figure 3.12**). The observation of three stable redox processes for this complex is promising for its ability as a catalyst as there are four different redox states which can now be accessed to facilitate oxidative or reductive transformations in catalysis. Further investigation into these new species are on going in the Baker group.

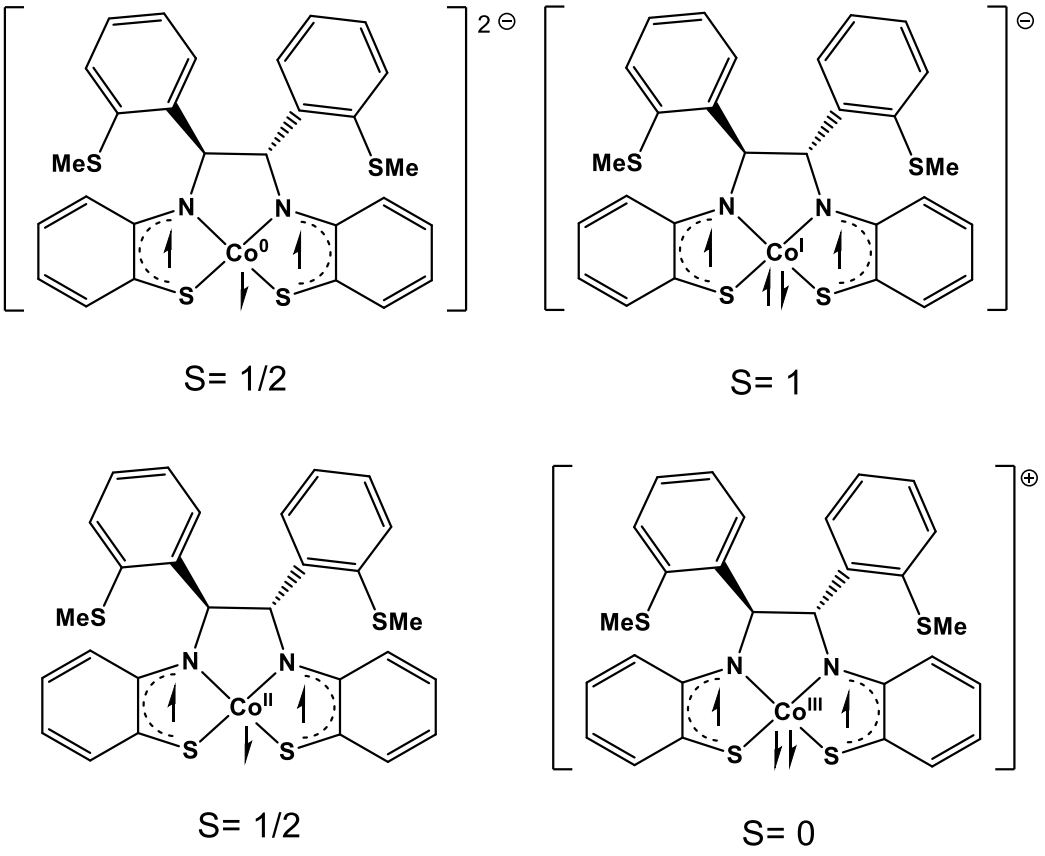

Figure 3.12: Different spin states of the four redox states of the Co(N_2S_2) complex.

3.4.2. Activity Towards the Hydroboration of Aldehydes and Ketones

Given the highly selective nature of the Fe(N_2S_2) complex when catalyzing the hydroboration of aldehydes, we thought it desirable to compare the reactivity of the analogous cobalt complex catalyzing the same reaction by performing a preliminary substrate scope (**Scheme 3.6**). The catalytic procedure is described in detail in section 3.6 but a brief summary is included here. A 1 mg/mL stock solution of **3-3** was prepared in THF and an identical volume of 0.3 mL was drawn and charged into an NMR tube for each catalytic experiment. The substrate and pinacolborane were added to achieve a catalyst loading of 0.1 mol% which is the same catalyst loading used in the iron

experiments. These reactions were allowed to stand at room temperature for 30 min before a ^{11}B NMR spectrum was acquired.

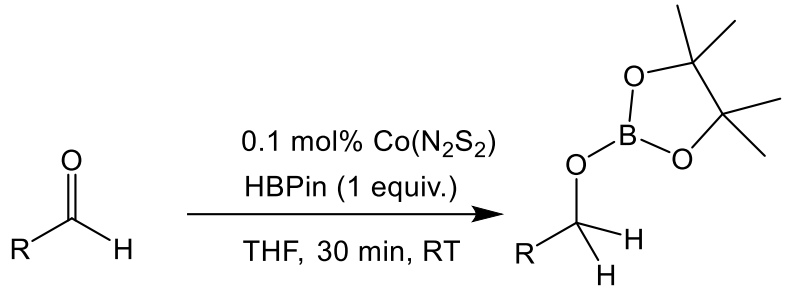

Scheme 3.6: Reaction scheme for the [Co(N_2S_2)][Li_2 (μ-Cl)] catalyzed hydroboration of aldehydes.

The first substrate examined was benzaldehyde which the Fe(N_2S_2) had shown to be highly effective at hydroborating. The iron catalyst was able to achieve a 95% conversion in less than 30 min at room temperature when dissolved in THF.[32] Performing a similar reaction with the cobalt analogue showed that cobalt was noticeably less efficient as a catalyst. After 30 min at room temperature, the initially pale yellow-brown solution had transitioned to a light turquoise-blue which is presumably the colour of the catalyst resting state. The ^{11}B NMR spectra revealed that the doublet belonging to the pinacolborane was still clearly visible and only a small amount of the corresponding borate ester was visible at 26.5 ppm (**Figure 3.13**). Leaving the reaction mixture for an additional 48 h however did show an almost complete conversion of the pinacolborane into the borate ester showing complete conversion is possible but at a much slower pace than with iron (**Figure 3.14**). During this time the solution had maintained its light turquoise colouration suggesting that the catalyst had survived for this period of time.

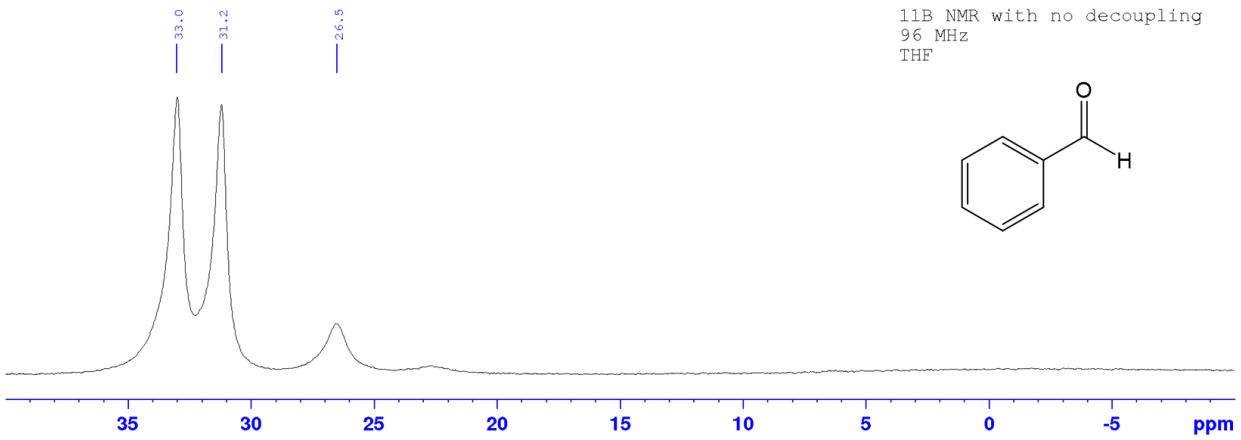

Figure 3.13: ^{11}B NMR spectrum of catalytic hydroboration of benzaldehyde in THF after 30 min at room temperature at 0.1 mol% catalyst loading.

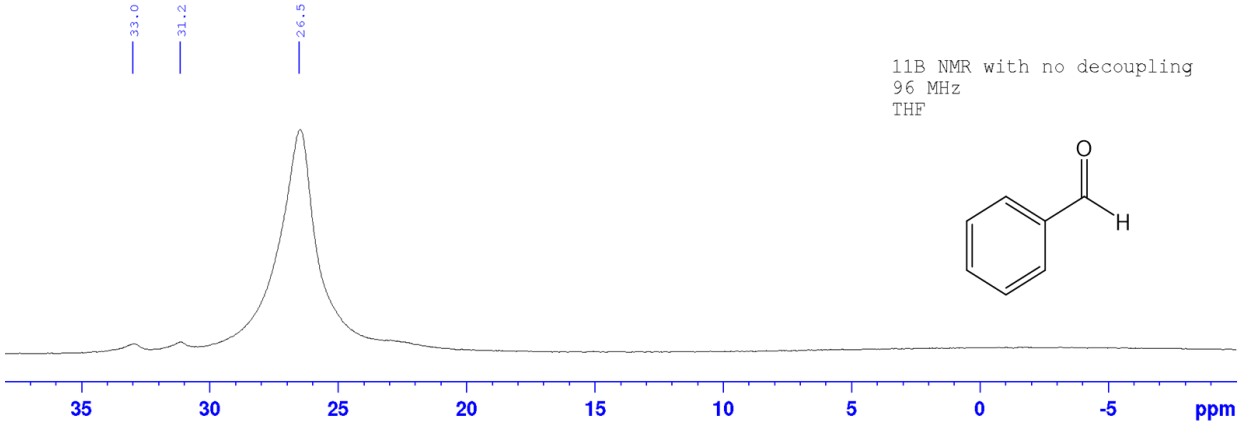

Figure 3.14: ^{11}B NMR spectrum of catalytic hydroboration of benzaldehyde in THF after 48 h at room temperature at 0.1 mol% catalyst loading.

The next substrate that was screened was cyclohexanal which possesses a higher electron density around the carbonyl carbon atom than benzaldehyde. This makes it a slightly more challenging substrate for the cobalt-hydride to attack due to the higher electron density around the electrophilic carbon. Performing a hydroboration with reaction conditions identical to those above resulted in similar observations: an initially pale brown solution that transitioned to a turquoise-blue after 30 min. The corresponding ^{11}B NMR spectrum showed that the cobalt catalyst was initially faster with this substrate than with benzaldehyde as can be seen by the relatively larger

borate-ester resonance compared to the pinacolborane (**Figure 3.15**). This however was still much slower than what was observed with the iron catalyst which effected complete conversion in 30 min. It should be noted that this reaction was performed in benzene with the iron catalyst, not THF. THF had an observable negative impact on the yield of the borate ester when optimizing reaction conditions with $Fe(N_2S_2)$ and benzaldehyde (99% yield in C_6D_6 vs 95% yield in THF). Even with this solvent effect in mind, the cobalt analogue is still markedly slower for the hydroboration of cyclohexanal.

While the cobalt catalyst was initially faster at hydroborating this substrate than benzaldehyde, it appears as though the catalyst cannot survive as long in its presence. After 16 h, a black solid began to appear in the bottom of the NMR tube which is presumably decomposed catalyst. The ^{11}B NMR spectrum after 48 h reveals only a marginal reduction in the amount of pinacolborane relative to the borate ester (**Figure 3.16**) suggesting that while the catalyst is initially more active with this substrate, it is not as long lived with cyclohexanal as it is with benzaldehyde.

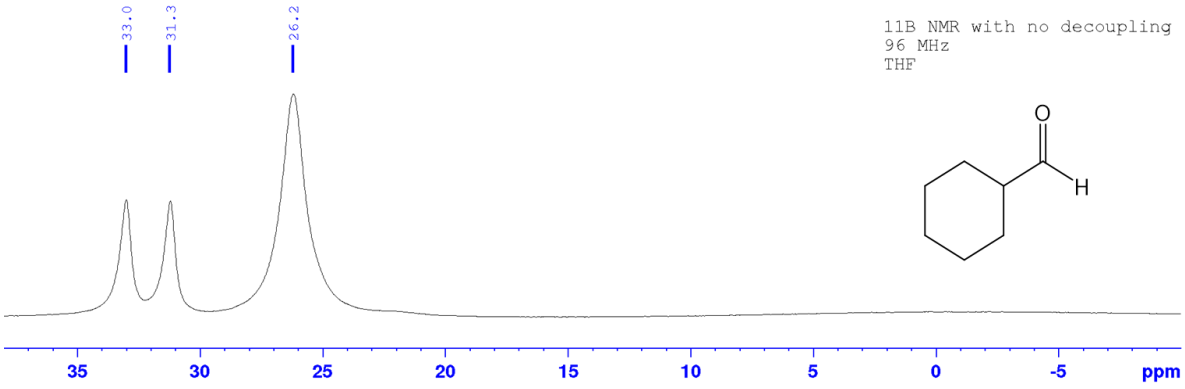

Figure 3.15: ^{11}B NMR spectrum of catalytic hydroboration of cyclohexanal in THF after 30 min at room temperature at 0.1 mol% catalyst loading.

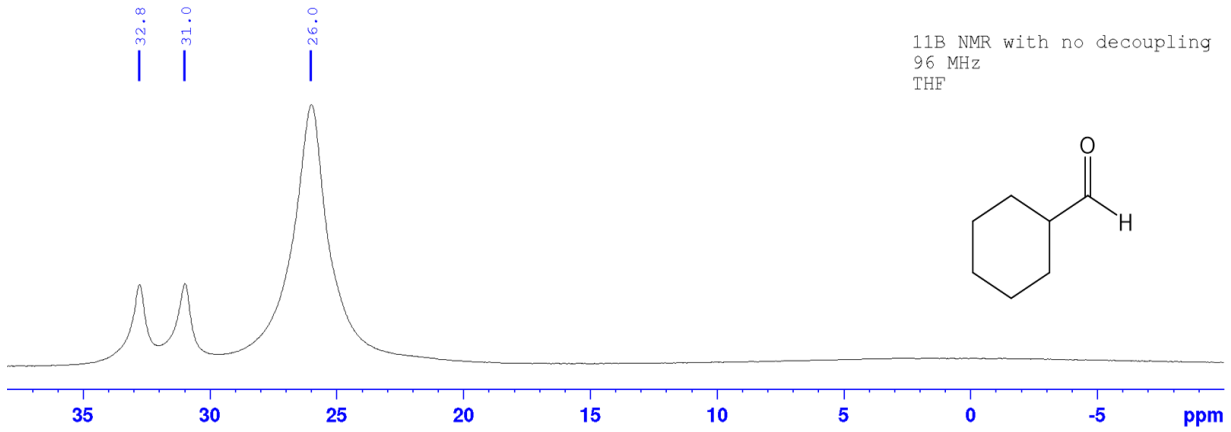

Figure 3.16: ^{11}B NMR spectrum of catalytic hydroboration of cyclohexanal in THF after 48 h at room temperature at 0.1 mol % catalyst loading.

One of the noticeable features with the Fe(N_2S_2) catalyst was its remarkable selectivity towards the hydroboration of carbonyls. While quite active when hydroborating aldehydes, it was almost completely inactive towards the hydroboration of ketones. The reaction of equimolar acetophenone and pinacolborane using 0.1 mol% of Fe(N_2S_2) at room temperature resulted in less than 5% of the borate ester. Even increasing the catalyst loading to 10 mol% and heating at 60 ^{o}C for 16 h yielded less than 10% of the hydroboration product.[32] To test if the cobalt precatalyst possessed the same selectivity as iron, a catalytic experiment was carried out with acetophenone. Initial combination of the acetophenone with the catalyst resulted in no obvious colour change over the course of ten minutes which is suggestive of no reaction between the ketone and the catalyst. Upon the addition of pinacolborane however the solution immediately changed to a clear dark-brown colour. The ^{11}B NMR spectrum revealed that the pinacolborane was being consumed and that a single borate ester was being produced at 26.2 ppm (**Figure 3.17**). This clearly shows that while the iron catalyst lacks reactivity towards ketone substrates, the cobalt catalyst does not exhibit the same selectivity. Leaving the reaction mixture for an additional 48 h resulted in only a

marginal decrease in the amount of pinacolborane relative to the borate ester resonance (**Figure 3.18**) suggesting that the catalyst is not substantially long lived to convert all of the starting material.

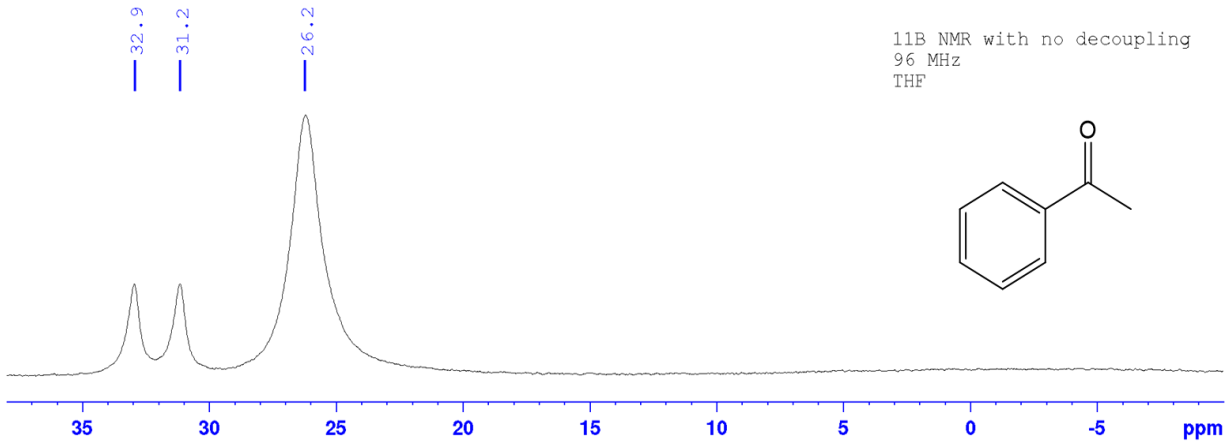

Figure 3.17: ^{11}B NMR spectrum of catalytic hydroboration of acetophenone in THF after 30 min at room temperature at 0.1 mol% catalyst loading.

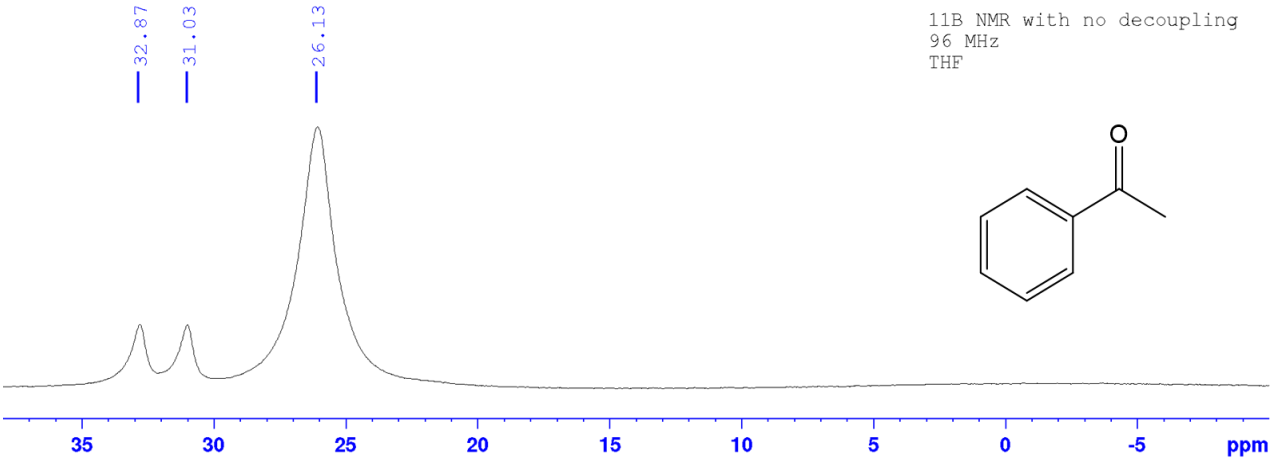

Figure 3.18: ^{11}B NMR spectrum of catalytic hydroboration of acetophenone in THF after 48 h at room temperature at 0.1 mol% catalyst loading.

3.5. Conclusion

In conclusion, attempts to compare the behaviour of the thiolate ligand with cobalt to that of iron show a noticeably different behaviour. To avoid forming multinuclear thiolate-bridged species that were observed with iron, the ancillary ligand

DEPE was added to the reaction mixture with cobalt. At the small scale, this had the unexpected effect of facilitating an oxidative addition into the C^{aryl}-S^{Me} bond forming a previously observed dianionic SNC ligand upon heating. Unlike with iron, however, which proceeded through a radical mechanism, cobalt undergoes the two-electron oxidative addition and was able to maintain possession of the SMe moiety which proved difficult to detect with the iron chemistry. Efforts to scale up this reaction had the undesirable effect of creating the imine-coupled N_2S_2 complex, behaviour which was also observed with iron.

Further characterization of the $[Co(N_2S_2)]^-$ anion revealed it to be a Co(I) 16 e^- square-planar species while DFT studies showed that two unpaired electrons of the same spin were delocalized throughout the ligand making the ground state of this species a triplet. This conclusion demonstrates the non-innocent nature of this N_2S_2 ligand. While the analogous iron complex proved to be quite an effective pre-catalyst for the hydroboration of aldehydes with a high selectivity against ketones, this behaviour was not observed with cobalt. While cobalt was almost able to accomplish complete conversion with benzaldehyde as a substrate, this took a significantly longer time than the iron. When using a less electrophilic substrate such as cyclohexanal, the conversion proved to be much lower and what appeared to be the decomposition of the catalyst was observed. Also, unlike the iron example, the cobalt complex showed a higher reactivity towards ketones, namely with acetophenone with which it showed a significant amount of pinacolborane conversion. This very interesting discrepancy in behaviour between the two metals illustrates the wide variety of chemistry that can be accomplished with this thiolate SNS ligand.

3.6. Experimental

3.6.1. General Considerations

All experiments were conducted under nitrogen using and MBraun glovebox unless otherwise stated. All solvents were deoxygenated/dried by purging with nitrogen on a column of activated alumina using a J.C. Meyer solvent purification system. In the case of the THF used for the catalytic reactions, the THF was passed through activated alumina a second time in the glovebox. Deuterated benzene was prepared by purging with nitrogen and then letting the liquid stand over activated alumina overnight. Deuterated acetonitrile was prepared by purging with nitrogen and then refluxing over CaH_2 overnight which was followed by distillation of the solvent the next day. All solvents were stored over activated 4 Å molecular sieves. Glassware was always oven-dried for at least 4 h at 150 ^{o}C before shipping into the glovebox. The following chemicals were purchased and used as is from the following suppliers: 2-(methylthio)benzaldehyde (Aldrich, 90%), 2-aminothiophenol (Aldrich, 90%), bis(diethylphosphino)ethane (Sigma, 98%), triphenylphosphine (Oakwood, 99%), pinacolborane (Aldrich, 97%). ^{1}H, ^{11}B NMR spectra were all recorded on a 300 MHz Bruker Avance or Avance II instrument and referenced to the residual solvent peak in the case of proton and to an external pinacolborane standard at 31 ppm in THF in the case of boron. Single-crystal X-ray diffraction was performed by Dr. Bulat Gabidullin

3.6.2. Synthesis of Co(SNC)(SMe)(DEPE), **3-2**

In a vial $CoCl(PPh_3)_3$ (69 mg, 0.08 mmol), $S^{Me}N^{H}S$ (21.5 mg, 0.08 mmol, 1 equiv.) and $KO^{t}Bu$ (9 mg, 0.08 mmol, 1 equiv.) were combined as solids. A solution of DEPE (18 µL in 3 mL of benzene, 0.08 mmol, 1 equiv.) was prepared and added

dropwise to the solids with rapid stirring causing the formation of a dark-brown suspension. The mixture was stirred for 16 h at 70 ^{o}C during which the colour transitioned to a black-blue with a brown solid visible on the sides. The solution was then filtered through Celite to remove the brown solid and the black-blue filtrate was concentrated under vacuum. The solution was then stored in the freezer causing the precipitation of a small amount of crystals which were suitable for single crystal X-ray diffraction.

3.6.3. Synthesis of $[Co(N_2S_2)][Li_2(\mu\text{-}Cl)]$, **3-3**

In a vial, anhydrous $CoCl_2$ (38.5 mg, 0.3 mmol), $S^{Me}N^{H}S$ (161.4 mg, 0.6 mmol, 2 equiv.) and lithium trimethylsilylimide (200 mg, 1.2 mmol, 4 equiv.) were combined as solids. THF was then added, forming a red solution due to the deprotonated SNS salt with the blue cobalt chloride largely in suspension. Stirring this mixture gradually dissolved the cobalt chloride, causing the colour of the solution to change to a brown colour. After stirring overnight for a total of 16 h the colour had transitioned to a dark navy-blue. The solution was then concentrated and toluene was added to precipitate white LiCl giving a dark purple solution. After filtration through Celite the solvent was removed *in vacuo* yielding a dark purple solid which was washed with 4 x 10 mL of hexanes to remove excess base and its conjugate acid. The purple solid was then dissolved in a minimal amount of THF regaining its navy-blue colouration, and stored in the freezer causing precipitation of a flaky blue solid. Yield 121 mg, 64 %. ^{1}H NMR (300 MHz, CD_3CN at 25 ^{o}C.) δ 13.49 (s, 2H), 11.88 (d, 2H), 7.57 (s, 2H), 2.96 (s, 6H, SCH_3), 2.60 (t, 2H), -1.98 (d, 2H), -20.24 (br s, 2H), -97.50 (s, 2H) and -103.52 (s, 2H).

3.6.4. Catalytic Procedure

In the glovebox, a precatalyst stock solution was prepared by dissolving $[Co(N_2S_2)][Li_2(\mu\text{-}Cl)]$ (5 mg, 0.005 mmol) in THF (5 mL, passed through activated alumina to remove water beforehand) to form the characteristic navy-blue solution. This solution was then stirred for 3 h to ensure homogeneity. From the stock solution, 0.3 mL (0.33 µmol) was extracted using a micropipette and added to an NMR tube. The aldehyde/ketone substrate (0.33 mmol) was then added with a micropipette causing an instant colour change to a dark-grey colour in the case of the aldehydes and with no colour change in the case of the ketone. Addition of pinacolborane (0.33 mmol, 1 equiv.) resulted in an instantaneous colour change to a pale yellow-brown. The reaction mixture was allowed to stand for 30 min after which time the colour had changed to a light turquoise and the ^{11}B NMR spectra were acquired. In cases where conversion was not complete after 30 min, the NMR tube was sealed with parafilm and stored in the glovebox. A ^{11}B NMR spectrum was then taken two days later to monitor the progress, if any.

3.7. References

(1) Ogata, H.; Mizoguchi, Y.; Mizuno, N.; Miki, K.; Adachi, S.; Yasuoka, N.; Yagi, T.; Yamauchi, O.; Hirota, S.; Higuchi, Y. *J. Am. Chem. Soc.* **2002**, *124* (39), 11628–11635.

(2) De Lacey, A. L.; Hatchikian, E. C.; Volbeda, A.; Frey, M.; Fontecilla-Camps, J. C.; Fernandez, V. M. *J. Am. Chem. Soc.* **1997**, *119* (31), 7181–7189.

(3) Niu, S.; Thomson, L. M.; Hall, M. B. *J. Am. Chem. Soc.* **1999**, *121* (16), 4000–4007.

(4) Amara, P.; Volbeda, A.; Fontecilla-Camps, J. C.; Field, M. J. *J. Am. Chem. Soc.* **1999**, *121* (18), 4468–4477.

(5) Lubitz, W.; Ogata, H.; Rüdiger, O.; Reijerse, E. *Chem. Rev.* **2014**, *114* (8), 4081–4148.

(6) Rose, M. J.; Betterley, N. M.; Mascharak, P. K. *J. Am. Chem. Soc.* **2009**, *131*, 8340–8341.

(7) Michael, J. R.; Nolan, M. B.; Allen, G. O.; Mascharak, P. K. *Inorg. Chem.* **2010**, *49*, 1854–1864.

(8) Harrop, T. C.; Mascharak, P. K. *Acc. Chem. Res.* **2004**, *37*, 253–260.

(9) Kovacs, J. A. *Chem. Rev.* **2004**, *104* (2), 825–848.

(10) Santos-Silva, T.; Trincão, J.; Carvalho, A. L.; Bonifácio, C.; Auchère, F.; Raleiras, P.; Moura, I.; Moura, J. J. G.; Romão, M. J. *J. Biol. Inorg. Chem.* **2006**, *11*, 548–558.

(11) Kovacs, J. A.; Brines, L. M. *Acc. Chem. Res.* **2007**, *40*, 501–509.

(12) Tchesnokov, E. P.; Wilbanks, S. M.; Jameson, G. N. L. *Biochemistry* **2012**, *51*, 257–264.

(13) Kumar, D.; Thiel, W.; De Visser, S. P. *J. Am. Chem. Soc.* **2011**, *133*, 3869–3882.

(14) Roy, N.; Sproules, S.; Weyhermu, T.; Wieghardt, K. *Inorg. Chem.* **2009**, *48*, 3783–3791.

(15) Hahn, R.; Nakamura, A.; Tanaka, K.; Nakayama, Y. *Inorg. Chem.* **1995**, *34*, 6562–6564.

(16) Shaffer, D. W.; Szigethy, G.; Ziller, J. W.; Heyduk, A. F. *Inorg. Chem.* **2013**, *52* (4), 2110–2118.

(17) Wong, Y.L.; Dilworth, J. R. *J. Chem. Soc. Dalton Trans.* **2002**, *0* (11), 2366–2370.

(18) Noveron, J. C.; Olmstead, M. M.; Mascharak, P. K. *Inorg. Chem.* **1998**, *37* (6), 1138–1139.

(19) Hirotsu, M.; Santo, K.; Tanaka, Y.; Kinoshita, I. *Polyhedron* **2018**, *143*, 201–208.

(20) Bouwman, E.; Henderson, R. K.; Powell, A. K.; Reedijk, J.; Smeets, W. J. J.; Spek, A. L.; Wocadlo, S. *J. Chem. Soc. Dalton Trans.* **1998**, *0*, 3495–3499.

(21) Sellmann, D.; Prakash, R.; Heinemann, F. W.; Moll, M.; Klimowicz, M. *Angew. Chem. - Int. Ed.* **2004**, *43* (14), 1877–1880.

(22) Rosenkoetter, K. E.; Wojnar, M. K.; Charette, B. J.; Ziller, J. W.; Heyduk, A. F. *Inorg. Chem.* **2018**,

(23) Singh, P.; Singh, A. K. *Organometallics* **2010**, *29* (23), 6433–6442.

(24) McGuinness, D. S.; Wasserscheid, P.; Keim, W.; Morgan, D.; Dixon, J. T.; Bollmann, A.; Maumela, H.; Hess, F.; Englert, U. *J. Am. Chem. Soc.* **2003**, *125* (18), 5272–5273.

(25) Takemoto, S.; Kawamura, H.; Yamada, Y.; Okada, T.; Ono, A.; Yoshikawa, E.; Mizobe, Y.; Hidai, M. *Organometallics* **2002**, *21*, 3897–3904.

(26) Miecznikowski, J. R.; Lo, W.; Lynn, M. A.; Jain, S.; Keilich, L. C.; Kloczko, N. F.; O'Loughlin, B. E.; Dimarzio, A. P.; Foley, K. M.; Lisi, G. P.; et al. *Inorg. Chim. Acta* **2012**, *387*, 25–36.

(27) Bassetti, M. *Eur. J. Inorg. Chem.* **2006**, *0* (22), 4473–4482.

(28) Bassetti, M.; Capone, A.; Salamone, M. *Organometallics* **2004**, *23* (2), 247–252.

(29) Braunstein, P.; Naud, F. *Angew. Chem. - Int. Ed.* **2001**, *40* (4), 680–699.

(30) Das, U. K.; Daifuku, S. L.; Gorelsky, S. I.; Korobkov, I.; Neidig, M. L.; Roy, J. J. Le; Murugesu, M.; Baker, R. T. *Inorg. Chem.* **2016**, *55*, 987–997.

(31) Das, U.K. *Iron Chemistry of Hemilabile SNS LIgands: Synthesis, Reactivity, and Catalytic Applications*, Ph. D. Dissertation, University of Ottawa, Ottawa, ON **2018**.

(32) Das, U. K.; Higman, C. S.; Gabidullin, B.; Hein, J. E.; Baker, R. T. *ACS Catal.* **2018**, *8*, 1076–1081.

(33) Koob, J. G. *A Tale of Two Metals: Come to Cobalt: Synthesis and Characterization of Novel Cobalt-SNS Complexes for Catalysis* and *Degradation of Organophosphates: Study and Characterization of a Novel Fusion of Oxygenase from* F. multimorphosa, B.Sc. Dissertation, Brandeis University, Waltham, MA, USA, **2017**.

(34) Sproules, S.; Kapre, R. R.; Roy, N.; Weyhermüller, T.; Wieghardt, K. *Inorg. Chim. Acta* **2010**, *363* (12), 2702–2714.

(35) Corwin, D. T.; Fikar, R.; Koch, S. A. *Inorg. Chem.* **1987**, *26* (19), 3079–3080.

(36) Franz, K. J.; Doerrer, L. H.; Spingler, B.; Lippard, S. J. *Inorg. Chem.* **2001**, *40* (15), 3774–3780.

(37) Fukui, K.; Masuda, H.; Ohya-Nishiguchi, H.; Kamada, H. *Inorg. Chim. Acta* **1995**, *238* (1–2), 73–81.

(38) Hung Kay Lee; Chung Hei Lam; Li, S. L.; Zhang, Z. Y.; Mak, T. C. W. *Inorg. Chem.* **2001**, *40* (18), 4691–4695.

Chapter 4: Conclusions and Future Outlook

With the ever-growing demand for more catalysts to produce the immense number of industrially prepared chemical products that are consumed everyday, our reliance on precious metals and expensive ligand systems must be significantly reduced. While these noble metals tend to exhibit high reactivity and selectivity, and often benefit from low catalyst loading, the health and environmental impacts of these toxic compounds are becoming of greater and greater concern as more inevitably leach into the environment. To accomplish truly sustainable homogeneous metal catalysis, alternatives using environmentally benign and earth-abundant first-row transition metals must be developed. While less expensive than precious metals, first-row transition metals do not as frequently exhibit the two-electron chemistry that makes the noble metals so attractive. Intelligently designing ligand systems to cooperate with the metal in order to mitigate or even eliminate the shortfalls of first-row transition metals is key to the further integration of these catalysts in industrial processes.

Bifunctional catalysis is at the centre of the study of metal-ligand cooperation and is pushing forward the use of first-row transition metals in catalysis. Ligands in these systems are designed to accomplish additional functions other than just the stabilization of the metal during its catalytic cycle. Bifunctional ligands are able to assist in the activation of small substrates through the use of Lewis bases incorporated into the ligand scaffold. Additionally, by possessing redox potentials which are on par with that of the metal, ligands can also act as electron reservoirs or sinks, facilitating two electron transfer reactions that are more challenging for first-row metals. Incorporating

hemilability into these ligands also allows them to stabilize the metal in the absence of substrate but can still free up a coordination site to allow access to the metal.

Like so many areas of chemistry, nature has had an almost unfathomable amount of time to tinker and optimize its catalytic systems through natural selection. As such, metalloenzyme chemistry acts as a source of inspiration and a template for the design of bifunctional ligand systems. In order to mimic the effectiveness that metalloenzymes exhibit, it is often desirable to incorporate similar functional groups into ligand design that are made use of in enzyme chemistry - namely S- and N-donor groups which are most frequently found in metalloenzymes that undergo a bifunctional mechanism such as [FeFe]-hydrogenases or superoxide reductase. These groups can both act as Lewis bases to assist in the activation of the substrate. With this in mind, our group has aimed to contribute to the field of bifunctional catalysis by preparing two sterically svelte, potentially redox-active, tridentate ligands containing both hard N and soft S donor groups. The ligands differ in that one contains an amido group when deprotonated which is envisioned to be bifunctionally active while the other possesses a thiolate group to fulfill the same role. This will allow for investigation into whether a hard or soft donor is better suited for certain catalytic applications with different substrates and metals.

While these ligands have been studied extensively within the context of iron chemistry, the objective of this Thesis was to develop a series of analogous cobalt complexes to compare the observed reactivity with that of iron. **Chapter 2** illustrated the reactivity that was observed with the amido ligand, $S^{Me}NS^{Me}$, when bonded to cobalt. Specifically, characterization of the $19e^-$ pseudooctahedral cobalt(II) bis-amido complex,

2-1, by ^{1}H NMR spectroscopy, single-crystal X-ray diffraction, and cyclic voltammetry demonstrated its sensitivity to water, likely a result of the basic amido nitrogen atoms. Most remarkable, however, was that this species was obtained starting from Co(I), Co(II) and Co(III) starting materials, demonstrating its high thermodynamic stability and inspiring the title of this thesis. In trying to replicate the reactivity observed with the analogous bis-amido iron complex, the hemilability of the two thioether arms was explored by the addition of ancillary ligands Bipy, DMPE, and CNAr, Surprisingly, Bipy was not able to permanently displace the thioether arms, even at lower temperatures, while DMPE and CNAr triggered redox chemistry, evidenced by disappearance of paramagnetic ^{1}H NMR signals and the appearance of new diamagnetic signals along with free protonated ligand. This is in stark contrast to the iron analog which easily accepted these ligands. Protonating one amido ligand resulted in the formation of $[Co(S^{Me}NS^{Me})(S^{Me}N^{H}S^{Me})](NTf_2)$, **2-2**, which dissolves in acetonitrile to give $[Co(S^{Me}NS^{Me})(NCMe)_n](NTf_2)$, **2-3**, displacing the protonated SNS ligand with a yet to be determined number of acetonitrile ligands. Preliminary attempts to coordinate triphenylphosphine and Bipy to **2-3** show promise from the ^{1}H NMR spectrum, but attempts to obtain crystals suitable for single-crystal X-ray diffraction have been unsuccessful thus far. Finally, probing the activity of **2-1** towards the dehydrogenation of ammonia-borane revealed that it cannot survive the highly reducing conditions on its own, but that in the presence of DMPE, forms an active species that demonstrates unprecedented selectivity towards the formation of linear N-B oligomers or cyclics in the case of MeAB.

Chapter 3 highlighted the reactivity of the SNS thiolate ligand, $S^{Me}NS^{-}$, with cobalt. In the presence of the electron rich bis(phosphine), DEPE, the cobalt(I) centre oxidatively added the C^{aryl}-S^{Me} bond giving Co^{III}(SNC)(SMe)(DEPE), **3-2**. In the presence of electron-rich PMe_3 ligands, iron also converted the $S^{Me}NS^{-}$ ligand into the new dianionic SNC ligand, but the instability of the iron(IV) oxidation state led instead to further reaction of the •SMe radical and a paramagnetic product, $Fe^{III}(S^{-}NC^{-})(PMe_3)_3$. In the absence of phosphine ligands, it was found that unlike iron, cobalt(II) salts did not yield trinuclear, thiolate-bridged complexes. Instead, the $[Co^{I}(N_2S_2)]^{-}$ anion, **3-3**, was formed by coupling the imines of two SNS ligands. Moreover, attempts to scale-up the DEPE reaction gave instead mostly **3-3**, again pointing to the stability of the latter. Characterization of **3-3** by single-crystal X-ray diffraction, cyclic voltammetry and ^{1}H NMR/EPR spectroscopy revealed a total of four stable redox states ranging from the formal Co(0) dianion to the Co(III) cation. DFT studies of **3-3** showed that the triplet ground state could be understood primarily in terms of a diamagnetic d^8 Co(I) centre with two unpaired electrons of the same spin delocalized on the ligand. In contrast, the two unpaired electrons in the neutral d^8 Fe(II) analogue are metal-based with the two ligand unpaired electrons of opposite spin. Mono-anion **3-3** showed inferior activity and selectivity towards the hydroboration of aldehydes compared to the iron species, but further work with the di-anion may lead to an expansion of the substrate scope to include alkenes.

This Thesis has contributed towards the advancement of the field of bifunctional catalysis by extending the pairing of these new SNS ligands from iron to cobalt. This has revealed interesting and unpredictable differences in reactivity between the two

metals. Most noticeable is the tendency of cobalt to undergo redox reactions even during supposedly ‘simple’ ligand substitutions, inspiring the title of this thesis. Major differences were also observed in the selectivity of amine-borane dehydrogenation. While the sluggish iron amido triphos complex gave the products typical of selective catalysts that afford multiple equiv. of H_2 (AB first to BCTB then to borazine and then to cross-linked borazine), the cobalt amido DMPE system showed unique selectivity, giving poly(aminoborane) along with small linear aminoborane oligomers from AB, but preferring to give only cyclic amino- and imino borane trimers from MeAB. We were unable to find another reported catalyst exhibiting this selectivity.

The work presented in this thesis opens a lot of doors for future students in the Baker group to pursue. Protonation of the cobalt(II) bis-amido complex in acetonitrile followed by substitution with hard nitrogen donor ligands such as di-imine, nacnac amidinate, or tris(pyrazolyl) borate may provide a promising new class of cationic and neutral Co(II) amido bifunctional catalysts. Oxidizing the cobalt(II) bis-amido with cationic silver in THF may lead to a family of Co(III) amido SNS species or, alternatively, reduction followed by soft phosphine, phosphite or NHC ligands could afford neutral Co(I) catalysts for reductive applications. While the stability of the $[Co(N_2S_2)]^-$ complex may hinder the isolation of analogous mono-thiolate cobalt catalysts, the multiple redox states of the former have initiated a search for redox-dependent catalysis, in which the activity and selectivity could be tuned by changing the charge on the $Co(N_2S_2)$ unit.

These findings also suggest that there may be a huge range of diversity in the chemistry of these SNS ligands that can be unlocked through the use of different first-row transition metals. Work with in the Baker group is already being extended to other

metals including manganese, nickel and copper with promising initial results that display distinct behaviour from iron and cobalt. Studies focused on furthering the understanding of transition metal SNS chemistry will continue to push the field of bifunctional catalysis forward, building a more sustainable future for the chemical industry.

Appendices:

NMR Spectra:

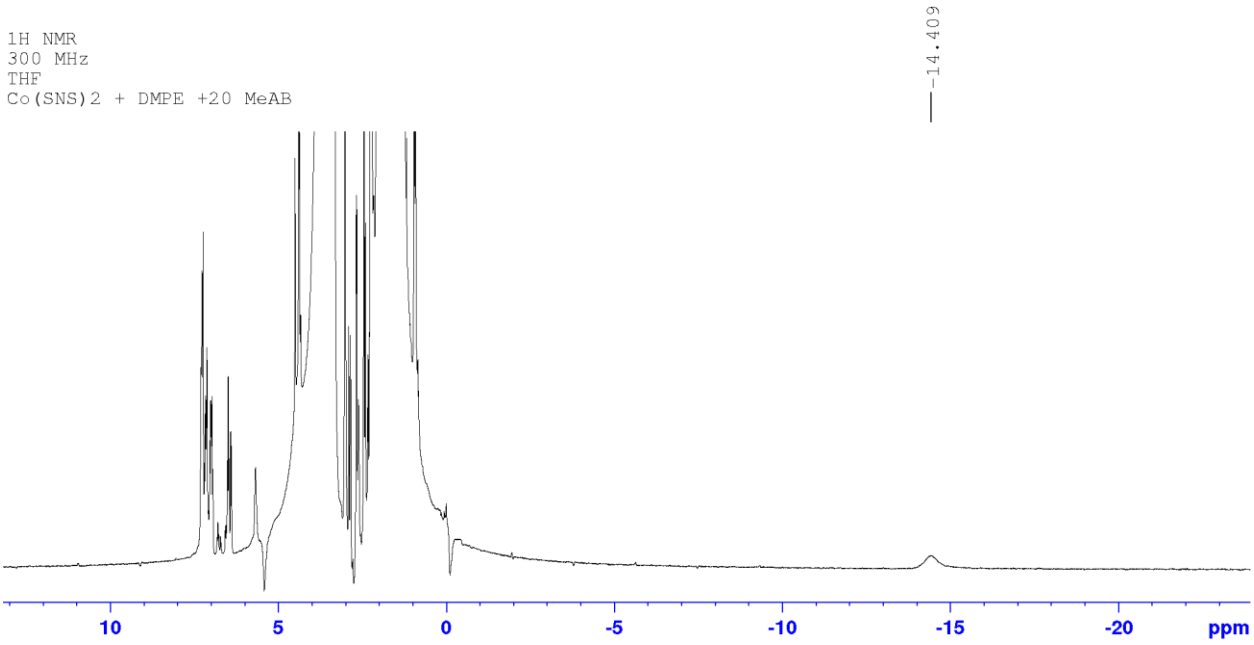

Figure S1: ^{1}H NMR spectrum of the catalytic dehydrogenation of MeAB using 5 mol% $Co(SNS)_2$ with 1 equiv. DMPE per Co.

X-Ray Crystallography:

Experimental: The crystals of **2-1** and **3-2** were mounted on thin glass fibers using paraffin oil. Prior to data collection the crystals were cooled to 200(2) K. The data was collected on a Bruker AXS single-crystal diffractometer equipped with a sealed Mo tube (λ=0.71073 Å) and APEX II CCD detector. The raw data collection and reduction were done with the Bruker APEXII software package.[1] Semi-empirical absorption corrections based on equivalent reflections were applied.[2] Systematic absences in the diffraction dataset and unit-cell parameters were consistent with monoclinic P21/n. The structures were solved by direct methods and refined with full-matrix least-squares procedures based on F^2, using SHELXL[3] and WinGX.[4] All non-H atoms were refined anisotropically. Hydrogen atoms were placed in idealized positions. For the crystal of **2-2**, a suitable crystal was selected and mounted on a cryoloop on a Bruker Venture Metaljet diffractometer. The crystal was kept at 150 K during data collection. Using Olex2,[5] the structure was solved with the XT[6] structure solution program using Intrinsic Phasing and refined with the XL[7] refinement package using Least Squares minimisation. For compound **3-3** crystals were analyzed in a similar method to **2-1** and **3-2** however the

crystals were not suitable enough for the accurate refinement of a unit cell. They were sufficient however to identify the same molecular structure that had been observed by former group member Dr. Cassandra E. Hayes previously.

Table S1: X-Ray diffraction data collection and refinement parameters for complexes **2-1**, **2-2** and **3-2**.

Parameters	**2-1**	**2-2**	**3-2**
Empirical Formula	C30 H32 Co N2 S4	C40 H34 Co F12 N4 O8 S8	C 24 H36 Co N P2 S2
Formula Weight	607.74	1254.20	523.53
Colour	Purple	Orange-yellow	Blue
Temperature, K	200(2)	150	200(2)
Crystal System	Monoclinic	Monoclinic	Monoclinic
Space Group	P21/n	P2/n	P21/n
a, Å	14.3526(5)	16.2712(5)	13.8067(13)
b, Å	10.3708(4)	9.0923(3)	12.1557(12)
c, Å	19.8110(6)	17.5024(5)	15.4526(14)
a, ^{o}	90	90	90
β, ^{o}	107.760(2)	97.5730(10)	107.477(2)
γ, ^{o}	90	90	90
V, Å^3	2808.29(17)	2566.77(14)	2473.7(4)
Z	4	2	4
ρ_{cal}, mg/m^3	1.437	1.623	1.406
μ, mm^{-1}	0.932	4.408	1.005
F(000)	1268	1270.0	1104
Crystal size, mm^3	0.542x0.211x0.0064	0.19x0.12x0.11	0.600x0.500x0.150
Reflections collected/unique	27717	404924	54216
θ range, ^{o}	2.241 to 28.379	3.033 to 60.84	1.737 to 32.612
Index range	-19<=h<19	-21<=h<=21	-20<=h<=20
	-13<=k<=13	-11<=k<=11	-18<=k<=18
	-26<=l<=21	-22<=l<=22	-21<=l<=23
R_{int}	0.0516	0.0429	0.0343
Completeness to θ	25.242, 99.9%	30.422, 99.9%	25.242, 100.0%
Max and Min transmission	0.746 and 0.674	0.752 and 0.550	0.747 and 0.641
Data/restraints/ parameters	7003/0/338	5923/168/381	8682/0/276
Goodness-of-fit of F^2	1.012	1.048	1.019

References:

1. Bruker AXS Inc., Bruker, APEX2, Madison, Wisconsin, USA, 2012.
2. Bruker AXS Inc., Bruker, SADABS, Madison, Wisconsin, USA, 2003.
3. Sheldrick, G. M. Crystal Structure Refinement with SHELXL. *Acta. Cryst.* **2015**, *C71*, 3-8.
4. Farrugia, L. J. WinGX Program Features. *J. Appl. Cryst.* **1999**, *32*, 837-838.
5. Dolomanov, O.V., Bourhis, L.J., Gildea, R.J, Howard, J.A.K. & Puschmann, H., *J. Appl. Cryst.* **2009**, 42, 339-341
6. Sheldrick, G.M. *Acta Cryst.* **2015**, A71, 3-8
7. Sheldrick, G.M. *Acta Cryst*. **2015**, C71, 3-8